농학박사학위논문

Poly(A)-specific ribonuclease에 의한 microRNA 3′ 말단 형성에 대한 연구

Study on the role of poly(A)-specific ribonuclease in microRNA 3′ end formation

2019년 2월

서울대학교 대학원

농생명공학부 응용생명화학전공

이 두 영

A Dissertation for the Degree of Doctor of Philosophy

Study on the role of poly(A)-specific ribonuclease in microRNA 3′ end formation

February 2019

Dooyoung Lee
Applied Life Chemistry Major
Department of Agricultural Biotechnology
Seoul National University

ABSTRACT

The 3′ ends of metazoan microRNAs (miRNAs) are initially defined by the RNase III enzymes during maturation, but subsequently experience extensive modifications by several enzymatic activities. For example, terminal nucleotidyltransferases (TENTs) elongate miRNAs by adding one or a few nucleotides to their 3′ ends, which occasionally leads to differential regulation of miRNA stability or function. However, the catalytic entities that shorten miRNAs and the molecular consequences of such shortening are less well understood, especially in vertebrates. Here, I report that poly(A)-specific ribonuclease (PARN) sculpts the 3′ ends of miRNAs in human cells. By generating *PARN* knockout cells and characterizing their miRNAome, I demonstrate that PARN digests the 3′ extensions of miRNAs that are either derived from the genome or attached by TENTs, thereby effectively reducing the length of miRNAs. Surprisingly, PARN-mediated shortening has little impact on miRNA stability, suggesting that this process likely operates to finalize miRNA maturation, rather than to initiate miRNA decay. PARN-mediated shortening is pervasive across most miRNAs and appears to be a conserved mechanism contributing to the 3′ end formation of vertebrate miRNAs. My findings add miRNAs to the expanding list of non-coding RNAs whose 3′ end formation depends on PARN.

Keywords: exoribonuclease, isomiR, microRNA, poly(A)-specific ribonuclease, PARN, tailing, trimming, untemplated nucleotide addition

***Student Number*:** 2010-23461

CONTENTS

LIST OF FIGURES AND TABLES

LITERATURE REVIEW

MATERIALS AND METHODS

RESULTS

DISCUSSION

LIST OF ABBREVIATIONS

ATP: adenosine triphosphate

BGH: bovine growth hormone

βME: 2-mercaptoethanol

CMV: cytomegalovirus

dATP: deoxyadenosine triphosphate

DNA: deoxyribonucleic acid

DNase: deoxyribonuclease

DTT: dithiothreitol

EDTA: ethylenediaminetetraacetic acid

GST: glutathione *S*-transferase

HCl: hydrochloric acid

hr: hour

IgG: immunoglobulin G

IPTG: isopropyl β-D-1-thiogalactopyranoside

KCl: potassium chloride

kDa: kilodalton

MBP: maltose binding protein

MEF: mouse embryonic fibroblast

MES: 2-(*N*-morpholino)ethanesulfonic acid

$MgCl_2$: magnesium chloride

$Mg(OAc)_2$: magnesium acetate

min: minute

mRNA: messenger RNA

NaCl: sodium chloride

NaOH: sodium hydroxide

NP-40: octylphenoxypolyethoxyethanol

PCR: polymerase chain reaction

PEG: polyethylene glycol

PVDF: polyvinylidene fluoride

RNA: ribonucleic acid

RNAi: RNA interference

RNase: ribonuclease

SDS: sodium dodecyl sulfate

siRNA: small-interfering RNA

SSC: saline-sodium citrate

Tris: tris(hydroxymethyl)aminomethane

tRNA: transfer RNA

UTP: uridine triphosphate

UV: ultraviolet

%(v/v): percentage by volume

INTRODUCTION

MicroRNAs (miRNAs) are small regulatory RNAs of ~22 nucleotides (nt) in length that are processed from characteristic hairpin structures embedded in longer precursor transcripts (Ha and Kim, 2014; Bartel, 2018). In the canonical biogenesis pathway, the RNase III enzymes DROSHA and DICER sequentially cleave the hairpin to produce a miRNA duplex, one strand of which is preferentially loaded into an Argonaute (AGO) protein. The resulting miRNA-induced silencing complex (miRISC) recognizes complementary sites within the 3′-untranslated regions (3′-UTRs) of mRNAs to target them for post-transcriptional repression (Jonas and Izaurralde, 2015). In mammals, each miRNA downregulates hundreds of mRNAs (Lim et al., 2005), and more than 60% of mRNAs have selectively maintained pairing to at least one miRNA (Friedman et al., 2009). Practically, this means that virtually every biological pathway is under the control of miRNAs. In this regard, it is not surprising that dysregulation of miRNAs is frequently associated with human diseases, including cancer and neurodevelopmental disorders (Im and Kenny, 2012; Lujambio and Lowe, 2012; Lin and Gregory, 2015).

With the advent of high-throughput sequencing technologies, it became clear that a single miRNA can exist in multiple isoforms in cells (Ameres and Zamore, 2013; Gebert and Macrae, 2019). These so-called “isomiRs” (Morin et al., 2008) arise from diverse sources, including alternative cleavage of precursors by the RNase III enzymes (Wu et al., 2009a; Chiang et al., 2010; Fukunaga et al., 2012; Kim et al., 2014; Seong et al., 2014; Wilson et al., 2015; Kim et al., 2017); exoribonucleolytic trimming (Han et al., 2011; Liu et al., 2011; Yoda et al., 2013); untemplated

nucleotide addition (Burroughs et al., 2010; Chiang et al., 2010; Wyman et al., 2011; Thornton et al., 2014); and adenosine-to-inosine (A-to-I) RNA editing (Luciano et al., 2004; Blow et al., 2006; Kawahara et al., 2007; Kawahara et al., 2008; Chiang et al., 2010). Because the targeting specificity of a metazoan miRNA is mainly determined by a short stretch of nucleotides located near the 5′ end, called the miRNA "seed" (Bartel, 2009), 5′ isomiRs are expected to regulate distinct sets of mRNAs. However, only a few exceptional miRNA genes produce alternative 5′ isoforms at levels sufficient to direct the repression, and most conserved miRNAs have very consistent 5′ ends (Ruby et al., 2006; Ruby et al., 2007b; Chiang et al., 2010).

On the other hand, variations near the 3′ ends of miRNAs are much more prevalent. In *Drosophila melanogaster*, the 3′-to-5′ exoribonuclease Nibbler trims the 3′ ends of more than a quarter of miRNAs (Han et al., 2011; Liu et al., 2011), and such 3′ trimming is thought to enhance miRNA targeting, at least for miR-34 (Han et al., 2011). In vertebrates, miR-451 exhibits significant 3′ heterogeneity, which is in part attributed to its non-canonical biogenesis: pre-miR-451 is too short to be processed by DICER and instead directly loaded into AGO2, which cleaves the 3′ arm of the hairpin to generate a ~30 nt AGO2-cleaved precursor miR-451 (ac-pre-miR-451) (Cheloufi et al., 2010; Cifuentes et al., 2010; Yang et al., 2010). Poly(A)-specific ribonuclease (PARN) finalizes the maturation of this atypical miRNA by trimming the 3′ end of ac-pre-miR-451 to produce the ~23-26 nt mature miR-451 (Yoda et al., 2013). Importantly, many canonical miRNAs in vertebrates also possess heterogeneous 3′ ends reminiscent of exoribonucleolytic trimming (Kozomara and Griffiths-Jones, 2014; Fromm et al., 2015), such that the overall 3′ heterogeneity of miRNAs is comparable in human and *Drosophila* cells (Han et al., 2011). However,

it is currently unclear whether a general miRNA trimmer, similar to Nibbler in *Drosophila*, exists in vertebrates.

In addition to ribonucleases, terminal nucleotidyltransferases (TENTs) also contribute to 3′ isomiR diversity by adding one or a few nucleotides, usually A or U, to the 3′ ends of miRNAs (Burroughs et al., 2010; Chiang et al., 2010; Wyman et al., 2011; Thornton et al., 2014). Such untemplated nucleotide addition or "tailing" occasionally modulates the stability or function of miRNAs. For example, TENT2 (also known as TUT2, GLD2, and PAPD4) catalyzes the mono-adenylation of miR-122, which is reportedly associated with its increased stability (Katoh et al., 2009; D'ambrogio et al., 2012). On the contrary, mono-adenylation of miR-21 by TENT4B (also known as TUT3, TRF4-2, and PAPD5) is proposed to serve as a decay signal (Boele et al., 2014). TUT4 (ZCCHC11)-mediated uridylation of miR-26 abrogates its regulatory activity and derepresses cytokine expression (Jones et al., 2009), while the same modification marks many miRNAs for degradation during T cell activation (Gutierrez-Vazquez et al., 2017). The basic enzymology of untemplated nucleotide addition to miRNAs has been established by virtue of several transcriptome-wide studies, with multiple TENTs often operating redundantly (Burroughs et al., 2010; Wyman et al., 2011; Thornton et al., 2014). On the other hand, it is poorly understood whether this type of modification is generally reversible, and if so, which ribonucleases are responsible for the clearance of untemplated nucleotides. Previously, PARN has been implicated in the degradation of adenylated miR-21 and miR-122 (Boele et al., 2014; Katoh et al., 2015), but the role of PARN here is described as a "reader/effector" rather than an "eraser".

PARN is a member of the DEDD family of 3′-to-5′ exonucleases with a marked nucleotide preference toward A (Zuo and Deutscher, 2001). Because of its

unique ability to interact with the 7-methylguanosine cap (m^7G) of mRNAs (Dehlin et al., 2000; Gao et al., 2000; Martinez et al., 2000; Martinez et al., 2001), PARN has long been thought to be primarily involved in the metabolism of mRNAs (Balatsos et al., 2012; Virtanen et al., 2013). However, accumulating evidence suggests that PARN-mediated deadenylation may be limited to a small subset of mRNAs and/or may occur mostly in particular biological contexts, rather than comprising the default pathway of mRNA deadenylation and decay (Yamashita et al., 2005; Lee et al., 2012; Son et al., 2018; Yi et al., 2018): for example, knockdown of PARN did not evidently alter the overall poly(A) tail length or abundance of mRNAs in HeLa cells (Son et al., 2018; Yi et al., 2018). Instead, PARN has recently emerged as a key player in the maturation of a wide variety of non-coding RNAs, including small nucleolar RNAs (snoRNAs) and small Cajal body-specific RNAs (scaRNAs) (Berndt et al., 2012; Son et al., 2018), telomerase RNA component (TERC) (Dhanraj et al., 2015; Moon et al., 2015; Nguyen et al., 2015a; Tseng et al., 2015; Boyraz et al., 2016; Shukla et al., 2016; Son et al., 2018), miR-451 (Yoda et al., 2013), 18S ribosomal RNA (rRNA) (Ishikawa et al., 2017; Montellese et al., 2017), and Y RNAs (Shukla and Parker, 2017). The precursors of these RNAs carry small extensions at their 3′ ends that are often followed by untemplated oligo(A) tails. PARN recognizes and removes the oligo(A) tails and subsequently polishes the 3′ ends of these non-coding RNAs to complete their biogenesis. Because oligo(A) tails in nuclear RNAs generally serve as a mark for exosome-mediated destruction (Houseley et al., 2006; Vanacova and Stefl, 2007), PARN-mediated deadenylation and 3′ end formation plays a pivotal role in maintaining the stability of many nuclear non-coding RNAs, including TERC (Berndt et al., 2012; Dhanraj et al., 2015; Moon et al., 2015; Nguyen et al., 2015a; Tseng et al., 2015; Boyraz et al., 2016; Shukla et al., 2016; Shukla and Parker, 2017;

Son et al., 2018). Indeed, mutations in *PARN* have recently been associated with telomere-related diseases, such as dyskeratosis congenita and pulmonary fibrosis (Dhanraj et al., 2015; Stuart et al., 2015; Tummala et al., 2015; Boyraz et al., 2016; Kropski et al., 2017; Petrovski et al., 2017).

In this study, I expand the repertoire of non-coding RNA substrates of PARN to canonical miRNAs, the biogenesis of which depends on both DROSHA and DICER. I reaffirm the notion that the sequence of a miRNA in cells does not necessarily correspond to that defined by the RNase III enzymes, because of frequent terminal modifications. I find that some miRNAs released by DICER processing possess slightly extended 3′ ends than their actual cellular populations, and that PARN is responsible for the 3′ shortening of such miRNAs in cells. By ablating *PARN* in HeLa cells, I demonstrate that PARN-mediated miRNA shortening is widespread across miRNAs and occurs through two distinct modes, depending on the origin of the resected nucleotide. PARN functions as a “trimmer” to digest the genome-encoded 3′ extensions of miRNAs, and as a “de-tailor” to erase or reduce the size of untemplated nucleotide additions. Collectively, my findings unveil the role of PARN in sculpting the 3′ ends of miRNAs, which contributes to miRNA diversity.

LITERATURE REVIEW

Metazoan miRNAs

The first miRNA, lin-4, was discovered in 1993 through genetic screens in the nematode worm, *Caenorhabditis elegans* (Lee et al., 1993; Wightman et al., 1993). It took seven years for the second miRNA, let-7, to be found in the same species (Reinhart et al., 2000). These RNAs were initially considered just an idiosyncrasy of the worm, perhaps because of their incredibly tiny size of ~22 nt—four times smaller than any other regulatory RNA known at that time—and their identification from one biological pathway in one fast-evolving nematode (Ruvkun et al., 2004). However, soon after the observation that the let-7 miRNA is evolutionarily conserved among a wide range of bilaterian organisms (Pasquinelli et al., 2000), efforts were made by several laboratories to identify additional miRNA genes in the genomes of worms, flies, and mammals (Lagos-Quintana et al., 2001; Lau et al., 2001; Lee and Ambros, 2001). The number of known miRNAs has since escalated at an exponential pace, with the aid of concurrent advances in sequencing technologies and computational prediction algorithms, and over two thousands of high-confidence miRNA sequences from over 250 species have been deposited in the miRNA database (miRBase, release 22) at the time of writing (Kozomara and Griffiths-Jones, 2014).

As with many other RNAs, miRNAs exist within cells in the form of functional ribonucleoprotein complexes, called the RNA-induced silencing complex (RISC), the major protein component of which is AGO proteins (Hutvagner and Zamore, 2002; Mourelatos et al., 2002; Khvorova et al., 2003; Schwarz et al., 2003; Liu et al., 2004; Meister et al., 2004). The mature miRNA guides the silencing

complex to target mRNAs through base-pairing and directs their post-transcriptional repression, the mechanism of which largely depends on the extent of pairing between the two nucleic acids (Figure 1). At sites with near-perfect complementarity, as shown in the pairing of most plant miRNAs with their targets (Jones-Rhoades et al., 2006), miRNAs can trigger AGO-catalyzed endoribonucleolytic cleavage of target mRNAs (Figure 1A) (Yekta et al., 2004; Karginov et al., 2010; Shin et al., 2010). In animals, however, miRNA-target pairing is often limited to a short stretch of the miRNA sequence at the 5′ end and mostly induces mRNA destabilization and/or translational repression without slicing the messages (Figure 1B). To elicit mRNA destabilization, AGO proteins recruit the adaptor protein TNRC6 (also known as GW182 and AIN-1/2 in flies and nematodes, respectively) (Ding et al., 2005; Liu et al., 2005; Meister et al., 2005; Rehwinkel et al., 2005), which in turn interacts with the poly(A)-binding protein (PABPC) and brings deadenylase complexes, such as the CCR4-NOT complex and the PAN2-PAN3 complex, to target mRNAs (Figure 1B) (Behm-Ansmant et al., 2006; Chen et al., 2009; Braun et al., 2011; Chekulaeva et al., 2011; Fabian et al., 2011). Deadenylation promotes decapping and subsequent 5′-to-3′ exoribonucleolytic degradation of the mRNAs (Chen et al., 2009; Braun et al., 2012). In most differentiated cells, mRNA destabilization provides a major contribution to miRNA-mediated repression (Baek et al., 2008; Hendrickson et al., 2009; Guo et al., 2010; Eichhorn et al., 2014), such that the repression mediated by a specific miRNA can be closely approximated by changes in mRNA levels.

In animals, contiguous Watson-Crick pairing to the 5′ region of the miRNA centered around nucleotides 2-8, termed the miRNA “seed”, is nearly always necessary and often sufficient to direct the repression (Figure 2A) (Bartel, 2009). The presumable importance of the 5′ region of the miRNA was initially hinted at by

the interaction of the lin-4 precedent with its target mRNA, *lin-14*, in which lin-4 binds to multiple sites within the 3′-UTR of the *lin-14* mRNA through ~8 nt "core elements" that match to the 5′ nucleotides of lin-4 (Lee et al., 1993; Wightman et al., 1993). Several lines of evidence have subsequently conceptualized the "seed rule" for metazoan miRNA-target interactions. From an evolutionary perspective, the seed region of a metazoan miRNA tends to be the most conserved portion across the sequence (Lim et al., 2003), and requiring conserved pairing to this region significantly improves the reliability of *in silico* target predictions (Lewis et al., 2003; Brennecke et al., 2005; Krek et al., 2005; Lewis et al., 2005). At the cellular level, overexpression or depletion of a specific miRNA leads to changes in the output of the sets of genes that are enriched for the corresponding seed matches (Krutzfeldt et al., 2005; Lim et al., 2005; Giraldez et al., 2006; Baek et al., 2008; Selbach et al., 2008). Biochemical and structural studies have provided a better understanding of the seed rule in molecular terms. Within the silencing complex, the seed region disproportionately contributes to the energy required for target recognition (Haley and Zamore, 2004; Ameres et al., 2007; Chandradoss et al., 2015; Salomon et al., 2015). The crystal structures of human AGO proteins loaded with guide nucleic acids reveal that the seed nucleotides are pre-organized such that their bases are exposed and positioned for pairing with target RNAs (Elkayam et al., 2012; Schirle and Macrae, 2012; Schirle et al., 2014; Klum et al., 2018).

Although seed pairing accounts for the majority of miRNA targeting events in animals, a minority of target sites extend pairing to the 3′ region of the miRNA to enhance the specificity of targeting (3′-supplementary sites), or even to compensate for imperfect seed pairing (3′-compensatory sites) (Figure 2A) (Bartel, 2009). In mammals, less than 7% of the conserved target sites have selectively maintained

pairing to the miRNA 3′ region (~4.9% and ~1.5% for 3′-supplementary and 3′-compensatory sites, respectively) (Friedman et al., 2009). The magnitude of benefits of retaining such additional pairing is generally modest (Grimson et al., 2007; Wee et al., 2012; Salomon et al., 2015), but nevertheless appears to be sufficient to impart a regulatory advantage in certain physiological contexts. The biological relevance of 3′ pairing is nicely illustrated by the let-7 sites present in the *lin-41* mRNA of *C. elegans* (Figure 2B). In this species, developmental timing is critically regulated by temporal expression of four miRNAs—let-7, miR-48, miR-84, and miR-241—, all of which have the same seed sequence but differ in their 3′ region, and are referred to as constituting the let-7 miRNA "family" (Lau et al., 2001; Lim et al., 2003). Because let-7 is expressed at the late stages of development (Reinhart et al., 2000; Slack et al., 2000; Vella et al., 2004; Abbott et al., 2005), target mRNAs for let-7 need to escape from the repression by earlier-expressed paralogous miRNAs, which would otherwise lead to precocious cell fate decisions. Perhaps as one such mechanism, the *lin-41* mRNA has evolved two highly conserved 3′-compensatory sites for let-7 (Reinhart et al., 2000; Vella et al., 2004), within which incomplete pairing to the seed sequence prevents targeting by other family members, and at the same time, extensive pairing to the 3′ region of let-7 allows only this particular miRNA to surmount the seed mismatches and effectively mediate the repression (Brennecke et al., 2005; Lewis et al., 2005).

The broad influence of miRNAs on the transcriptome is manifested by the observations that each mammalian miRNA can downregulate hundreds of target mRNAs (Lim et al., 2005; Baek et al., 2008), and more than 60% of mammalian mRNAs have been under selective pressure to retain at least one miRNA target site (Friedman et al., 2009). In animals, the miRNAs as a whole are indispensable for

normal functioning of cells, because the combined loss of all miRNAs results in severe cellular, physiological, and developmental defects, including retarded cell proliferation (Murchison et al., 2005; Wang et al., 2007; Kim et al., 2016), aberrant differentiation (Kanellopoulou et al., 2005; Wang et al., 2007; De Pietri Tonelli et al., 2008; Chong et al., 2010; Johanson et al., 2015), and embryonic lethality (Kataoka et al., 2001; Bernstein et al., 2003; Wienholds et al., 2003; Wang et al., 2007; Vasquez-Rifo et al., 2012). On the other hand, individual miRNAs play roles in a spectrum of biological processes, with regulatory effects that are modest and often redundant with one another. For example, ablation of a single miRNA rarely causes apparent developmental or physiological defects, and simultaneous deletion of multiple family members is often necessary to uncover phenotypic consequences (Miska et al., 2007; Park et al., 2012; Chen et al., 2014). Nevertheless, recent advances in genome-engineering techniques have greatly accelerated the surveys, and abnormal knockout phenotypes for more than two thirds of conserved miRNA families have been reported in mice (Bartel, 2018). The defects caused by the loss of individual miRNA families are surprisingly diverse, spanning from a broad range of physiological, developmental, and behavioral abnormalities to altered susceptibility to diseases (Bartel, 2018). Considering the pervasive regulation by miRNAs, it is not surprising that aberrant miRNA expression emerges as a common feature of human diseases, including cancer and neurodevelopmental disorders (Im and Kenny, 2012; Lujambio and Lowe, 2012; Lin and Gregory, 2015).

Figure 1. Mechanisms of miRNA-mediated gene silencing.

(A) The miRNA associated with slicing-competent AGO proteins (for example, AGO2 in mammals) can induce endoribonucleolytic cleavage of target mRNAs if pairing between the two nucleic acids is extensive enough. However, this mechanism is rarely employed by metazoan miRNAs for endogenous regulation.

(B) Paring between a metazoan miRNA and its target mRNAs is usually confined to a short stretch of miRNA nucleotides near the 5′ end. In this case, the silencing complex interacts with the adaptor protein TNRC6, which in turn recruits poly(A)-binding protein PABPC and several deadenylase complexes such as the CCR4-NOT complex and the PAN2-PAN3 complex. Deadenylation is followed by the recruitment of the DCP1/DCP2 complex, which removes the m^7G cap from target mRNAs and makes them susceptible to 5′-to-3′ exoribonucleolytic degradation. In animals, mRNA destabilization generally provides a major contribution to miRNA-mediated repression, although the silencing complex can mediate translational repression in certain biological contexts (not shown).

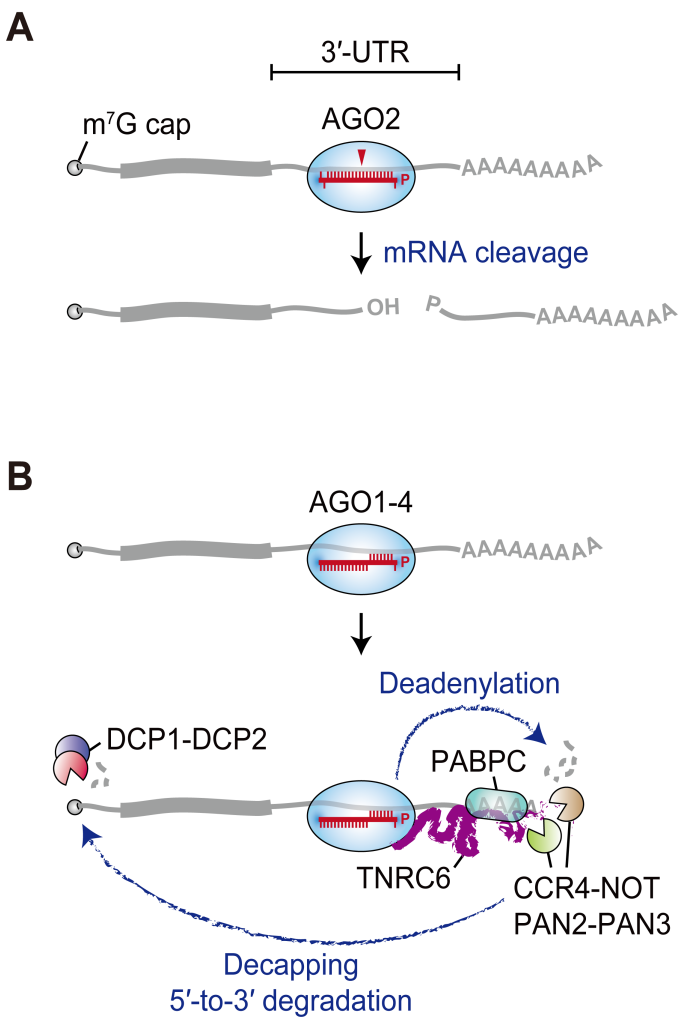
A
3′-UTR
m7G cap
AGO2
AAAAAAAA
mRNA cleavage
OH
P
AAAAAAAA
B
AGO1-4
AAAAAAAA
Deadenylation
DCP1-DCP2
PABPC
TNRC6
CCR4-NOT
PAN2-PAN3
Decapping
5′-to-3′ degradation

Figure 2. Metazoan miRNA target sites.

(A) Canonical and non-canonical miRNA target sites in animals. Watson-Crick base-pairs are indicated by solid lines and G:U wobble pairs by open circles. Note that the first nucleotide of the miRNA is buried within the MID domain of AGO proteins and does not engage in pairing with target RNAs (Lewis et al., 2005; Elkayam et al., 2012; Schirle and Macrae, 2012). Canonical targets sites exhibit 6-7 contiguous Watson-Crick paring to the 5′ region of the miRNA centered on nucleotides 2-8, known as the miRNA "seed". Paring to the seed region, or "seed pairing", is often sufficient to direct the miRNA-mediated repression, as exemplified by the lin-4 site in the *C. elegans lin-14* mRNA. Apart from canonical seed sites, a minority of target sites extend pairing to the 3′ region of the miRNA. Note that 3′-compensatory sites display more substantial pairing (≥4-5 base-pairs) than 3′-supplementary sites (≥3-4 base-pairs) to compensate for incomplete seed pairing. Examples of target sites were obtained elsewhere (Bartel, 2009).

(B) Potential regulatory advantage of acquiring additional 3′ pairing. In *C. elegans*, developmental timing is controlled by temporal expression of four paralogous miRNAs, let-7, miR-48, miR-84, and miR-241. These miRNAs have the same seed and are known to constitute the let-7 miRNA "family". Because of the latest accumulation of let-7, its target mRNAs should escape from the repression by earlier-expressed paralogous miRNAs. As one such mechanism, the *lin-41* mRNA has evolved two highly conserved 3′-compensatory sites for let-7, within which only this specific miRNA can surmount imperfect seed pairing through extensive 3′ pairing and direct the repression.

A

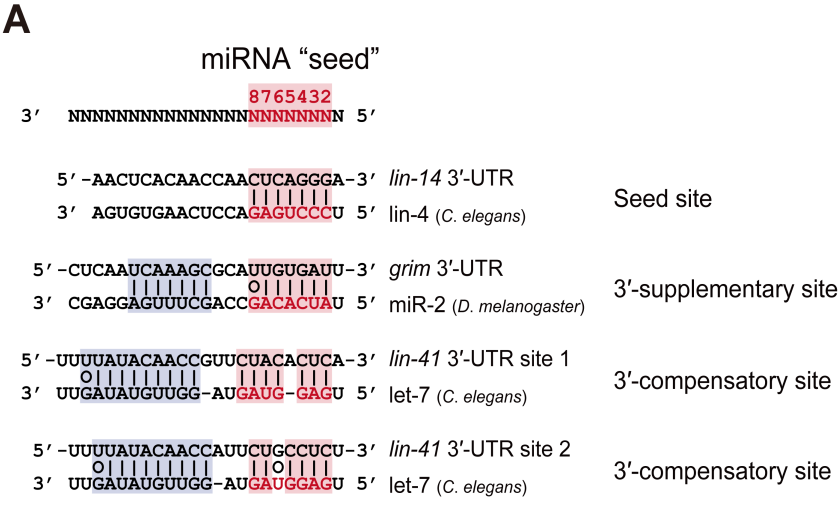
miRNA "seed"
8765432
3′ NNNNNNNNNNNNNNNNNNNNNN 5′
5′-AACUCACAACCAACUCAGGGA-3′ lin-14 3′-UTR
3′ AGUGUGAACUCCAGAGUCCCU 5′ lin-4 (C. elegans)
Seed site
5′-CUCAAUCAAAGCGCAUUGUGAUU-3′ grim 3′-UTR
3′ CGAGGAGUUUCGACCGACACUAU 5′ miR-2 (D. melanogaster)
3′-supplementary site
5′-UUUUAUACAACCGUUCUACACUCA-3′ lin-41 3′-UTR site 1
3′ UUGAUAUGUUGG-AUGAUG-GAGU 5′ let-7 (C. elegans)
3′-compensatory site
5′-UUUUAUACAACCAUUCUGCCUCU-3′ lin-41 3′-UTR site 2
3′ UUGAUAUGUUGG-AUGAUGGAGU 5′ let-7 (C. elegans)
3′-compensatory site

B

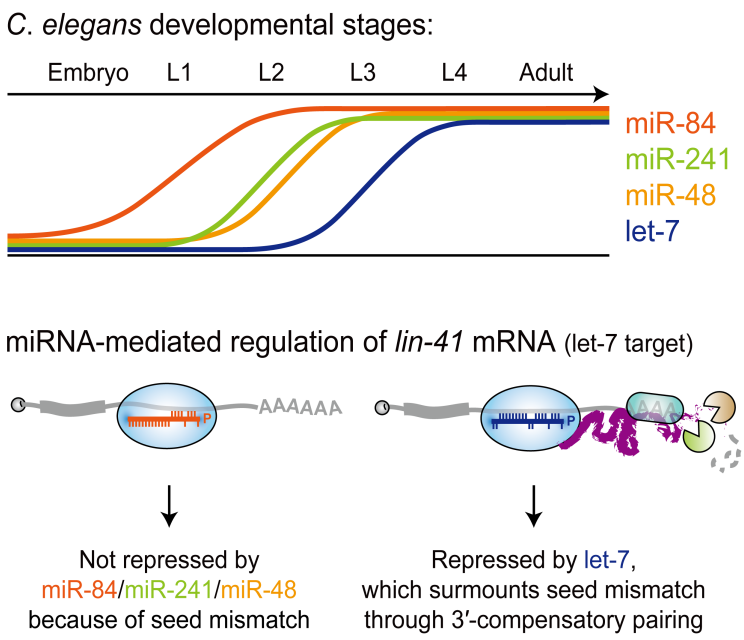
C. elegans developmental stages:
Embryo
L1
L2
L3
L4
Adult
miR-84
miR-241
miR-48
let-7
miRNA-mediated regulation of lin-41 mRNA (let-7 target)
AAAAAA
Not repressed by
miR-84/miR-241/miR-48
because of seed mismatch
Repressed by let-7,
which surmounts seed mismatch
through 3′-compensatory pairing

Biogenesis of metazoan miRNAs

By virtue of intensified efforts over the past two decades, much is now known about how metazoan miRNAs are generated (Figure 3) (Ha and Kim, 2014). In the canonical biogenesis pathway, miRNA genes are transcribed by RNA polymerase II (Pol II) into long primary transcripts, called primary miRNAs (pri-miRNAs), containing one or more characteristic hairpin structures (Lee et al., 2004). These miRNA hairpins are initially cleaved by the nuclear Microprocessor complex, the catalytic subunit of which is DROSHA, an RNase III, to release ~60-80 nt precursor miRNAs (pre-miRNAs) (Lee et al., 2003; Denli et al., 2004; Gregory et al., 2004; Han et al., 2004). Pre-miRNAs are then exported to the cytoplasm with the aid of Exportin-5 (Yi et al., 2003; Bohnsack et al., 2004; Lund et al., 2004), where they undergo further processing by a second RNase III, DICER (Grishok et al., 2001; Hutvagner et al., 2001; Ketting et al., 2001). Of the resulting ~20 base-pair (bp) miRNA duplex, one strand (called the "guide" strand or "miRNA") is preferentially selected by an AGO protein to form a functional silencing complex (Hutvagner and Zamore, 2002; Mourelatos et al., 2002; Khvorova et al., 2003; Schwarz et al., 2003; Liu et al., 2004; Meister et al., 2004), while the opposite strand (the "passenger" strand or "miRNA*") is discarded (Matranga et al., 2005; Rand et al., 2005; Leuschner et al., 2006; Kawamata et al., 2009; Park and Shin, 2015). The suffix "5p" or "3p" can be added to the miRNA name to indicate the arm of the pre-miRNA hairpin from which the strand originates. Because the strand choice by AGO proteins depends on the properties that are not predisposed by the duplex orientation within the pre-miRNA (discussed below), either 5p or 3p strand can serve as a guide strand.

The irreplaceable roles of RNase III enzymes in metazoan miRNA biogenesis are manifested by the loss of the vast majority of miRNAs in *DROSHA* or *DICER*

knockout cells (Kim et al., 2016). RNase III family enzymes are double-stranded RNA (dsRNA)-specific endoribonucleases that cut each strand of the RNA duplex with a 2 bp offset (Court et al., 2013; Nicholson, 2014). Based on domain structures, they are divided into four classes, with DROSHA and DICER constituting the two, respectively (Liang et al., 2014). Both enzymes possess tandem RNase III domains followed by a single dsRNA-binding domain in their C-terminal regions (Filippov et al., 2000; Wu et al., 2000; Bernstein et al., 2001), with the two RNase III domains dimerizing intramolecularly to form a single processing center (Figure 4) (Han et al., 2004; Zhang et al., 2004; Macrae et al., 2006; Kwon et al., 2016; Liu et al., 2018). The overall structures of DROSHA and DICER are markedly similar, despite their distant sequence homology apart from the catalytic core, suggesting that DROSHA may have evolved from an ancestral DICER (Kwon et al., 2016).

Both DROSHA and DICER require dsRNA-binding protein partners for full activity. Human DROSHA purified to homogeneity fails to process pri-miRNAs *in vitro* (Gregory et al., 2004; Han et al., 2004). In human and *Drosophila* lysates, DROSHA fractionates as a large protein complex, termed the Microprocessor, in which it is tightly associated with a dsRNA-binding protein, called DGCR8 (also known as Pasha in invertebrates) (Denli et al., 2004; Gregory et al., 2004; Han et al., 2004). DROSHA and DGCR8/Pasha together are minimally required for pri-miRNA processing activity both *in vitro* and in cells (Denli et al., 2004; Gregory et al., 2004; Han et al., 2004). Within the Microprocessor, two molecules of DGCR8 bind to the two RNase III domains of DROSHA, respectively, allowing it to fold properly and cleave pri-miRNAs both efficiently and accurately (Nguyen et al., 2015b; Kwon et al., 2016). While recombinant DICER alone is capable of cleaving pre-miRNA and long dsRNA substrates *in vitro* (Provost et al., 2002; Chendrimada et al., 2005), its

catalytic activity is modulated by the association with protein partners, similarly as that of DROSHA. In mammals, DICER utilizes the N-terminal helicase domain to interact with the dsRNA-binding protein TRBP or its paralogue PACT (Chendrimada et al., 2005; Haase et al., 2005; Lee et al., 2006). In *Drosophila*, Dicer-1 and Dicer-2 associate with Loquacious (Loqs) and R2D2, respectively, both of which are fly orthologues of TRBP (Liu et al., 2003; Forstemann et al., 2005; Jiang et al., 2005; Saito et al., 2005). For a subset of pre-miRNAs, TRBP/Loqs increases the efficiency of DICER processing (Forstemann et al., 2005; Jiang et al., 2005; Saito et al., 2005; Chakravarthy et al., 2010; Lee et al., 2013; Fareh et al., 2016), and even alters the choice of cleavage sites by DICER (Fukunaga et al., 2012; Lee and Doudna, 2012; Kim et al., 2014; Wilson et al., 2015). In the presence of TRBP, mammalian DICER also forms a complex with AGO2, termed the miRISC-loading complex (miRLC), which is believed to streamline the cytoplasmic maturation processes (Gregory et al., 2005; Maniataki and Mourelatos, 2005; Macrae et al., 2008; Wang et al., 2009; Liu et al., 2012).

As the gatekeeper of the miRNA biogenesis pathway, the Microprocessor discriminates authentic pri-miRNA hairpins from tens of millions of other hairpins (Bentwich et al., 2005). Structurally, bilaterian pri-miRNAs are approximated to an imperfect stem of ~3 helical turns (35±1 bp) flanked by unpaired basal segments at the base and an apical loop at the top (Lim et al., 2003; Han et al., 2006; Fang and Bartel, 2015). The Microprocessor recognizes the single-stranded RNA (ssRNA)-dsRNA junctions at both ends of the stem, introducing staggered cuts ~1 helical turn away from the basal junction and ~2 helical turns away from the apical junction (Figure 4) (Zeng et al., 2005; Han et al., 2006; Ma et al., 2013; Fang and Bartel, 2015; Nguyen et al., 2015b). The crystal structure of minimal Microprocessor

reveals that DROSHA is the subunit that not only executes the catalysis, but also determines the sites for cleavage by measuring the distance from the basal junction (Kwon et al., 2016). In addition to structural determinants, most bilaterian pri-miRNAs also possess several conserved primary-sequence motifs, including a UG motif at the basal junction, a CNNC motif in the 3′ basal segment, a mismatched GHG motif in the middle of the basal stem, and a UGU/GUG motif in the 5′ end of the apical loop (Figure 4) (Auyeung et al., 2013; Mori et al., 2014; Fang and Bartel, 2015; Nguyen et al., 2015b; Roden et al., 2017). These motifs stimulate pri-miRNA processing by recruiting the subunits or auxiliary co-factors of the Microprocessor: for example, the basal UG and apical UGU/GUG motifs are directly recognized by DROSHA and DGCR8, respectively (Nguyen et al., 2015b), while the CNNC motif is bound by SRSF3 (Auyeung et al., 2013; Fernandez et al., 2017), which in turn recruits DROSHA to pri-miRNAs (Kim et al., 2018). The motifs also impart a degree of asymmetry to pri-miRNAs, which forces the Microprocessor to bind substrates only in the productive orientation (Fang and Bartel, 2015; Nguyen et al., 2015b).

Pre-miRNAs excised by the Microprocessor features a 5′ monophosphate, a 3′ hydroxyl, and a ~2 nt 3′ overhang (Lee et al., 2003), the hallmarks of RNase III products (Nicholson, 2014). DICER ideally recognizes these terminal structures of pre-miRNAs using a sequence-independent RNA-binding module, called the PAZ domain, and introduces another staggered cuts ~22 bp away from the ends (Figure 4) (Macrae et al., 2007; Park et al., 2011; Tsutsumi et al., 2011; Tian et al., 2014; Liu et al., 2018). The PAZ domain displays a marked preference toward a 2 nt 3′ overhang (Ma et al., 2004), such that substrates with blunt ends or ≥3 nt overhangs are cleaved by DICER much less efficiently than those with canonical 2 nt overhangs (Vermeulen et al., 2005; Park et al., 2011). This structural preference forms in part

the basis of a cellular strategy to suppress let-7 biogenesis in embryonic stem cells, in which the combined activity of LIN28 and TUT4 elongates the 3′ overhang of pre-let-7 and effectively blocks its DICER processing (Heo et al., 2008; Heo et al., 2009). In addition to the overhang structure, DICER also recognizes the terminal loop of pre-miRNAs using the helicase domain to ensure the accuracy of cleavage (Zhang and Zeng, 2010; Tsutsumi et al., 2011; Gu et al., 2012; Liu et al., 2018). Unlike the Microprocessor, which senses primary-sequence determinants to a certain extent (Auyeung et al., 2013; Fang and Bartel, 2015; Nguyen et al., 2015b), DICER has negligible, if any, sequence preferences, as illustrated by the artificial short hairpin RNA (shRNA) technology that has become routine in biological research as a means of silencing desired target genes. By design, shRNAs are transcribed into short transcripts similar in structure to pre-miRNAs, which are directly cleaved by DICER and loaded into AGO proteins (Brummelkamp et al., 2002; Paddison et al., 2002). In a typical loss-of-function screen, hundreds of thousands of shRNAs with different sequences are designed to cover, for example, all protein-coding genes. Despite their extremely diverse sequences, most shRNAs are functional (Moffat et al., 2006), and by inference, are likely cleaved by DICER in cells without much variation in cleavage efficiency.

Two consecutive cleavage of pri-miRNA hairpins by DROSHA and DICER releases ~20 bp miRNA duplexes containing a ~2 nt 3′ overhang on each strand. In mammals, four AGO proteins (AGO1-4) recognize and incorporate these duplexes almost indistinguishably from one another (Azuma-Mukai et al., 2008; Burroughs et al., 2011; Dueck et al., 2012), although only AGO2 is capable of cleaving perfectly matched target RNAs (Liu et al., 2004; Meister et al., 2004). The miRNA duplex associates with an AGO protein to form an intermediate species called pre-RISC,

during which the chaperon complex HSC70/HSP90 assists the protein to undergo a conformational opening to accommodate the rigid dsRNA structure (Iwasaki et al., 2010; Yoda et al., 2010; Naruse et al., 2018). The choice of which strand of the duplex is selected as a guide strand primarily depends on the composition of the first nucleotide and the relative thermodynamic stability at the ends of the duplex: AGO retains the strand less stably paired at the 5′ end (Khvorova et al., 2003; Schwarz et al., 2003), with a preference for U or A at nucleotide position 1 (Frank et al., 2010; Suzuki et al., 2015). Upon strand selection, pre-RISC unwinds the duplex and discards the passenger strand to generate a mature RISC (Matranga et al., 2005; Rand et al., 2005; Leuschner et al., 2006; Kawamata et al., 2009; Park and Shin, 2015), in which AGO tightly anchors the 5′ and 3′ ends of the miRNA in the MID and PAZ domains, respectively (Elkayam et al., 2012; Schirle and Macrae, 2012).

Although the vast majority of miRNAs are generated through the canonical biogenesis pathway that relies on both DROSHA and DICER, a minority of miRNAs requires only one of the two factors for maturation (Babiarz et al., 2008; Kim et al., 2016). For example, precursors for some miRNAs are biochemically defined by the spliceosome (called “mirtrons”) (Berezikov et al., 2007; Okamura et al., 2007; Ruby et al., 2007a) or RNA polymerases (endogenous shRNAs) (Andersson et al., 2005; Xie et al., 2013; Zamudio et al., 2014; Bellutti et al., 2015; Kim et al., 2016), rather than by the Microprocessor. On the other hand, there is a single known miRNA that bypasses DICER processing: vertebrate miR-451 (Figure 5). The precursor of this miRNA released by the Microprocessor is too short to be cleaved by DICER, and is directly loaded into AGO proteins (Cheloufi et al., 2010; Cifuentes et al., 2010; Yang et al., 2010). The pairing in the pre-miR-451 stem is so extensive that AGO2 can cleave the 3′ arm of the hairpin in the middle to generate a ~30 nt ac-pre-miR-451

(Cheloufi et al., 2010; Cifuentes et al., 2010; Yang et al., 2010), which is trimmed at the 3′ end by the PARN exonuclease to eventually produce the ~23-26 nt mature miRNA (Yoda et al., 2013).

Figure 3. Biogenesis of metazoan miRNAs.

In the canonical pathway, miRNA genes are transcribed by RNA polymerase II (Pol II) into long primary transcripts, referred to as primary miRNAs (pri-miRNAs), which contain at least one characteristic hairpin structure. These hairpins are cleaved in the basal stem by the nuclear Microprocessor, a heterotrimeric complex consisting of one molecule of DROSHA, an RNase III, and two molecules of DGCR8, a double-stranded RNA (dsRNA)-binding protein. The resulting ~60-80 nt precursor miRNAs (pre-miRNAs) are exported to the cytoplasm through the action of Exportin-5 and Ran-GTP, and further cleaved near the terminal loop by another RNase III, DICER, whose activity is modulated by dsRNA-binding protein partners such as TRBP. Of the ~20 bp miRNA duplex liberated by DICER processing, one strand is preferentially loaded into an AGO protein to form a mature miRNA-induced silencing complex (miRISC). Within this complex, the 5′ and 3′ ends of the miRNA are tightly anchored in the MID and PAZ domains of AGO, respectively.

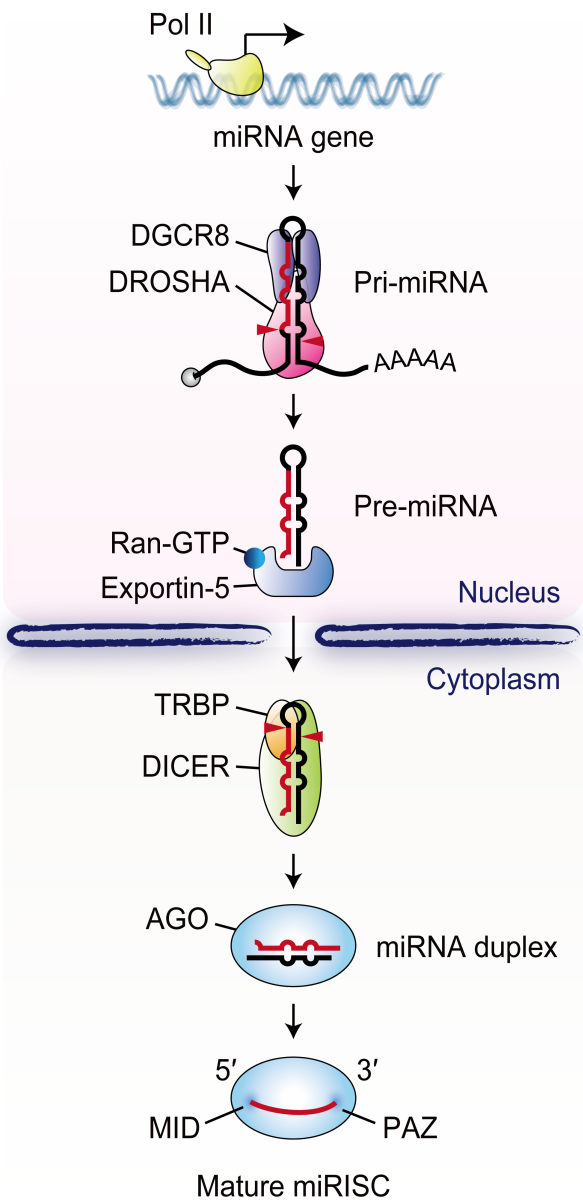
Pol II
miRNA gene
DGCR8
DROSHA
Pri-miRNA
AAAAA
Pre-miRNA
Ran-GTP
Exportin-5
Nucleus
Cytoplasm
TRBP
DICER
AGO
miRNA duplex
5′
3′
MID
PAZ
Mature miRISC

Figure 4. Two consecutive cleavage of pri-miRNA hairpins by DROSHA and DICER.

A representative pri-miRNA molecule is illustrated at the top. Pri-miRNAs are characterized by an imperfect stem of ~3 helical turns (35±1 bp) flanked by a stretch of unstructured nucleotides at both ends, termed the basal segment and apical loop. The Microprocessor introduces staggered cuts ~1 helical turn (~13 bp) away from the basal junction and ~2 helical turns (~22 bp) away from the apical junction. Primary sequence motifs that are known to enhance the processing efficiency of the Microprocessor are indicated, including a basal UG motif, a flanking CNNC motif, a mismatched GHG motif, and an apical UGU/GUG motif. DICER recognizes both ends of the resulting pre-miRNA and introduces staggered cuts ~2 helical turns (~22 bp) away from them to produce a ~20 bp miRNA duplex. Thus, both DROSHA and DICER function as molecular rulers. Note that, unlike the Microprocessor, DICER does not depend on primary sequence motifs.

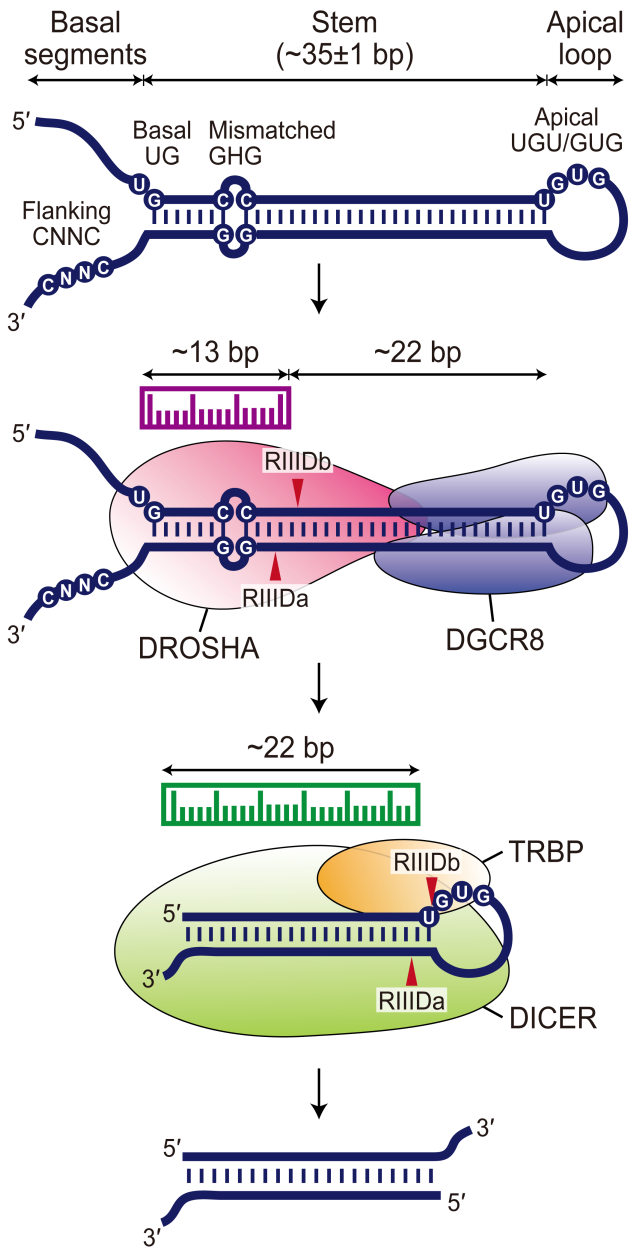
Basal segments
Stem (~35±1 bp)
Apical loop
5′
Basal UG
Mismatched GHG
Apical UGU/GUG
Flanking CNNC
3′
~13 bp
~22 bp
RIIIDb
RIIIDa
DROSHA
DGCR8
~22 bp
TRBP
RIIIDb
5′
3′
RIIIDa
DICER
5′
3′
3′
5′

Figure 5. Atypical maturation of miR-451 mediated by AGO2 and PARN.

Pri-miR-451 is processed by the Microprocessor into an unusually short, ~41-42 nt pre-miR-451 hairpin with a ~17 bp extensively paired stem. This atypical precursor bypasses DICER processing and is directly loaded into AGO proteins. Once AGO2 incorporates pre-miR-451, it cleaves the 3′ arm of the hairpin in the middle to generate a ~30 nt AGO2-cleaved pre-miR-451 (ac-pre-miR-451), which is subsequently trimmed at the 3′ end by PARN into ~23-26 nt mature miR-451.

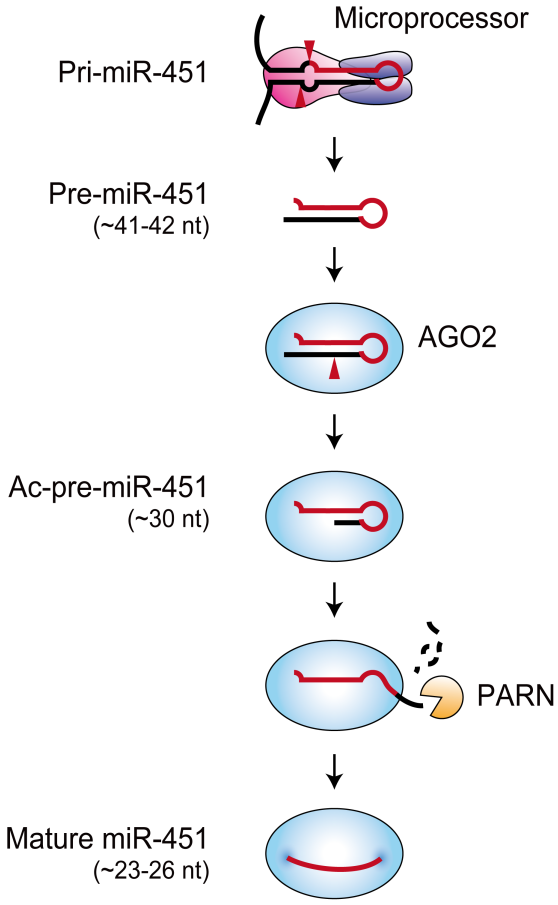
Microprocessor
Pri-miR-451
Pre-miR-451
(~41-42 nt)
AGO2
Ac-pre-miR-451
(~30 nt)
PARN
Mature miR-451
(~23-26 nt)

Diversifying miRNA sequence

High-throughput sequencing of cellular small RNAs often retrieves a collection of different sequences mapped to a single miRNA locus, called isomiRs (Figure 6) (Morin et al., 2008). Practically, the miRNA repository provides one reference sequence for each miRNA, which usually corresponds to the most abundant isoform (Kozomara and Griffiths-Jones, 2014). Individual miRNAs display varying degrees of heterogeneity (Ruby et al., 2006; Ruby et al., 2007b; Chiang et al., 2010), and certain miRNAs exhibit differential patterns of isomiR distribution among different developmental stages (Fernandez-Valverde et al., 2010; Lee et al., 2014) or between normal tissue and cancer (Telonis et al., 2017). These observations imply that the generation of isomiRs might be a regulated process with the potential biological importance.

Depending on the site of variation, isomiRs are categorized into 5′, 3′, and internal isomiRs: the sequence may be extended or truncated at either end or have different nucleotides in the middle, compared with the reference sequence (Figure 6) (Ameres and Zamore, 2013; Gebert and Macrae, 2019). Internal modifications are primarily generated through A-to-I RNA editing of miRNA precursors, which is mediated by the dsRNA-specific adenosine deaminases (ADARs) and most frequently occurs in the brain (Luciano et al., 2004; Blow et al., 2006; Kawahara et al., 2007; Kawahara et al., 2008; Chiang et al., 2010). On the other hand, terminal variations can be introduced to a miRNA at various stages in the biogenesis pathway. For example, DROSHA and DICER occasionally cleave their substrates at more than one site, leading to multiple miRNA isoforms with different ends (Wu et al., 2009a; Chiang et al., 2010; Fukunaga et al., 2012; Kim et al., 2014; Seong et al., 2014; Wilson et al., 2015; Kim et al., 2017). Even once loaded into AGO proteins, miRNAs

undergo extensive terminal modifications, mainly at their 3′ ends, by post-processing enzymatic activities such as trimming (Han et al., 2011; Liu et al., 2011; Yoda et al., 2013) and untemplated nucleotide addition (Burroughs et al., 2010; Chiang et al., 2010; Wyman et al., 2011; Thornton et al., 2014).

Regarding the consequence of sequence variations, any modification altering the seed sequence is expected to produce the miRNA isoforms exhibiting different targeting specificity. For example, alternative cleavage by DROSHA or DICER can shift the 5′ end position of 5p or 3p miRNAs, respectively (Wu et al., 2009a; Chiang et al., 2010; Fukunaga et al., 2012; Kim et al., 2017). A-to-I RNA editing within the seed also impacts on miRNA targeting, because I pairs with C, not U (Kawahara et al., 2007). However, only a few exceptional miRNAs generate such 5′ isomiRs at levels sufficient to mediate the repression and most metazoan miRNAs have evolved to retain very consistent 5′ ends, perhaps to maximize targeting specificity (Ruby et al., 2006; Ruby et al., 2007b; Chiang et al., 2010). In this regard, requiring 5′ homogeneity has been one of the main criteria for discriminating authentic miRNAs from dubious annotations (Fromm et al., 2015).

On the other hand, modifications at the 3′ ends of miRNAs are much more frequently observed (Figure 6). The best-characterized mechanism of generating 3′ isomiRs is untemplated nucleotide addition or “tailing”, in which one or a few nucleotides, usually A or U, are added to the 3′ ends of miRNAs (Figure 7A). Tailing of miRNAs is catalyzed by a set of related enzymes known as TENTs. In mammals, seven TENTs with different nucleotide preferences remodel the 3′ ends of partially overlapping sets of miRNAs, as elucidated by several transcriptome-wide studies (Burroughs et al., 2010; Wyman et al., 2011; Thornton et al., 2014). Depending on the type of modification and the miRNA being modified, tailing can lead to various

outcomes, including stabilization (Katoh et al., 2009; D'ambrogio et al., 2012), destabilization (Boele et al., 2014; Lee et al., 2014; Gutierrez-Vazquez et al., 2017) and altered regulatory activity (Jones et al., 2009). Another mechanism contributing to 3′ isomiR diversity is 3′-to-5′ exoribonucleolytic trimming (Figure 7A). On an intellectual level, exoribonucleases comprise one of the most prevalent enzymatic activities in cells (Deutscher and Li, 2001; Zuo and Deutscher, 2001), and one might say with confidence that miRNAs are also likely influenced by them. On a practical level, high-throughput sequencing often retrieves a considerable fraction of reads that are shorter at their 3′ ends than the reference sequence (Kozomara and Griffiths-Jones, 2014; Fromm et al., 2015), which are not attributable to RNA degradation during sample preparation (Lee et al., 2010). In principle, they could represent either naturally occurring isoforms and/or decay intermediates from a cellular degradation pathway. Currently, the enzymology and consequences of 3′-to-5′ exoribonucleolytic trimming are known for only a few individual miRNAs and less well characterized on a global scale, especially in vertebrates (Figure 7B).

In *Drosophila*, the 3′-to-5′ exoribonuclease Nibbler trims more than a quarter of miRNAs without apparently altering their abundance (Han et al., 2011; Liu et al., 2011). Trimming by Nibbler takes places within the miRISC and is likely supported by the interaction between Nibbler and Ago1 (Han et al., 2011; Liu et al., 2011). Nibbler-mediated trimming is reported to enhance the regulatory activity of a model miRNA, miR-34 (Han et al., 2011). In vertebrates, PARN trims the 3′ end of ac-pre-miR-451, an atypical intermediate species generated during the biogenesis of miR-451 (Figure 5) (Yoda et al., 2013). Trimming does not apparently affect the stability or function of this miRNA, such that untrimmed ac-pre-miR-451 mediates the repression as efficiently as mature miR-451 (Yoda et al., 2013). During mammalian

nervous system development, unknown nuclease(s) globally shortens the 3′ ends of miRNAs loaded into AGO2 but not the other AGO proteins (Juvvuna et al., 2012). These examples illustrate how 3′-to-5′ exoribonucleolytic trimming influences the 3′ end formation of metazoan miRNAs and contributes to 3′ isomiR diversity. On the other hand, the same process is also closely linked to miRNA degradation. For example, PNPT1, an interferon-inducible 3′-to-5′ exoribonuclease, selectively and preferentially degrades miR-221 in human melanoma cells (Das et al., 2010). The exosome complex serves as the primary nuclease activity responsible for the rapid decay of miR-382 in HEK293T cells (Bail et al., 2010). PARN is believed to promote the degradation of adenylated miR-21 and miR-122 (Boele et al., 2014; Katoh et al., 2015). In target RNA-directed miRNA degradation (TDMD) (Fuchs Wightman et al., 2018), destabilization of the miRNA by highly complementary target RNAs is accompanied by 3′ tailing and trimming of the degraded miRNA (Ameres et al., 2010; De et al., 2013; De La Mata et al., 2015; Haas et al., 2016; Park et al., 2017). In summary, the consequences of 3′-to-5′ trimming of miRNAs are highly context-dependent and not easily predictable (Figure 7B).

By inference, enzymatic activities that counteract miRNA tailing by TENTs or reduce the length of tails should belong to 3′-to-5′ exoribonucleases. Such enzyme has never been described to date, and only those acting as a “reader/effector” are known. For example, PARN recognizes and degrades some miRNAs carrying mono or oligo(A) tails (Boele et al., 2014; Katoh et al., 2015). The exosome complex degrades defective pre-miRNAs marked with uridine tails (Liu et al., 2014), while DIS3L2 specifically targets oligo-uridylated pre-let-7 for destruction in embryonic stem cells (Chang et al., 2013). The existence of “eraser” for miRNA tailing is currently obscure.

Figure 6. miRNA isoforms or isomiRs.

The sequences of human miR-21-5p isoforms, revealed by high-throughput small RNA sequencing (Fromm et al., 2015), are presented with their read counts. The reference sequence of miR-21-5p annotated in miRBase is shown in red. Untemplated nucleotides (nucleotides that do not match to the genome) or "tails" are indicated (white letters within dark blue rectangles). Note that the variations are mostly enriched near the 3′ end of the miRNA.

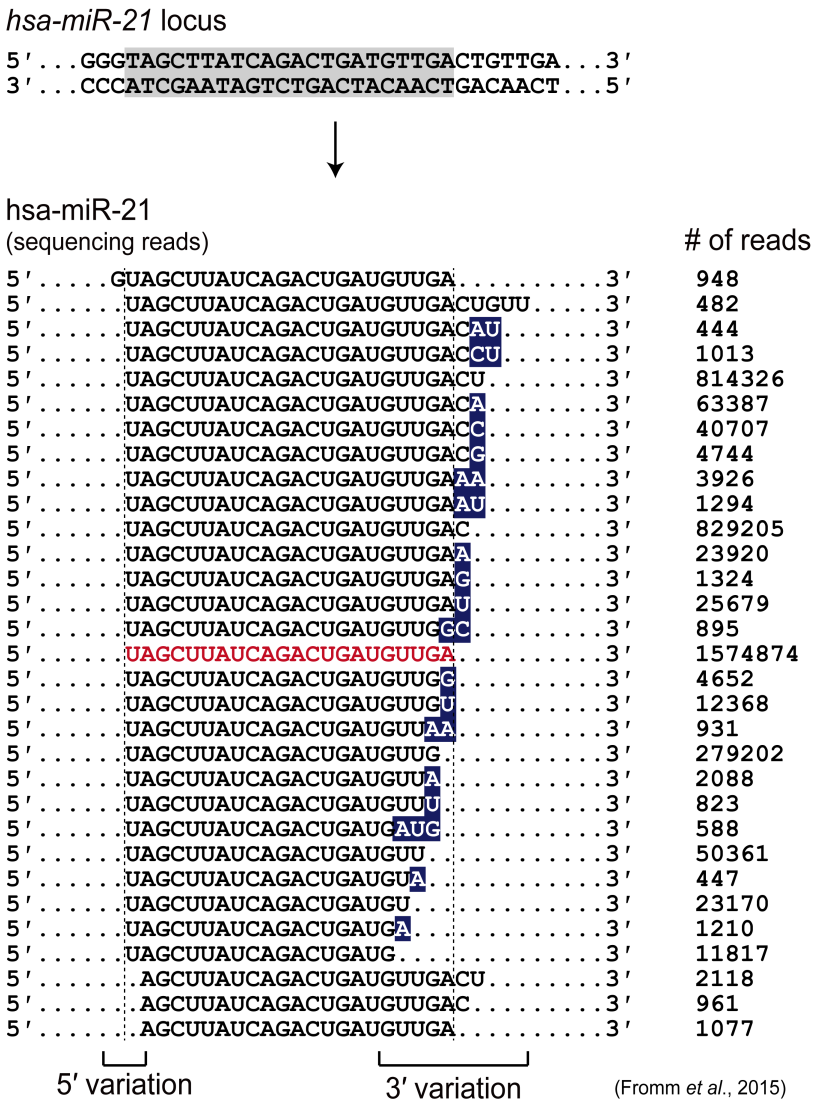
hsa-miR-21 locus
5′...GGGTAGCTTATCAGACTGATGTTGACTGTTGA...3′
3′...CCCATCGAATAGTCTGACTACAACTGACAACT...5′
hsa-miR-21
(sequencing reads)
# of reads
5′.....GUAGCUUAUCAGACUGAUGUUGA.....3′ 948
5′.....UAGCUUAUCAGACUGAUGUUGACUGUU.....3′ 482
5′.....UAGCUUAUCAGACUGAUGUUGACAU.....3′ 444
5′.....UAGCUUAUCAGACUGAUGUUGACCU.....3′ 1013
5′.....UAGCUUAUCAGACUGAUGUUGACU.....3′ 814326
5′.....UAGCUUAUCAGACUGAUGUUGACA.....3′ 63387
5′.....UAGCUUAUCAGACUGAUGUUGACC.....3′ 40707
5′.....UAGCUUAUCAGACUGAUGUUGACG.....3′ 4744
5′.....UAGCUUAUCAGACUGAUGUUGAAA.....3′ 3926
5′.....UAGCUUAUCAGACUGAUGUUGAAU.....3′ 1294
5′.....UAGCUUAUCAGACUGAUGUUGAC.....3′ 829205
5′.....UAGCUUAUCAGACUGAUGUUGAA.....3′ 23920
5′.....UAGCUUAUCAGACUGAUGUUGAG.....3′ 1324
5′.....UAGCUUAUCAGACUGAUGUUGAU.....3′ 25679
5′.....UAGCUUAUCAGACUGAUGUUGGC.....3′ 895
5′.....UAGCUUAUCAGACUGAUGUUGA.....3′ 1574874
5′.....UAGCUUAUCAGACUGAUGUUGG.....3′ 4652
5′.....UAGCUUAUCAGACUGAUGUUGU.....3′ 12368
5′.....UAGCUUAUCAGACUGAUGUUAA.....3′ 931
5′.....UAGCUUAUCAGACUGAUGUUG.....3′ 279202
5′.....UAGCUUAUCAGACUGAUGUUA.....3′ 2088
5′.....UAGCUUAUCAGACUGAUGUUU.....3′ 823
5′.....UAGCUUAUCAGACUGAUGAUG.....3′ 588
5′.....UAGCUUAUCAGACUGAUGUU.....3′ 50361
5′.....UAGCUUAUCAGACUGAUGUA.....3′ 447
5′.....UAGCUUAUCAGACUGAUGU.....3′ 23170
5′.....UAGCUUAUCAGACUGAUGA.....3′ 1210
5′.....UAGCUUAUCAGACUGAUG.....3′ 11817
5′.....AGCUUAUCAGACUGAUGUUGACU.....3′ 2118
5′.....AGCUUAUCAGACUGAUGUUGAC.....3′ 961
5′.....AGCUUAUCAGACUGAUGUUGA.....3′ 1077
5′ variation
3′ variation
(Fromm *et al.*, 2015)

Figure 7. Post-processing enzymatic activities acting on the 3′ ends of miRNAs.

(A) Enzymatic activities diversifying the 3′ ends of miRNAs. TENTs elongate miRNAs by adding one of a few nucleotides, usually A or U, to their 3′ ends. In mammals, seven TENTs mediate miRNA tailing redundantly. Depending on the nucleotide specificity, they are classified as adenylyltransferases (TENT2, TENT4A, TENT4B, MTPAP) and uridylyltransferases (TUT1, TUT4, TUT7). Tailing occasionally alters the stability or regulatory activity of miRNAs. In addition to TENTs, 3′-to-5′ exoribonucleases also contribute to 3′ isomiR diversity.

(B) 3′-to-5′ exoribonucleases previously implicated in the metabolism of metazoan miRNAs. Note that although DIS3L2 trims the 3′ end of miR-27a/b during target RNA-directed miRNA degradation (TDMD), it is unclear whether the 3′ trimming directly destabilizes the miRNA (Haas et al., 2016).

A

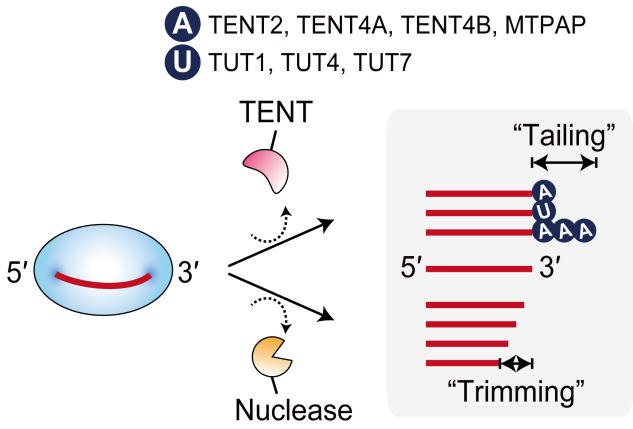

B

Enzyme	Substrate	Outcome	Reference
Nibbler	>1/4 of miRNAs	Maturation	Han *et al.*, 2011 Liu *et al.*, 2011
Exosome	Defective pre-miRNAs	Degradation	Liu *et al.*, 2014
	miR-382	Degradation	Bail *et al.*, 2010
DIS3L2	Oligo-uridylated pre-let-7	Degradation	Chang *et al.*, 2013
	miR-27a/b	Degradation (?)	Haas *et al.*, 2016
PNPT1	miR-221	Degradation	Das *et al.*, 2010
PARN	AGO2-cleaved pre-miR-451	Maturation	Yoda *et al.*, 2013
	Adenylated miR-21, miR-122	Degradation	Boele *et al.*, 2014 Katoh *et al.*, 2015

D. melanogaster
Mammals

Poly(A)-specific ribonuclease

The stability and translational efficiency of eukaryotic mRNAs critically depend on their two defining features: the m^7G cap at the 5′ end and the poly(A) tail at the 3′ end. Because 3′-to-5′ exoribonucleolytic degradation of the poly(A) tail often serves as the first and rate-limiting step in mRNA turnover (Parker and Song, 2004), the catalytic entities responsible for this process, known as “deadenylases”, have been subjected to intense scrutiny. The discovery of poly(A)-degrading activities in cell-free extracts dates back to the 1960s (Lazarus and Sporin, 1967), and intensified efforts to characterize them eventually led to the identification of more than ten deadenylases in vertebrates, including the PAN2-PAN3 and CCR4-NOT complexes and PARN (Goldstrohm and Wickens, 2008).

PARN was first identified and characterized as a 3′-to-5′ exoribonuclease activity present in HeLa nuclear extracts (Astrom et al., 1991; Astrom et al., 1992). The nuclease activity was hydrolytic, Mg^{2+}-dependent, and more importantly, was highly specific for a single-stranded stretch of adenosines: it efficiently degraded the poly(A) tail of an artificial mRNA substrate, leaving the mRNA body intact (Astrom et al., 1991; Astrom et al., 1992). Later a similar activity was identified in HeLa cytoplasmic extracts (Korner and Wahle, 1997; Ford et al., 1999; Gao et al., 2000), and extracts of calf thymus (Korner and Wahle, 1997; Martinez et al., 2000), *Xenopus laevis* oocytes (Korner et al., 1998; Copeland and Wormington, 2001), and mosquito cells (Opyrchal et al., 2005). Molecular cloning of human and *Xenopus* PARN revealed that they consist of 639 and 631 amino acids, respectively (now annotated as NP_002573.1 and NP_001081143.1 in NCBI RefSeq, respectively) (Korner et al., 1998; Martinez et al., 2000; Copeland and Wormington, 2001). PARN is ubiquitously expressed across multiple tissues and cell lines (Uhlen et al., 2010) and

shuttles between the nucleus and the cytoplasm (Yamashita et al., 2005). PARN orthologues are found in the genomes of almost all eukaryotic species, including vertebrates, insects, nematodes, and plants, but appear to be notably absent in *Drosophila melanogaster* and *Saccharomyces cerevisiae* (Parker and Song, 2004; Opyrchal et al., 2005; Goldstrohm and Wickens, 2008).

PARN belongs to the DEDD superfamily of 3′-to-5′ exoribonucleases, which are named after the characteristic catalytic core consisting of four acidic amino acids (Zuo and Deutscher, 2001). The catalytic residues of PARN are distributed in the nuclease domain (D28, E30, D292, and D382 in human PARN) (Ren et al., 2002; Ren et al., 2004), which is centrally interrupted by an RNA-binding domain known as the R3H domain (Wu et al., 2005), and followed by another RNA-binding domain, the RNA recognition motif (RRM) (Figure 8A) (Copeland and Wormington, 2001; Nilsson et al., 2007; Monecke et al., 2008; Nagata et al., 2008; Wu et al., 2009b). Based on its nuclease domain, PARN is further classified as a member of the CAF1 family of deadenylases, which includes CAF1a and CAF1b (one of the two catalytic subunits of the CCR4-NOT complex), PAN2 (the calaytic subunit of the PAN2-PAN3 complex), TOE1, and PNLDC1 in mammals (Virtanen et al., 2013). The R3H domain and the RRM differentially contribute to substrate binding and structural integrity of PARN (Wu et al., 2005; Liu et al., 2007; Zhang et al., 2007; He et al., 2013; He and Yan, 2014). The determinants of strong preference of PARN for A are thought to reside in the nuclease domain and the RRM (Wu et al., 2005; Nilsson et al., 2007; Henriksson et al., 2010). Importantly, the RRM confers the feature that is unique to PARN among the CAF1 family of deadenylases: through its RRM, PARN recognizes and strongly interacts with the m^7G cap, (Nilsson et al., 2007; Monecke et al., 2008; Nagata et al., 2008; Wu et al., 2009b), which increases the processivity

of the enzyme in an allosteric fashion (Martinez et al., 2001; Wu et al., 2005; Liu et al., 2009). The nuclease domain and RNA-binding domains are highly conserved among PARN orthologues (Figure 8A) (Korner et al., 1998; Martinez et al., 2000; Copeland and Wormington, 2001). On the other hand, the C-terminal region of PARN is less well conserved (Figure 8A) (Copeland and Wormington, 2001), unstructured (He et al., 2009), and appears to serve as a regulatory platform for the protein, for example, by mediating nuclear localization (Copeland and Wormington, 2001; Martinez et al., 2001) and protein-protein interactions (Balatsos et al., 2006; Cevher et al., 2010), and/or by undergoing inducible post-translational modifications (Reinhardt et al., 2010). PARN forms a homodimer (Martinez et al., 2000; Wu et al., 2005; Wu et al., 2009b) and dimerization is essential for its activity (Wu et al., 2005) (Figure 8B).

Given its preference for the m^7G cap and poly(A), PARN appears to be best suited for the role in mRNA metabolism. As it turns out, PARN does indeed degrade the poly(A) tails of mRNAs in several physiological contexts, including the early development of *Xenopus* oocytes (Korner et al., 1998; Copeland and Wormington, 2001; Kim and Richter, 2006), nonsense-mediated decay (Lejeune et al., 2003), miRNA-mediated regulation (Zhang et al., 2015), UV-induced stress responses (Cevher et al., 2010; Reinhardt et al., 2010; Devany et al., 2013), synaptic plasticity (Udagawa et al., 2012), cell cycle progression (Zhang and Yan, 2015), and viral defense (Zhu et al., 2011). PARN-mediated mRNA deadenylation controls cell motility in mouse myoblasts (Lee et al., 2012), and its dysregulation has been observed in some types of human cancers (Zhang and Yan, 2015; Miller and Gomez-Cambronero, 2017). Several *trans*-acting factors are known to promote PARN-mediated deadenylation of mRNAs containing AU-rich elements (AREs) in their 3′-

UTRs (Figure 9A) (Lin et al., 2007), including Tristetraprolin (TTP) (Lai et al., 2003), KSRP (Gherzi et al., 2004), and CUGBP1 (Moraes et al., 2006). Although these findings suggest a role of PARN in mRNA metabolism, it was controversial until recently whether PARN is the enzyme responsible for the default deadenylation and decay of mRNAs (Yamashita et al., 2005), perhaps because there was no technique available to accurately measure the poly(A) tail length of mRNAs on a global scale.

Unexpectedly, the functional repertoire of PARN began to be expanded beyond mRNA metabolism in the early 2010, when Berndt and colleagues reported that the maturation of a specific class of snoRNAs, known as H/ACA box snoRNAs, requires PARN (Figure 9B) (Berndt et al., 2012). In mammals, the precursors of these RNAs contain additional nucleotides at their 3′ ends that are first trimmed by exoribonuclease(s) to the size of ~5-8 nt (Kiss and Filipowicz, 1993; Tycowski et al., 1993; Kiss and Filipowicz, 1995). TENT4B then adds oligo(A) tails to these intermediate species, which are preferentially recognized by PARN (Berndt et al., 2012; Son et al., 2018). PARN not only removes the oligo(A) tails but also tailors the 3′ ends of pre-snoRNAs to the mature species by trimming the remaining 3′ extension (Berndt et al., 2012; Son et al., 2018). In the absence of PARN, H/ACA box snoRNAs become significantly destabilized (Berndt et al., 2012; Son et al., 2018), because oligo(A) tails in nuclear RNAs tend to recruit the exosome complex (Houseley et al., 2006; Vanacova and Stefl, 2007). Similar maturation modules are utilized by various non-coding RNAs, including scaRNAs (Son et al., 2018), TERC (Dhanraj et al., 2015; Moon et al., 2015; Nguyen et al., 2015a; Tseng et al., 2015; Boyraz et al., 2016; Shukla et al., 2016; Son et al., 2018), 18S rRNAs (Ishikawa et al., 2017; Montellese et al., 2017), and Y RNAs (Shukla and Parker, 2017).

Accumulating evidence challenges the notion that the primary role of PARN is in mRNA metabolism. Technical advances have made it possible to determine the poly(A) tail length of mRNAs on a transcriptome-wide scale (Chang et al., 2014; Subtelny et al., 2014), and recent studies reveal that downregulation of PARN causes no significant change in the poly(A) tail length or steady-state abundance of mRNAs (Moon et al., 2015; Son et al., 2018; Yi et al., 2018). In summary, all these observations suggest that PARN may primarily function in the maturation of non-coding RNAs, with a minor or context-dependent role in mRNA metabolism (Figure 9).

The aim and scope of this dissertation

The 3′ ends of miRNAs are extensively modified by several enzymatic activities, such as tailing and trimming. Although the enzymology and extent of miRNA tailing is well established by virtue of several transcriptome-wide studies, little is known about the catalytic entities that pervasively shorten miRNAs and the molecular consequences of such shortening, especially in vertebrates. Existing studies suggest a role of PARN in miRNA metabolism (Figure 9C). However, they were focused on a few specific miRNAs, including miR-451 whose biogenesis is quite idiosyncratic, raising the question as to whether miRNAs generally serve as substrates for PARN. In this study, I rigorously evaluate the contribution of PARN to the biogenesis and 3′ end formation of a model miRNA, miR-362-5p, using various biochemical and cell-based assays. By generating *PARN* KO cells and characterizing their miRNAome by deep sequencing, I extend my findings to many canonical miRNAs and provide a comprehensive picture of the roles of PARN in miRNA metabolism.

Figure 8. Structure and evolutionary conservation of PARN.

(A) Domain architecture and evolutionary conservation of PARN. The domains of human PARN (NP_002573.1) are shown at the top, with the four catalytic residues indicated. The conservation plot is presented below. To calculate the conservation score at each residue, 150 non-redundant, phylogenetically distributed protein sequences of PARN were collected and aligned at the ConSurf Server (http://consurf.tau.ac.il/2016/) with default options (Ashkenazy et al., 2016). The resulting multiple sequence alignment was subjected to conservation analysis at the Scorecons Server (https://www.ebi.ac.uk/thornton-srv/databases/cgi-bin/valdar/scorecons_server.pl/) with the scoring method of "valdar01" (Valdar, 2002).

(B) Model of homodimeric PARN. A proposed structural model of a PARN dimer is presented on the left side (Wu et al., 2009b). The structures of human PARN (residues 1-430) (PDB ID: 2A1S) (Wu et al., 2005) and mouse PARN (residues 1-510) (Wu et al., 2009b) were aligned using the PyMOL software (https://www.pymol.org/). Domains are colored as in (A). A model for the recognition and subsequent deadenylation of mRNA substrates by the PARN dimer is shown on the right side. The illustration was adopted from a previous report with minor modifications (Virtanen et al., 2013).

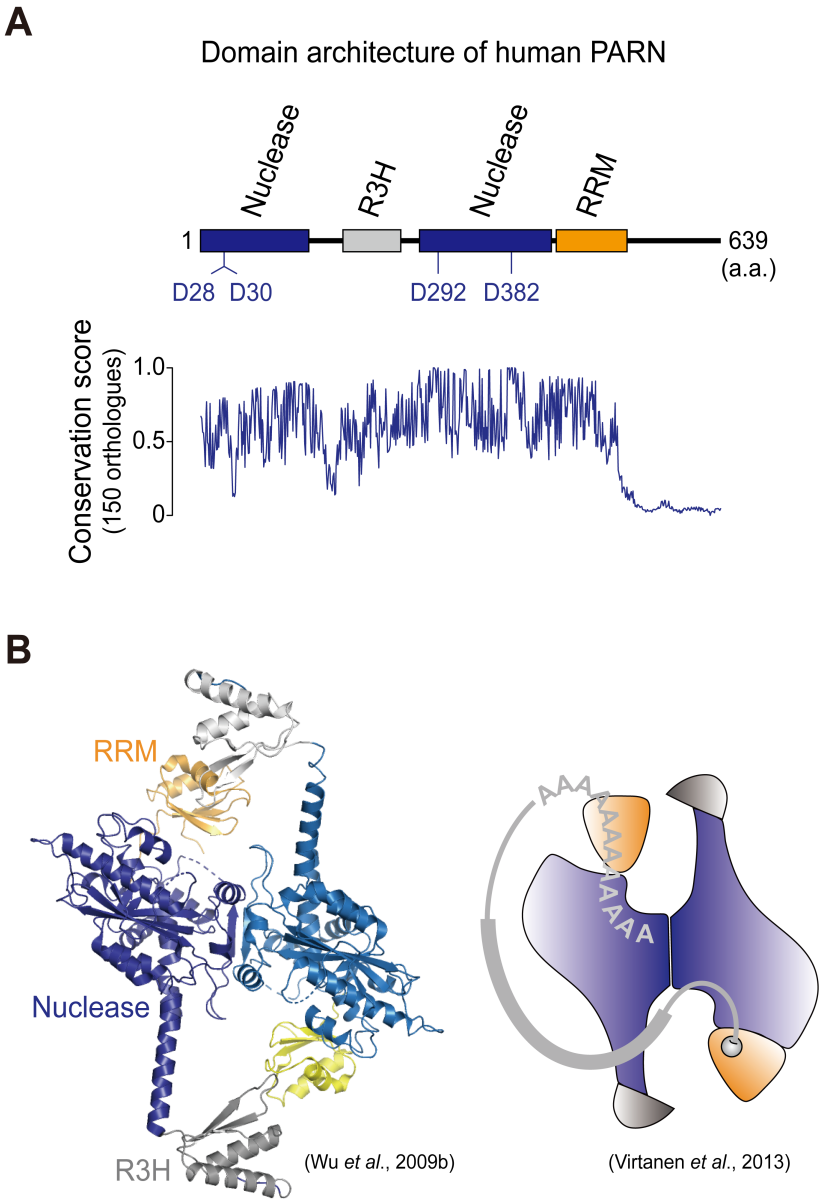
A
Domain architecture of human PARN
Nuclease
R3H
Nuclease
RRM
1
639
(a.a.)
D28 D30
D292 D382
Conservation score
(150 orthologues)
1.0
0.5
0
B
RRM
Nuclease
R3H
(Wu et al., 2009b)
AAAA
AAAA
AAAA
(Virtanen et al., 2013)

Figure 9. The known roles of PARN in RNA metabolism.

(A) PARN degrades the poly(A) tails of mRNAs in several physiological contexts, leading to their destabilization. Note that PARN interacts with both the m^7G cap and the poly(A) tail. Several *trans*-acting factors are known to bind AU-rich elements in the 3′-UTR of mRNAs and recruit PARN.

(B) PARN finalizes the maturation of non-coding RNAs. The precursors of many nuclear non-coding RNAs, including snoRNAs, scaRNAs, TERC, and Y RNAs, contain 3′ genomic extensions that are initially trimmed by exoribonucleases to ~5-8 nt. TENT4B adds oligo(A) tails to these intermediate species, which are preferentially recognized by PARN. PARN not only removes the oligo(A) tails but also trims the residual extension, finalizing the maturation. Because oligo(A) tails in nuclear RNAs serve as a mark for exosome-mediated destruction, PARN-mediated deadenylation and 3′ end formation is pivotal for maintaining the stability of nuclear non-coding RNAs.

(C) PARN is associated with the metabolism of a few miRNAs, including the maturation of miR-451 (Figure 5) and the degradation of adenylated miR-21 and miR-122. However, it is unclear whether miRNAs generally serve as substrates for PARN.

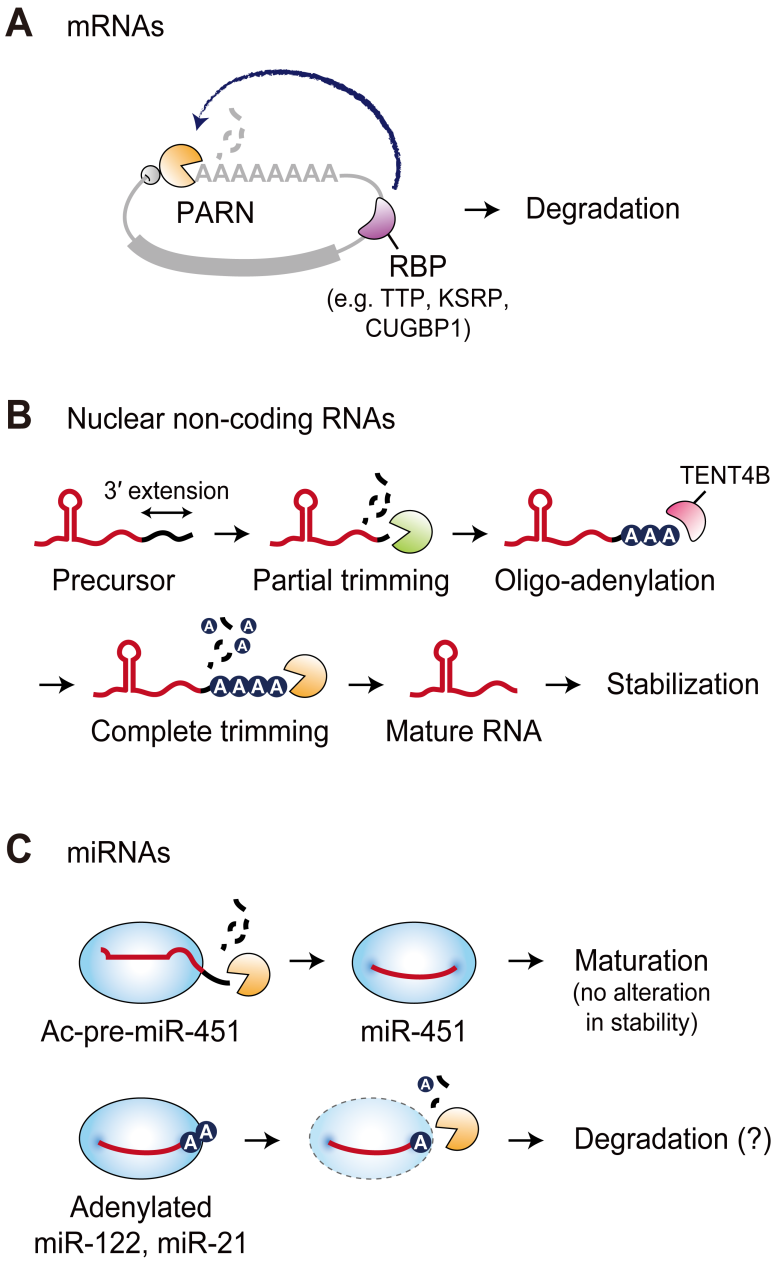
A
mRNAs
AAAAAAAA
PARN
Degradation
RBP
(e.g. TTP, KSRP,
CUGBP1)
B
Nuclear non-coding RNAs
3′ extension
TENT4B
Precursor
Partial trimming
Oligo-adenylation
Complete trimming
Mature RNA
Stabilization
C
miRNAs
Ac-pre-miR-451
miR-451
Maturation
(no alteration
in stability)
Adenylated
miR-122, miR-21
Degradation (?)

MATERIALS AND METHODS

Plasmids

To generate pri-miRNA expression plasmids, 300 bp fragments containing the pre-miRNA and genomic sequences on each side of the hairpin (~110-120 bp) were amplified from HeLa S3 or MEF genomic DNA and subcloned into the NheI/XbaI sites of pcDNA3.1(+) (Thermo Fisher Scientific). For high-level protein expression in mammalian cells, pDY-CMV, a modified mammalian expression vector, was generated. To this end, a ~1.5-kb fragment containing the promoter and downstream 5′-UTR of the human CMV immediately early gene was amplified from pCK-DROSHA-FLAG[1] and overlap-extended by PCR to the BGH polyadenylation signal obtained from pcDNA3.1(+). The resulting expression unit was then ligated to the minimal backbone of pcDNA3.1(+), consisting of the pUC origin and *bla* expression cassette, to generate pDY-CMV. The coding sequences of candidate genes were amplified from existing plasmids or HeLa S3 cDNA and subcloned into pDY-CMV, using the Overlap Cloner DNA Cloning Kit (Elpis Biotech). Of note, pDY-CMV lacks traditional multiple cloning sites, and therefore, subcloning into this vector should be performed with methods that do not rely on the use of restriction sites, such as homology-directed recombination. For miRNA reporters, the miRNA target site of interest was inserted into the XhoI/NotI sites of psiCHECK-2 (Promega). For expression of recombinant proteins in *Escherichia coli*, pHis-GST, a modified bacterial expression vector, was constructed by replacing the coding sequence of

[1] This plasmid is a generous gift from Dr. V. Narry Kim.

MBP present in pMAL-c2x (New England Biolabs) by that of hexahistidine and GST. The coding sequence of GST was amplified from pGEX-6p-1 (GE Healthcare). The coding sequence of full-length human PARN (wild-type or D28A) or the human TNRC6B peptide (599-683; designated T6B) was subcloned into pHis-GST using the Overlap Cloner DNA Cloning Kit. Site-directed mutagenesis was carried out by standard inverse PCR with Phusion High-Fidelity DNA Polymerase (New England Biolabs). All plasmid constructs were verified by Sanger sequencing. The sequences of oligonucleotides used for cloning are listed in Table 1.

Cell culture and transfection

HeLa S3 (and its *PARN* knockout derivatives), HEK293T, A549, Huh7, MCF7, BE(2)-C, MDA-MB-231, and SW480 cells were cultured in DMEM (Welgene) supplemented with 9%(v/v) FBS (Welgene). NIH-3T3 cells were grown in DMEM with 9%(v/v) BCS (Welgene). Mouse mesenchymal stem cells (mMCS) were cultivated in MEMα (Welgene) containing 9%(v/v) FBS. For RNAi-mediated gene silencing, cells were transfected with siRNAs (Bioneer) at a concentration of ~18 nM twice over the course of 72-hr incubation. For transfection of miRNA duplexes, synthetic 5p and 3p RNA strands (Bioneer) were mixed at an equimolar ratio and annealed immediately before transfection by boiling the mixture at 90°C for 3 min then slowly cooling it down to 25°C at a rate of -1°C per 4 min. The resulting duplexes were introduced at a concentration of ~0.1 nM and the cells were harvested 48 hr after the transfection. For plasmid transfection, cells were co-transfected with 1 μg of pri-miRNA expression plasmid and the indicated amount of effector plasmid per 35-mm dish and incubated for 48 hr. For miRNA targeting studies, cells pre-treated with siRNAs for 72 hr were transfected with ~100 nM anti-miRs (Bioneer)

(and 50 ng of empty reporter or miRNA targeting reporter per well of a 24-well plate in the case of luciferase reporter assays) and incubated further for 24 hr. All transfection procedures were performed with Lipofectamine 2000 (Thermo Fisher Scientific) according to the manufacturer's instructions. The sequences of oligonucleotides used for transfection are listed in Table 1.

CRISPR/Cas9-mediated gene knockout[2]

Gene knockout in mammalian cells was performed as described elsewhere (Ran et al., 2013), with minor modifications. Briefly, a single guide RNA was designed to target the second exon of the human *PARN* gene using the CRISPR Design Tool (http://crispr.mit.edu/). A pair of complementary DNA oligonucleotides matching the guide sequence was annealed and inserted into the BbsI site of pSpCas9(BB)-2A-Puro (Addgene; ID 48139). The resulting gene-editing construct was introduced into HeLa S3 cells by Lipofectamine 2000. Forty eight hours after the transfection, puromycin (Thermo Fisher Scientific) was added to the medium at a concentration of 3 μg/ml and incubated for 3 days. The surviving transfectants were trypsinized, freshly seeded into 100-mm dishes at low densities (~100-1,000 cells per 100-mm dish), and allowed to form colonies, which were individually transferred to the wells of 24-well plates and screened for the absence of the PARN protein by western blotting. For the candidate clones, the genomic region flanking the targeted locus was PCR-amplified, cloned into TA Cloning Vector (RBC Bioscience), and subjected to Sanger sequencing. The clones containing the frame-shifting mutations at the targeted locus were chosen as genuine knockouts and used in study. The sequences

[2] This experiment was carried out in collaboration with Dr. June Hyun Park.

of oligonucleotides used for genotyping are listed in Table 1.

In vitro DROSHA processing assay

To generate body-labeled pri-miRNA substrates, *in vitro* transcription was performed using in-house T7 RNA polymerase in the presence of [α-^{32}P]UTP (PerkinElmer) at 37°C for 3 hr. The resulting run-off transcripts were gel-purified on a 6% urea-polyacrylamide gel before the use in *in vitro* DROSHA processing. To prepare the Microprocessor, HEK293T cells grown on a 100-mm dish were co-transfected with 8 μg of pCK-DROSHA-FLAG and 2 μg of pCK-V5-DGCR8[3] and incubated for 2 days. Approximately one quarter of the cells from a single 100-mm dish were used for immunoprecipitation. The cells were dispersed in 300 μl of ice-cold Buffer T100 [20 mM Tris-HCl at pH 7.4, 100 mM KCl, 0.2 mM EDTA, 10%(v/v) glycerol, and 1x cOmplete Protease Inhibitor Cocktail (Roche Life Science)], sonicated on ice, and spun at 15,000 rpm at 4°C for 10 min. The resulting supernatant was incubated with 5 μl of ANTI-FLAG M2 Affinity Gel (Sigma) at 4°C for 2 hr with constant rotation. The beads were washed with 1 ml of Buffer T100 four times and the volume of immunoprecipitate was adjusted to 100 μl with Buffer T100. *In vitro* DROSHA processing was performed in 10-μl reactions containing ~10 nM pri-miRNA substrate, 50%(v/v) FLAG-immunoprecipitate (FLAG-IP), and 6.4 mM $Mg(OAc)_2$ with incubation at 37°C for 30 min. The reactions were quenched by treating with Proteinase K (Roche Life Science) at 60°C for 20 min and purified by phenol extraction and ethanol precipitation. The reaction products were resolved on a 8% urea-polyacrylamide gel and analyzed by phosphorimaging with the Typhoon FLA

[3] This plasmid is a generous gift from Dr. V. Narry Kim.

7000 laser scanner (GE Healthcare).

***In vitro* DICER processing assay**

The exact end structures of pre-miRNAs are critical for DICER processing (Park et al., 2011). Because *in vitro* transcription using phage RNA polymerases leaves a degree of heterogeneity at both ends of the run-off transcript (Milligan et al., 1987; Krupp, 1988), self-cleaving ribozymes were utilized to generate pre-miRNAs with homogenous ends (Schurer et al., 2002; Walker et al., 2003). To this end, the pre-miRNA sequence of interest was fused to a hammerhead (HH) ribozyme and a hepatitis delta virus (HDV) ribozyme at the 5′ and 3′ end, respectively, through two rounds of PCR. The primary structure of the resulting transcription template was then expected to be 5′-[T7 promoter][Reverse complement of the first 11 nt of the pre-miRNA][HH][Pre-miRNA][HDV]-3′. The nucleotide sequences of the HH and HDV ribozymes used here were 5′-CTGATGAGTCCGTGAGGACGAAACGGTACCCGGTACCGTC-3′ and 5′-GGGTCGGCATGGCATCTCCACCTCCTCGCGGTCCGACCTGGGCATCCGAGGAAACTCGGATGGCTAAGGGAGAGCCAACGAGTAGTGGGATCCGGG-3′, respectively. The sequences of oligonucleotides used for ribozyme construction are listed in Table 1. The templates were transcribed *in vitro* using T7 RNA polymerase at 37°C for 1-3 hr. Following *in vitro* transcription, the reactions were further subjected to 3 cycles of incubation at 72°C for 1 min, at 65°C for 5 min, then at 37°C for 10 min to ensure ribozyme cleavage. The released pre-miRNA fragments were gel-purified on a 6% urea-polyacrylamide gel. To heal 2′,3′-cyclic phosphates, an undesirable remnant of ribozyme-catalyzed cleavage, the pre-miRNAs were treated with T4 Polynucleotide Kinase (Takara) in home-made Dephosphorylation Buffer (100 mM MES-NaOH at pH 5.5, 10 mM $MgCl_2$, 10 mM βME, and 300 mM NaCl) at 37°C for 6 hr and

purified by phenol extraction and ethanol precipitation. The pre-miRNAs were then phosphorylated at the 5′ ends by standard kinasing reactions using T4 Polynucleotide Kinase, gel-purified on a 6% urea-polyacrylamide gel, and used as substrates for *in vitro* DICER processing. For body-labeling of substrates, the initial transcription reactions were supplemented with [α-^{32}P]UTP. For 5′-labeling of substrates, [γ-^{32}P]ATP (PerkinElmer) was used instead of cold ATP in the final kinasing reactions.

To prepare the DICER complex, HEK293T cells grown on a 100-mm dish were co-transfected with 6 μg of pCK-FLAG-DICER1[4] and 3 μg of pCK-myc-TRBP and incubated for 2 days. Approximately one quarter of the cells from a single 100-mm dish were used for immunoprecipitation. The cells were lysed in 300 μl of ice-cold Hypotonic Lysis Buffer [10 mM Tris-HCl at pH 7.4, 10 mM KCl, 1.5 mM $MgCl_2$, 0.1%(v/v) NP-40, and 1x cOmplete Protease Inhibitor Cocktail] on ice for 10 min and spun at 15,000 rpm at 4°C for 10 min. The resulting supernatant was incubated with 5 μl of ANTI-FLAG M2 Affinity Gel at 4°C for 2 hr with constant rotation. The beads were washed with 1 ml of Buffer T2000 [20 mM Tris-HCl at pH 7.4, 2 M KCl, 0.2 mM EDTA, and 10%(v/v) glycerol] twice, then with 1 ml of Buffer T100 four times. After washing, the volume of immunoprecipitate was adjusted to 100 μl with Buffer T100. *In vitro* DICER processing was carried out in 10-μl reactions containing ~10 nM pre-miRNA substrate, 50%(v/v) FLAG-IP, and 2 mM $Mg(OAc)_2$ with incubation at 37°C for the indicated time period. The reactions were quenched and purified essentially as described in *in vitro* DROSHA processing assay. The reaction products were resolved on a 15% urea-polyacrylamide gel and analyzed by phosphorimaging (for the reactions performed with radiolabeled substrates) or

[4] This plasmid is a generous gift from Dr. V. Narry Kim.

small RNA northern blotting (for the reactions with cold substrates).

Directional cloning of RNA fragments

Adaptors for small-scale directional cloning were designed such that each contains a central BmeT110I site. The 3′ adaptor was pre-adenylated using an established protocol (Song et al., 2015). Briefly, 1 nmole of 5′-phosphorylated 3′ adaptor was incubated with 300 U of T4 RNA Ligase (Ambion) in the presence of 25%(v/v) PEG 8000 (New England Biolabs) in a 500-μl reaction at 37°C for 2 hr. The adenylated adaptor was gel-purified on a 20% urea-polyacrylamide gel. The RNA fragments to be characterized were gel-purified and ligated to the pre-adenylated 3′ adaptor using T4 RNA Ligase 2, truncated (New England Biolabs) in the presence of 25%(v/v) PEG 8000 at 16°C overnight. The ligation reaction was separated on a 15% urea-polyacrylamide gel and the ligated RNA was gel-purified. The purified RNA was then ligated to the 5′ adaptor using T4 RNA Ligase in the presence of 25%(v/v) PEG 8000 at 22°C overnight. The RNA ligated to both adaptors was reverse transcribed using PrimeScript Reverse Transcriptase (Takara) and amplified by Phusion High-Fidelity DNA Polymerase. The PCR product was digested with BmeT110I (Takara) and treated with T4 DNA Ligase (Takara) to form concatemers, which were subsequently cloned into the TA Cloning Vector and sequenced. The sequences of adaptors and primers used for directional cloning are listed in Table 1.

***In vitro* trimming assay**

The strand of interest was 5′-radiolabeled and annealed to the cold opposite strand to form a miRNA duplex. To prepare AGO proteins, HEK293T cells grown on a 100-mm dish were transfected with 9 μg of pDY-CMV-AGO and incubated for 2 days.

Approximately one-eighth of the cells were lysed in 25 µl of ice-cold Hypotonic Lysis Buffer on ice for 10 min and spun at 15,000 rpm at 4°C for 10 min to obtain a cytoplasmic lysate. Small RNA loading was performed in 50-µl reactions containing ~20 nM miRNA duplex, 50%(v/v) AGO cytoplasmic lysate (~18 µg/µl), 50 mM KCl, 1 mM ATP, 25 mM creatine phosphate, and 2 mM $Mg(OAc)_2$ with incubation at 25°C for 1 hr. The reactions were then incubated with 5 µl of ANTI-FLAG M2 Affinity Gel at 4°C for 2 hr with constant rotation. The beads were washed with 1 ml of Buffer T2000 twice, then with 1 ml of Buffer T100 four times. After washing, the volume of immunoprecipitate was adjusted to 50 µl with Buffer T100. To prepare HeLa S3 whole cell lysate, cells grown on a single 100-mm dish were dispersed in 250 µl of ice-cold Hypotonic Lysis Buffer, sonicated, and spun at 15,000 rpm at 4°C for 10 min. *In vitro* trimming was carried out in 10-µl reactions containing 50%(v/v) FLAG-IP, 40%(v/v) HeLa S3 whole cell lysate (~18 µg/µl), and 2 mM $Mg(OAc)_2$ at 37°C for the indicated time period. For trimming assays with recombinant proteins, His-GST-PARN (wild-type or D28A) was used at a final concentration of ~700 nM instead of whole cell lysate. The reactions were quenched and purified essentially as described above. The reaction products were resolved on a 15% urea-polyacrylamide gel and analyzed by phosphorimaging. Densitometric calculation of the fraction of trimmed species was carried out with Multi Gauge V3.0 (Fujifilm).

Western blot analysis

Cells were dispersed in ice-cold Hypotonic Lysis Buffer, lysed by sonication, and spun at 15,000 rpm at 4°C for 10 min. Thirty to fifty micrograms of the cleared lysate was separated on a 10% SDS-polyacrylamide gel and electrotransferred to an Immobilon-P PVDF membrane (EMD Millipore). The primary antibodies used in

this study include rabbit anti-PARN (Abcam, ab27778), rabbit anti-FLAG (Sigma, F7425), mouse anti-c-myc (9E10; Santa Cruz Biotechnology, sc-40), rabbit anti-α-tubulin (Abcam, ab52866), and mouse anti-β-actin (Abcam, ab8224). The blots probed with primary antibodies were incubated with HRP-conjugated goat anti-rabbit IgG(H+L) or donkey anti-mouse IgG(H+L) (Jackson Laboratories) and treated with PicoEPD Western Reagent (Elpis Biotech) to develop chemiluminescent signals, which were subsequently exposed to and imaged on X-ray films (Agfa).

Expression and purification of recombinant proteins

The bacterial expression plasmids were introduced into Rosetta2(DE3) *E. coli* cells (EMD Millipore), which were grown at 37°C to an OD_{600} of ~0.7 and treated with 0.5 mM IPTG at 16°C overnight to induce protein expression. His-GST (from empty pHis-GST) and His-GST-T6B were purified by immobilized metal ion affinity chromatography. Briefly, 500 ml of bacterial culture was harvested, resuspended in 15 ml of ice-cold Buffer P500 (20 mM Tris-HCl at pH 7.4, 500 mM NaCl, and 2 mM βME), and sonicated. The crude lysate was cleared by centrifugation at 15,000 rpm at 4°C for 20 min and the resulting supernatant was filtered through a 0.22 μm polyethersulfone Millex-GP Syringe Filter Unit (EMD Millipore). The cleared lysate was applied to a HisTrap HP column (GE Healthcare). The column was washed with 20 ml of Buffer P500/I50 (20 mM Tris-HCl at pH 7.4, 500 mM NaCl, 2 mM βME, and 50 mM imidazole) and the immobilized protein was eluted with 5 ml of Buffer P250/I500 (20 mM Tris-HCl at pH 7.4, 250 mM NaCl, 2 mM βME, and 500 mM imidazole). The eluate was loaded into the SnakeSkin Dialysis Tubing (10 kDa cut-off; Thermo Fisher Scientific) and dialyzed against 2 L of Storage Buffer I [1x PBS, 20%(v/v) glycerol, and 1 mM DTT] at 4°C overnight. His-GST-PARN (wild-type or

D28A) was batch-purified using GST-Bind Agarose Resin (Elpis Biotech). To this end, the bacterial pellet was resuspended in ice-cold Buffer T500 [20 mM Tris-HCl at pH 7.4, 500 mM KCl, 0.2 mM EDTA, and 10%(v/v) glycerol], and lysed and cleared as described above. The cleared lysate was supplemented with Triton X-100 at a final concentration of 10%(v/v) and incubated with the resin (1 ml per 500 ml culture) at 4°C for 1 hr with constant rotation. The resin was washed with 10 ml of Buffer T500 three times and the bound protein was eluted with 5 ml of GST Elution Buffer (100 mM Tris-HCl at pH 7.4, 100 mM KCl, 1 mM DTT, and 10 mM reduced glutathione). The eluate was dialyzed against 2 L of Storage Buffer II [20 mM Tris-HCl at pH 7.4, 100 mM KCl, 0.2 mM EDTA, 20%(v/v) glycerol, and 1 mM DTT] at 4°C overnight. The concentration of purified protein was determined by Bradford assay (Protein Assay Dye Reagent Concentrate; Bio-Rad) or by densitometric analysis in parallel with serial dilutions of BSA on a SDS-polyacrylamide gel. The purified protein was distributed into single-use aliquots, snap-cooled with liquid nitrogen, and stored at -80°C.

Small RNA northern blot analysis and primer extension assay

Total RNA was prepared using Tri Reagent (Thermo Fisher Scientific). For small RNA northern blotting, ~5-50 μg of total RNA was mixed with an aqual volume of home-made 2x Formamide Loading Buffer [95%(v/v) formamide, 25 mM EDTA, 0.1%(w/v) SDS, 0.05%(w/v) bromophenol blue, and 0.05%(w/v) xylene cyanol], denatured at 95°C for 5 min, and separated on a 12.5% urea-polyacrylamide gel. The resulting size-fractionated RNA was electrotransferred to a Hybond N+ membrane (GE Healthcare) and fixed by UV crosslinking (0.12 J). Pre-hybridization and hybridization of northern blots were performed with 10 ml of PerfectHyb Plus

Hybridization Buffer (Sigma). To prepare regular hybridization probes, DNA oligonucleotides complementary to the miRNA sequences were 5′-radiolabeled using T4 Polynucleotide Kinase and purified by ethanol precipitation. Regular probes were added to the hybridization buffer and incubated at 42°C overnight. To prepare high-specific-activity probes to detect miRNAs expressed at low levels, both the 5′ and 3′ ends of the probe were radiolabeled. To this end, a DNA oligonucleotide was designed such that a small extension (5′-ACCCGAGG-3′) was added to the 3′ end of the regular probe sequence. The oligonucleotide was 5′-radiolabeled and gel-purified on a 15% urea-polyacrylamide gel to remove unincorporated [γ-^{32}P]ATP. One picomole of the resulting 5′-labaled probe was annealed to 25 pmoles of the universal template oligonucleotide, 5′-TTTTTTTTTTTTCCTCGGGT-NH_2 3′, in a 5-μl reaction. The annealing mixture was incubated with ~6.7-20 pmoles of [α-^{32}P]dATP (PerkinElmer) and 5 U Klenow Fragment, exo- (Elpis Biotech) in a 20-μl reaction at 25°C for 1 hr and purified by ethanol precipitation. The amount of [α-^{32}P]dATP to be added was determined empirically based on the abundance of the miRNA to be examined. High-specific-activity probes were added to the hybridization buffer and incubated at 42°C for 6 hr. Upon completion of hybridization, the blots were washed twice with 25 ml of Low-Stringency Wash Buffer [2x SSC and 0.1%(w/v) SDS] for 5 min twice, and then with 25 ml of High-Stringency Wash Buffer [0.5x SSC and 0.1%(w/v) SDS] for 20 min twice. After washing, the radioactive signals on the blots were analyzed by phosphorimaging. Densitometric analysis of miRNA isoforms was carried out with Multi Gauge v3.0. For primer extension of miR-362-5p, 1 pmole of the 5′-labeled DNA oligonucleotide complementary to nucleotides 5-22 of miR-362-5p was mixed with 5-10 μg of total RNA, denatured at 65°C for 5 min, and annealed at 50°C for 20 min in 10-μl reactions. Reverse transcription was performed in 20-μl

reactions with PrimeScript Reverse Transcriptase at 42°C for 30 min. The reactions were quenched at 70°C for 15 min and purified by ethanol precipitation. The reaction products were separated on a 15% urea-polyacrylamide gel and analyzed by phosphorimaging. The sequences of oligonucleotides used for northern blotting and primer extension are listed in Table 1.

Small RNA sequencing and analysis[5]

The TruSeq Small RNA Library Preparation Kit (Illumina) was used to prepare small RNA sequencing libraries, with minor modifications. Total RNA isolated with Tri Reagent was further enriched for small RNA using the mirVana miRNA Isolation Kit (Thermo Fisher Scientific). Five micrograms of small RNA was fractionated on a 15% urea-polyacrylamide gel, and ~18-30 nt RNA was gel-purified and ligated to the TruSeq 3′ adaptor with T4 RNA Ligase 2, truncated. The ligation reaction was separated on a 15% urea-polyacrylamide gel, ~35-52 nt RNA was gel-purified, and ligated the TruSeq 5′ adaptor using T4 RNA Ligase. The ligated RNA was reverse transcribed with SuperScript III Reverse Transcriptase (Thermo Fisher Scientific), PCR-amplified with Phusion High-Fidelity DNA Polymerase, and sequenced on the HiSeq 2500 platform (Illumina). For sequencing data analysis, adaptor sequences were trimmed using the cutadapt tool (Martin, 2011) and reads shorter than 18 nt were discarded. After merging technical replicates, structural RNAs were filtered out by mapping onto the human tRNA and rRNA sequences with BWA (version 0.6.2) (Li and Durbin, 2009). The resulting preprocessed reads were locally aligned to

[5] Sequencing library preparation and data analysis were carried out in collaboration with Dr. June Hyun Park and Dr. Daechan Park, respectively.

human miRBase 21 using BOWTIE2 (version 2.2.6) with the following parameters: -D 50 -R 5 -N 0 -L 10 -i C,1,0 --score-min=C,32,0 (Langmead and Salzberg, 2012). The reads that included soft-clip (S) at the 3′ end in the CIGAR string were defined as prefix-matching miRNA reads, whereas those consisting of only M in the CIGAR were considered as genome-matching miRNA reads. To explore the role of PARN as a miRNA de-tailor, the non-genome-matching nucleotide sequences were extracted from prefix-matching reads using regular expression based on the parsed CIGAR strings. Finally, read coverages were calculated for 5p and 3p strands, respectively, using the mirUtils package (version 1.0.0-r27). The small RNA sequencing data generated in this study were submitted to the Gene Expression Omnibus (GEO; http://www.ncbi.nlm.nih.gov/geo/) under the accession number GSE121466.

AGO protein affinity purification by peptides (AGO-APP)

AGO-APP was performed as described previously (Hauptmann et al., 2015), with minor modifications. Briefly, ~1 mg of His-GST or His-GST-T6B was incubated with ~300 µl of GST-Bind Agarose Resin, which was pre-washed with 1x PBS, at 4°C for at least 1 hr with constant rotation. The beads were then washed with Buffer APP [50 mM Tris-HCl at pH 7.4, 150 mM NaCl, 5 mM EDTA, 0.1%(v/v) NP-40, 10%(v/v) glycerol, 1 mM DTT, and 1x cOmplete Protease Inhibitor Cocktail] to remove the unbound proteins. HeLa S3 whole cell lysate was prepared as described in *in vitro* trimming assay, with the exception that Buffer APP was used instead of Hypotonic Lysis Buffer. Cytoplasmic lysates of HEK293T cells overexpressing AGO proteins were prepared as in *in vitro* trimming assay and, prior to AGO-APP, mixed with an equal volume of 2x Buffer APP to adjust the salt concentration to ~150 mM. It is noted that salt concentrations as low as that in the Hypotonic Lysis

Buffer strongly reduce the efficiency of AGO-APP, probably due to the hydrophobic nature of AGO-TNRC6 interactions. Approximately 8-10 mg of HeLa S3 whole cell lysate was incubated with the washed beads in a total volume of 1.5 ml at 4°C for 4 hr with constant rotation. The beads were washed with 1 ml of Buffer APP six times and treated with Tri Reagent to isolate co-purifying RNAs. For AGO-APP with HEK293T cytoplasmic lysates containing overexpressed AGO proteins, ~25 μl of the resin saturated with the bait proteins were incubated with ~450 μg of lysate in a total volume of 350 μl, washed with 1 ml of Buffer APP three times, and co-purifying proteins were eluted and analyzed by western blotting.

Quantitative RT-PCR (qRT-PCR) and luciferase reporter assay

To measure mRNA levels, total RNA isolated by Tri Reagent was treated with Recombinant DNase I (Takara) and reverse transcribed with oligo$(dT)_{20}$ (Bioneer) and PrimeScript Reverse Transcriptase. The resulting cDNA was amplified with LightCycler 480 SYBR Green I Master (Roche Life Science). The human *GAPDH* mRNA was amplified in parallel as an endogenous control and the fold changes were calculated based on the comparative C_T method (Schmittgen and Livak, 2008). Primer sequences are listed in Table 1. To detect miRNA expression by qRT-PCR, TaqMan MicroRNA Assays (Thermo Fisher Scientific) were performed according to the manufacturer's instructions. All qRT-PCR experiments were conducted with the LightCycler 480 Instrument II (Roche Life Science). The Dual-Luciferase Reporter Assay System (Promega) was used for miRNA reporter assays, with the *Renilla* luminescence signal normalized to that of firefly luminescence. The relative *Renilla* signal from the miRNA targeting reporter was then normalized to that from the empty reporter to calculate the fold derepression.

Table 1. The sequences of oligonucleotides used in this study.

DNA Oligo	Sequence (5′→3′)	Description
hsa-miR-362_F	CCCAAGCTGGCTAGCAGTCCCTAGTAAATGACACTGTATATACATGAGAGTGA	Cloning of pri-miR-362 plasmids
hsa-miR-362_R	AACGGGCCCTCTAGATATTTACCGTTGTATCTCCACCACCC	
mmu-miR-362_F	CCCAAGCTGGCTAGCCCTTTGTGTTTGTAAAGGACAGAGCGCATC	
mmu-miR-362_R	AACGGGCCCTCTAGAATGTGTAGAACCAAGTCTGACAGCTAAAACCAAAA	
Pre-miR-362_RZ_F1	CTGATGAGTCCGTGAGGACGAAACGGTACCCGGTACCGTCAATCCTTGGAACCTAGGTGT	*In vitro* transcription of pre-miR-362 and pri-miR-362 and cloning of processing product
Pre-miR-362_RZ_F2	GAATTAATACGACTCACTATAGGGTTCCAAGGATTCTGATGAGTCCGTGAGGACG	
hsa-pre-miR-362_RZ_R1	CAGGTCGGACCGCGAGGAGGTGGAGATGCCATGCCGACCCTGAATCCTTGAATAGGTGTG	
mmu-pre-miR-362_RZ_R1	CAGGTCGGACCGCGAGGAGGTGGAGATGCCATGCCGACCCTGAATCCTTGAACAGGTGTG	
Polishing_HDV_RZ_R2	CCCGGATCCCACTACTCGTTGGCTCTCCCTTAGCCATCCGAGTTTCCTCGGATGCCCAGGTCGGACCGCGAGGAGG	
hsa-pri-miR-362_F	GAATTAATACGACTCACTATAGGGAGTCCCTAGTAAATGACACTGTATATACAT	
hsa-pri-miR-362_R	TATTTACCGTTGTATCTCCACCACC	
mmu-pri-miR-362_F	GAATTAATACGACTCACTATAGGGCCTTTGTGTTTGTAAAGGACAGAGC	
mmu-pri-miR-362_R	ATGTGTAGAACCAAGTCTGACAGCTAAAAC	
17_5A_DY_F	ATCGTACCCGAGTGAAA	
17_3A_DY_R	ATTGATCTCGGGTACAG	
miR-362-5p_PE	TCACACCTAGGTTCCAAG	Primer extension
PE_22nt_marker	TCACACCTAGGTTCCAAGGA	
PE_24nt_marker	TCACACCTAGGTTCCAAGGATT	
myc-PARN_F	TCAGAAGAGGATCTGATGGAGATAATCAGGAGCAATTTTA	Cloning of PARN plasmids and site-directed mutagenesis
myc-PARN_R	AGGCACAGTCGAGGCTTACCATGTGTCAGGAACTTCAAA	
His-GST-PARN_F	CTGTATTTCCAGGGCATGGAGATAATCAGGAGCAATTTTA	
His-GST-PARN_R	AGAGGATCCGAATTCTTACCATGTGTCAGGAACTTCAAA	
PARN_ΔsiRNA_F	GCGCCAACTCAGAGAGCAGTATGATGAAAAACGTTCA	
PARN_ΔsiRNA_R	TCCTCCTCTTGATTTAAATATGGAATTCCATTTCGAA	
PARN_genotyping_F	AGCAGGAATTCAGGCCACTGGTTCT	Knockout genotyping
PARN_genotyping_R	GTGAAACCCGCCCAAGGCTACTAAC	
anti-miR-362-5p	TCACACCTAGGTTCCAAGGATT	Small RNA northern blot probes (R and Y indicate purine and pyrimidine, respectively)
anti-miR-362-3p	TGAATCCTTGAAYAGGTGTGTT	
anti-miR-362-5p_HS	TCACACCTAGGTTCCAAGGATTACCCGAGG	
anti-miR-224-5p_HS	AACGGAACCACTAGTGACTTGACCCGAGG	
anti-miR-182-5p_HS	AGTGTGAGTTCTACCATTGCCAAAACCCGAGG	
anti-miR-425-5p_HS	TCAACGGGAGTGATCGTGTCATTACCCGAGG	
anti-miR-361-3p_HS	AAATCAGAATCACACCTGGGGGAACCCGAGG	
anti-miR-301a-3p_HS	GCTTTGACAATACTATTGCACTGACCCGAGG	
anti-miR-454-3p_HS	ACCCTATAAGCAATATTGCACTAACCCGAGG	

anti-miR-186-5p_HS	AGCCCAAAAGGAGAATTCTTTGACCCGAGG	
anti-miR-16-5p	CGCCAATATTTACGTGCTGCTA	
anti-miR-27a-3p	GCGGAACTTAGCCACTGTGAA	
anti-hsa-miR-17/20a-5p	CTACCTGCACTRTAAGCACTTT	
anti-hsa-miR-18a-5p_HS	CTATCTGCACTAGATGCACCTTAACCCGAGG	
anti-hsa-miR-19a/b-3p	TCAGTTTTGCATRGATTTGCACA	
anti_SNORA63_HS	CATGTATGAGACCAAGCGTCACCCGAGG	
anti-U1 snRNA	CAAATTATGCAGTCGAGTTTCCCACATTTG	
anti-U6 snRNA	TTGCGTGTCATCCTTGCGCAGG	
anti-tRNA^{Lys}	GAGATTAAGAGTCTCATGCTC	
HS_universal	TTTTTTTTTTTTCCTCGGGT-NH_2 (3′-amine modification)	
qPCR_EXOSC10_F	TGAGAGCCTCACAGACCCAG	Quantitative RT-PCR
qPCR_EXOSC10_R	AGGTTAAGAAGGCGTGCTGC	
qPCR_DIS3_F	TAAGGCAGCCAGGTCAAGGA	
qPCR_DIS3_R	TGCATCATACAGCGAGTGGC	
qPCR_DIS3L_F	GGAGAGCCATGGGAAGGAGT	
qPCR_DIS3L_R	CTGCTGGCTCCTTGAAGTCG	
qPCR_DIS3L2_F	CTGTGTGAGGAGCTGTGCAG	
qPCR_DIS3L2_R	GGTCCGGCCAAACCATTCAT	
qPCR_PARN_F	GCTCTTGGACGTCATGCACA	
qPCR_PARN_R	AAAAGGTTGTGTGCTGGCCA	
qPCR_ERI1_F	GTGTCAACTCAGCAGGCTCA	
qPCR_ERI1_R	GGCCGCCCATCATAATCCAT	
qPCR_FRS2_F	GACCATGTGATCCTTCTTTTTGGTT	
qPCR_FRS2_R	AGCATGGGATAGATGCTGTTATGAT	
qPCR_CUGBP1_F	TGATCAGGACCTGCTGCAGA	
qPCR_CUGBP1_R	GGCCGAAACAGGATTGTCGT	
psiCHECK2_FRS2_F	TACCATTGCCAAATTGTATATGAAATATGGCGGCCGCTGGCCGCAATAAAATA	Reporter construction
psiCHECK2_FRS2_R	GTCCCACTGTTGGACAATTTTTTATAAAACTCGAGCGATCGCCTAGAATTACTGCTC	

RNA Oligo	Sequence (5′→3′)	Description
17_5A_DY	AUCGUACCCGAGUGAAA	Cloning of processing product
17_3A_DY	AppCTGTACCCGAGATCAATddC	
siGFP	UGAAUUAGAUGGCGAUGUU(dTdT)	RNAi-mediated gene knockdown (the type of 3′ overhang indicated within parentheses)
siEXOSC10-1	CACAGUUUGGCGAUGAGUA(dTdT)	
siEXOSC10-2	CAUUAAGGAUCGAAGUAAA(dTdT)	
siDIS3	AGGUAGAGUUGUAGGAAUA(UU)	
siDIS3L	CGUAAAGACUUGAGGAAAA(dTdT)	
siDIS3L2-1	GGUUGAUGGUGUUAAGAAA(dTdT)	
siDIS3L2-2	UGAGAAAGGAAGAGAGGAU(dTdT)	
siDIS3L2-3	GCACAGAGCAUGAUUGAAA(UU)	
siPARN	GGAAGAAGAAAGACAGUUA(dTdT)	
siERI1	GCUUGAAACUAGAGGAGUA(UU)	
siCUGBP1-1	GACAAGCAGACAAACCUGA(dTdT)	
siCUGBP1-2	ACAAAGAACAGAAGAGAAU(dTdT)	

ASO-hsa-miR-182-5p	$A_mG_mU_mG_mU_mG_mA_mG_mU_mU_mC_mU_mA_mC_mC_mA_mU_mU_mG_mC_mC_mA_mA_mA_m$	anti-miR
ASO-hsa-miR-1-3p	$A_mU_mA_mC_mA_mU_mA_mC_mU_mU_mC_mU_mU_mU_mA_mC_mA_mU_mU_mC_mC_mA_m$	
hsa-miR-362-5p_WT	AAUCCUUGGAACCUAGGUGUGAGUGC	Duplex formation followed by transfection into HeLa S3 cells or *in vitro* trimming
hsa-miR-362-5p_m1	AAUCCUUGGAACCUAGGUGUGAGUG$_m$C	
hsa-miR-362-5p_m2	AAUCCUUGGAACCUAGGUGUGAG$_m$UGC	
hsa-miR-362-3p	AACACACCUAUUCAAGGAUUCA	
mmu-miR-362-5p_WT	AAUCCUUGGAACCUAGGUGUGAAUGC	
mmu-miR-362-5p_m1	AAUCCUUGGAACCUAGGUGUGAAUG$_m$C	
mmu-miR-362-5p_m2	AAUCCUUGGAACCUAGGUGUGAA$_m$UGC	
mmu-miR-362-3p	AACACACCUGUUCAAGGAUUCA	

RESULTS

The "cellular definition" of miR-362-5p

The stem region of natural miRNA hairpins is frequently enriched for various structural imperfections, such as wobbles, mismatches, and bulges (Fang and Bartel, 2015; Liu et al., 2016). While examining the effect of such structural motifs on DICER processing (Starega-Roslan et al., 2011), I became interested in miR-362, a mammalian miRNA whose precursor contains a relatively large bulge compared with other pre-miRNAs (Figure 10A) (Fang and Bartel, 2015). Both the 5′ and 3′ ends of human and mouse pre-miR-362 were consistently annotated by two different miRNA databases based on small RNA sequencing (Kozomara and Griffiths-Jones, 2014; Fromm et al., 2015). In addition, those of human pre-miR-362 exactly matched the sites of DROSHA-mediated cleavage on endogenous pri-miR-362 (Kim et al., 2017). Lastly, characterization of pre-miR-362 liberated from *in vitro* DROSHA processing of human and mouse pri-miR-362 confirmed the annotations (Figures 10B and 11). *In silico* prediction of RNA secondary structure (Zuker, 2003) indicated that pre-miR-362 is a 59 nt fragment containing a canonical 2 nt overhang at its 3′ end and a tri-nucleotide bulge in the middle of the 5p strand (nt 11-13; Figure 10B).

To characterize DICER processing of pre-miR-362 *in vitro*, body-labeled pre-miR-362 was prepared and incubated with FLAG-immunoprecipitate obtained from HEK293T cells overexpressing FLAG-DICER1 and myc-TRBP. *In vitro* processing of pre-miR-362 with the immunopurified DICER complex released three major products, plausibly corresponding to the 5p strand, 3p strand, and terminal loop (Figure 12A; lanes 1-10). When 5′-labeled pre-miR-362 was used as a substrate,

only the uppermost band was produced, demonstrating that this largest product represented the 5p strand of the miR-362 duplex (Figure 12A; lanes 11-16). Small RNA northern blot analysis of the DICER processing products corroborated this finding and further identified the middle band as the 3p strand (data not shown). Cloning and sequencing of the DICER products (~20-30 nt) enabled to precisely map the cleavage sites on pre-miR-362, which divide the 59 nt hairpin into the 26 nt 5p strand, the 22 nt 3p strand, and the 11 nt terminal loop (Figures 10B and 12B). Collectively, these results indicate that miR-362-5p defined by DROSHA and DICER is 26 nt in length, which is somewhat longer than the miRBase annotation of 24 nt (Figure 10B).

Next, the expression of endogenous miR-362-5p in a panel of human and mouse cells was investigated by northern hybridization. Curiously, all cell lines tested expressed fragments that were ~2-4 nt shorter than the 26 nt miR-362-5p defined *in vitro*, with the heterogeneity more prominent in mouse cells (Figure 13A). Primer extension experiments using a centrally designed primer (complementary to nt 5-22 of miR-362-5p) demonstrated that the endogenous miR-362-5p isoforms share the 5′ end, suggesting the possibility of 3′ end variation (Figure 13B). To comprehensively catalog the isomiR repertoire of miR-362-5p, small RNA deep sequencing data obtained from HeLa S3 cells and mouse tissues were analyzed. Consistent with the results of northern blotting and primer extension assays, miR-362-5p was represented by more than two dominantly abundant isoforms of 22-26 nt that differed in their 3′ ends (Figure 14). Taken together, these findings suggest that the “cellular definition” of a miRNA does not necessarily coincide with the definition made by the core miRNA biogenesis enzymes.

Figure 10. Predicted secondary structure of pri-miR-362.

(A) Bulges and Watson-Crick pairing across the 35 bp stem of 186 conserved human pri-miRNAs. Data from a previous report (Fang and Bartel, 2015) was re-analyzed. Pri-miR-362 was chosen for further investigation because it is well structured except for the tri-nucleotide bulge (i.e., pri-miR-362 has the highest number of Watson-Crick pairing across the pri-miRNAs containing ≥3 nt bulges).

(B) Predicted secondary structure of pri-miR-362. Predictions were carried out using the mfold RNA folding algorithm (Zuker 2003). The sequences of miR-362-5p and miR-362-3p annotated in miRBase are shown in red. The purple and green arrowheads indicate the DROSHA and DICER cleavage sites determined *in vitro*, respectively. Note that mouse pri-miR-362 is processed into 59 nt or 60 nt precursors to a similar extent (see Figure 11). The 59 nt fragment was annotated as mouse pre-miR-362 because it carries a canonical 2 nt overhang.

A

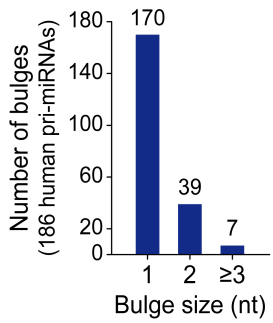

Pri-miRNAs w/ ≥3 nt bulge	Number of W-C pairing
Pri-miR-362	31
Pri-miR-802	30
Pri-miR-19b-2	28
Pri-miR-221	28
Pri-miR-1249	26
Pri-miR-182	25
Pri-miR-134	22

(Fang and Bartel, 2015)

B

Human pri-miR-362

Mouse pri-miR-362

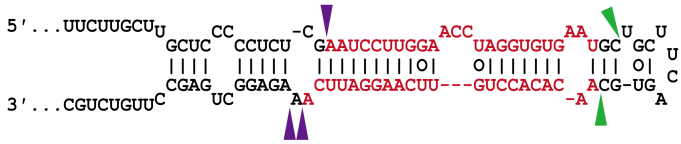

In vitro DROSHA cleavage sites
In vitro DICER cleavage sites

Figure 11. Characterization of pri-miR-362 processing *in vitro*.

(A) *In vitro* DROSHA processing of human and mouse pri-miR-362. A body-labeled pri-miRNA substrate of ~300 nt in length was incubated with the Microprocessor complex immunopurified from HEK293T cells overexpressing DROSHA-FLAG and V5-DGCR8 for 30 min and the reaction products were analyzed by phosphorimaging. Pre-miR-362 liberated by the Microprocessor is indicated. The dashed line indicates discontinuous lanes from the same gel.

(B) Mapping of DROSHA cleavage sites on pri-miR-362. To increase the specificity, the 5′ and 3′ cleavage sites were mapped separately, by pairing one primer complementary to the adaptor and the other to the internal sequence of pre-miR-362. The frequency of each cleavage site is indicated, with the major cleavage sites marked in bold.

A

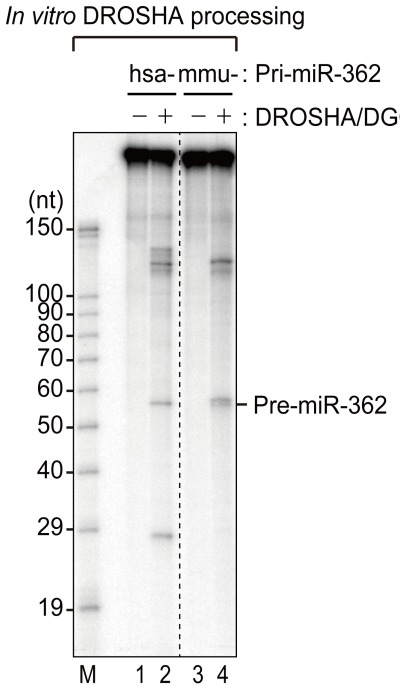
In vitro DROSHA processing
hsa- mmu- : Pri-miR-362
− + − + : DROSHA/DGCR8
(nt)
150
100
90
80
70
60
50
40
29
19
Pre-miR-362
M 1 2 3 4

B

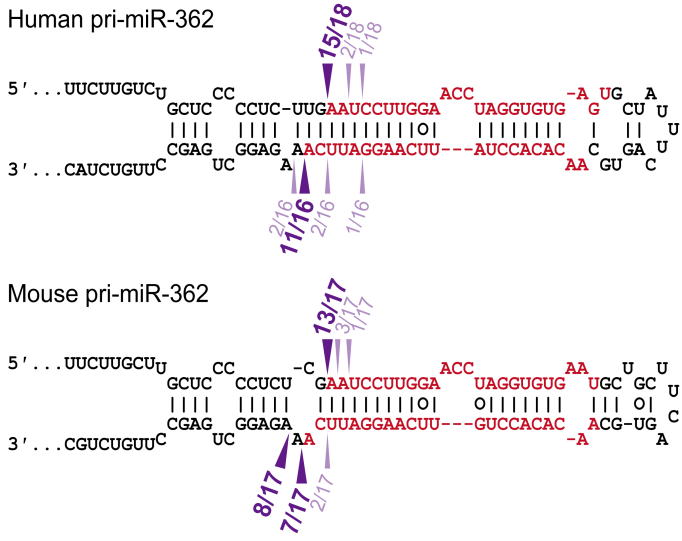
Human pri-miR-362
15/18
2/18
1/18
5′...UUCUUGUCU
CC
ACC
-A UG A
GCUC CCUC-UUGAAUCCUUGGA UAGGUGUG G CU U
CGAG GGAG AACUUAGGAACUU---AUCCACAC C GA U
3′...CAUCUGUUC
UC A
AA GU C
2/16
11/16
2/16
1/16
Mouse pri-miR-362
13/17
3/17
1/17
5′...UUCUUGCUU
CC -C
ACC
AA U U
GCUC CCUCU GAAUCCUUGGA UAGGUGUG UGC GC U
CGAG GGAGA CUUAGGAACUU---GUCCACAC ACG-UG C
3′...CGUCUGUUC
UC AA
-A A
8/17
7/17
2/17

Figure 12. Characterization of pre-miR-362 processing *in vitro*.

(A) *In vitro* DICER processing of human and mouse pre-miR-362. Body-labeled (lanes 1-10) or 5′-labeled pre-miR-362 (lanes 11-16) was incubated with the immunopurified DICER/TRBP complex for the indicated time period. The suspected identity of each reaction product is shown on the right side. Dashed lines indicate discontinuous lanes from the same gel.

(B) Mapping of DICER cleavage sites on pre-miR-362. The frequency of each cleavage site is indicated, with the major cleavage sites marked in bold.

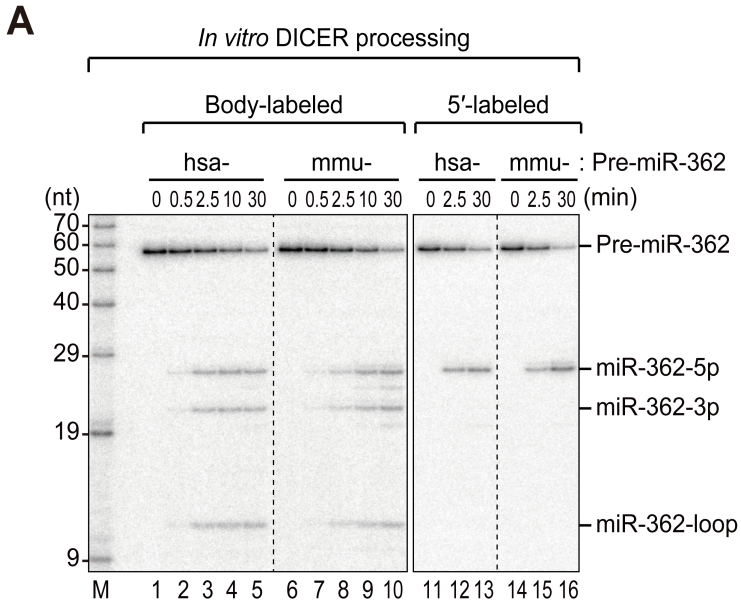
A
In vitro DICER processing
Body-labeled
5′-labeled
hsa-
mmu-
hsa-
mmu-
: Pre-miR-362
(nt)
0 0.5 2.5 10 30 0 0.5 2.5 10 30
0 2.5 30 0 2.5 30 (min)
70
60
50
40
29
19
9
Pre-miR-362
miR-362-5p
miR-362-3p
miR-362-loop
M 1 2 3 4 5 6 7 8 9 10 11 12 13 14 15 16

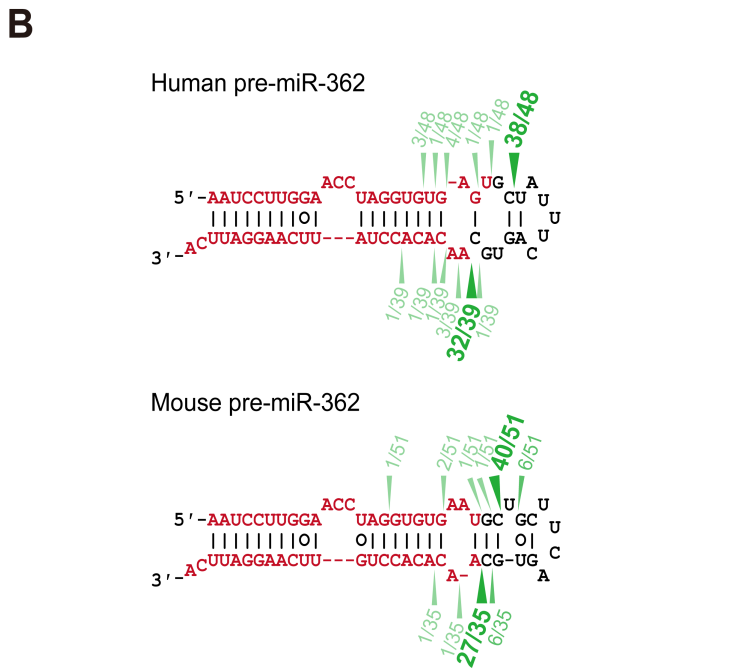
B
Human pre-miR-362
5′-AAUCCUUGGA ACC UAGGUGUG -A UG G CU A U U
3′-ACUUAGGAACUU---AUCCACAC AA C GU GA C U
3/48 1/48 4/48 1/48 1/48 38/48
1/39 1/39 1/39 3/39 32/39 1/39
Mouse pre-miR-362
5′-AAUCCUUGGA ACC UAGGUGUG AA UGC U GC U C
3′-ACUUAGGAACUU---GUCCACAC A- ACG-UG A
1/51 2/51 1/51 1/51 40/51 6/51
1/35 1/35 27/35 6/35

Figure 13. Characterization of miR-362-5p expression in cells (1).

(A) miR-362-5p expression in cells. Total RNA isolated from human (BE(2)-C, MDA-MB-231, SW480) or mouse (MEF, mMSC, NIH-3T3) cell lines was subjected to northern hybridization. One femtomole of synthetic human miR-362-5p (26 nt) was loaded in the same gel to serve as a positive control and size reference (lane 1). U6 snRNA and 5S rRNA served as loading controls.

(B) Primer extension analysis of miR-362-5p. A 5′-labeled DNA oligonucleotide complementary to the central region of miR-362-5p (nt 5-22) was annealed to the total RNA used in (A) and reverse transcribed. The capital "R" in the sequence of miR-362-5p indicates G or A in the human or mouse orthologues, respectively. Antisense DNA oligonucleotides corresponding to nt 3-22 and nt 1-22 of miR-362-5p were 5′-labeled and used as size markers. Reactions with water (No RNA) and 1 fmole of synthetic human miR-362-5p (26 nt) served as a negative and positive control, respectively (lanes 1 and 2). Ethidium bromide staining of tRNAs served as a loading control.

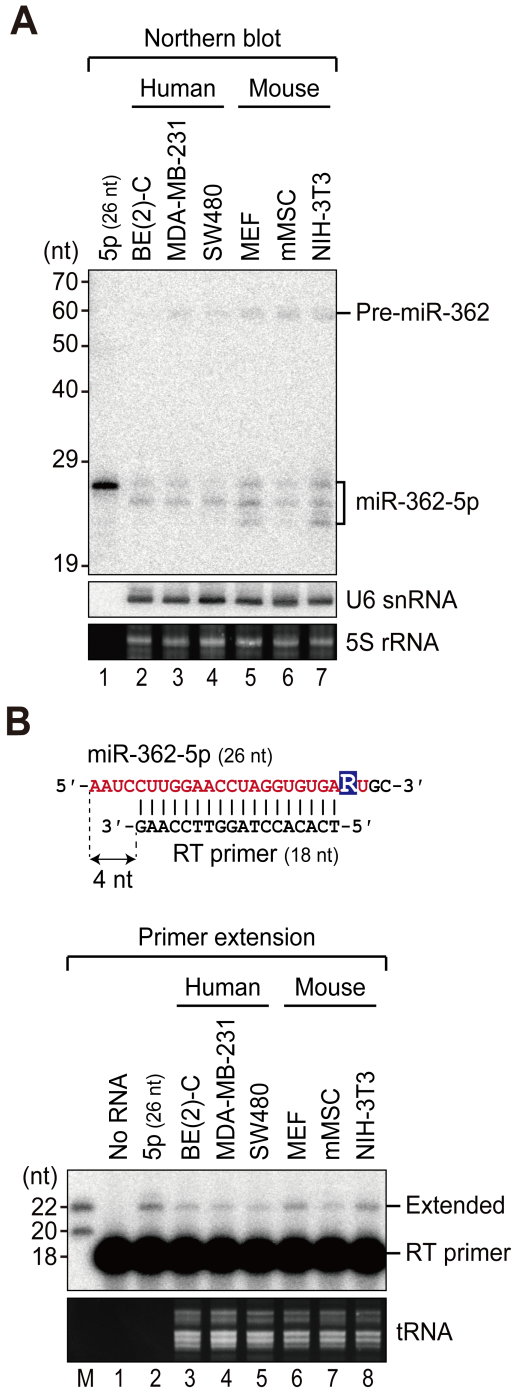
A
Northern blot
Human
Mouse
5p (26 nt)
BE(2)-C
MDA-MB-231
SW480
MEF
mMSC
NIH-3T3
(nt)
70
60
50
40
29
19
Pre-miR-362
miR-362-5p
U6 snRNA
5S rRNA
1 2 3 4 5 6 7
B
miR-362-5p (26 nt)
5′-AAUCCUUGGAACCUAGGUGUGAUGC-3′
3′-GAACCTTGGATCCACACT-5′
RT primer (18 nt)
4 nt
Primer extension
Human
Mouse
No RNA
5p (26 nt)
BE(2)-C
MDA-MB-231
SW480
MEF
mMSC
NIH-3T3
(nt)
22
20
18
Extended
RT primer
tRNA
M 1 2 3 4 5 6 7 8

Figure 14. Characterization of miR-362-5p expression in cells (2).

Small RNA sequencing reads mapped to the miR-362 locus. Reads from mouse tissues were obtained elsewhere (Chiang et al. 2010). For simplicity, only the reads that share the 5′ end with the miRBase sequence and that do not contain untemplated nucleotides at the 3′ end were displayed. The sequence of miR-362-5p defined by DICER *in vitro* is shown in green, with the cleavage site indicated by a green arrowhead. The sequence of miR-362-5p annotated in miRBase is shown in red. The fraction of each read was calculated and is plotted on the right side.

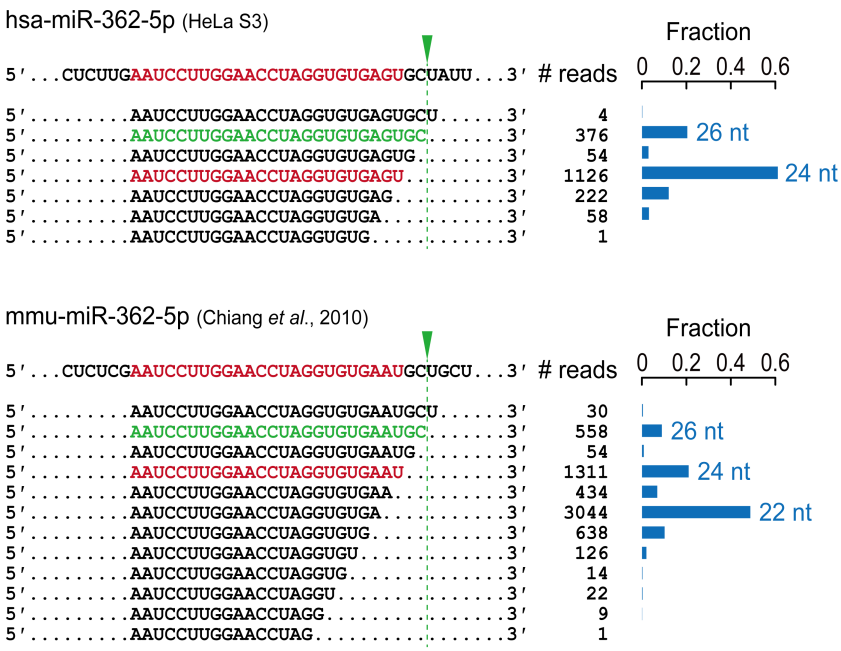
hsa-miR-362-5p (HeLa S3)
Fraction
5′...CUCUUGAAUCCUUGGAACCUAGGUGUGAGUGCUAUU...3′ # reads
0 0.2 0.4 0.6
5′.....AAUCCUUGGAACCUAGGUGUGAGUGCU.....3′ 4
5′.....AAUCCUUGGAACCUAGGUGUGAGUGC.....3′ 376
5′.....AAUCCUUGGAACCUAGGUGUGAGUG.....3′ 54
5′.....AAUCCUUGGAACCUAGGUGUGAGU.....3′ 1126
5′.....AAUCCUUGGAACCUAGGUGUGAG.....3′ 222
5′.....AAUCCUUGGAACCUAGGUGUGA.....3′ 58
5′.....AAUCCUUGGAACCUAGGUGUG.....3′ 1
26 nt
24 nt
mmu-miR-362-5p (Chiang et al., 2010)
Fraction
5′...CUCUCGAAUCCUUGGAACCUAGGUGUGAAUGCUGCU...3′ # reads
0 0.2 0.4 0.6
5′.....AAUCCUUGGAACCUAGGUGUGAAUGCU.....3′ 30
5′.....AAUCCUUGGAACCUAGGUGUGAAUGC.....3′ 558
5′.....AAUCCUUGGAACCUAGGUGUGAAUG.....3′ 54
5′.....AAUCCUUGGAACCUAGGUGUGAAU.....3′ 1311
5′.....AAUCCUUGGAACCUAGGUGUGAA.....3′ 434
5′.....AAUCCUUGGAACCUAGGUGUGA.....3′ 3044
5′.....AAUCCUUGGAACCUAGGUGUG.....3′ 638
5′.....AAUCCUUGGAACCUAGGUGU.....3′ 126
5′.....AAUCCUUGGAACCUAGGUG.....3′ 14
5′.....AAUCCUUGGAACCUAGGU.....3′ 22
5′.....AAUCCUUGGAACCUAGG.....3′ 9
5′.....AAUCCUUGGAACCUAG.....3′ 1
26 nt
24 nt
22 nt

Biogenesis of miR-362-5p involves 3′-to-5′ exoribonucleolytic trimming

To gain insights into how the shorter isoforms of miR-362-5p are generated, pri-miR-362 was overexpressed in HEK293T cells and the expression of miR-362-5p was analyzed by northern blotting. Ectopic expression of pri-miR-362 faithfully recapitulated the production of two distinct isoforms of miR-362-5p (Figure 15A), suggesting that the observed 3′ heterogeneity may be a sequence-driven feature of miR-362-5p biogenesis. Because pre-miR-362 was cleaved by DICER without much variation *in vitro* (Figure 12), it was suspected that the 26 nt miR-362-5p liberated by DICER may be subsequently resected at the 3′ end by unknown ribonuclease(s). To test this possibility, HeLa S3 cells were transfected with a synthetic miR-362 duplex consisting of the 26 nt 5p strand and the 22 nt 3p strand. Notably, miR-362-5p from the synthetic duplex was trimmed down to ~22-24 nt species with a pattern similar to that observed for its endogenous or ectopically expressed counterpart, implying the existence of 3′ trimming activity toward this specific miRNA *after* DICER processing (Figure 15B; lanes 3 and 6). Next, an RNase-resistant 2′-*O*-methyl (2′-*O*Me) modification was incorporated at the 25th or 23rd position of miR-362-5p (designated m1 or m2, respectively) and a duplex bearing the mutant 5p strand was introduced into HeLa S3 cells. The m1 duplex no longer produced the shorter isoforms (Figure 15B; lanes 4 and 7), while the m2 substitution abolished the production of miR-362-5p isoforms shorter than 24 nt (Figure 15B; lanes 5 and 8). These results suggest that the characteristic 3′ heterogeneity of miR-362-5p is conferred after DICER processing by the action of 3′-to-5′ *exo*ribonuclease(s).

To further demonstrate the existence of such 3′ trimming activity in cells, it was tested whether the 3′ end of miR-362-5p could be resected *in vitro*. To this end, the miR-362 duplex containing 5′-labeled 26 nt miR-362-5p was incubated with a

cytoplasmic lysate obtained from HEK293T cells overexpressing FLAG-AGO2. The resulting FLAG-AGO2/miR-362-5p complex was immunopurified and subjected to further incubation with HeLa whole cell lysate (Figure 16A). Notably, wild-type miR-362-5p, but not the m1 mutant, was trimmed over time (Figure 16B), with the size distribution of trimming products resembling that of miR-362-5p isoforms in cells (Figures 13-15). Trimming was consistently observed when the other three human AGO proteins (AGO1, AGO3, and AGO4) were used for miRNA loading (Figure 17A), excluding the possibility that the identity of AGO proteins may specify the 3′ trimming of miR-362-5p, as previously reported for other miRNAs (Juvvuna et al., 2012). Although miRNAs tend to become highly stable once loaded into AGO proteins (De et al., 2013; Park et al., 2017), because their 5′ and 3′ ends are anchored in the MID and PAZ domains, respectively (Elkayam et al., 2012; Schirle and Macrae, 2012), my data suggest that the 3′ ends of certain miRNAs can be exposed to and subsequently trimmed by cellular 3′-to-5′ exoribonucleases. To investigate whether the interaction between the miRNA 3′ end and the AGO protein plays a role in trimming, Y311 of AGO2 was mutated, which is located within the PAZ domain and makes contact with the 3′ nucleotides of miRNAs (Figure 17B) (Elkayam et al., 2012; Park et al., 2017). Strikingly, miR-362-5p loaded into this mutant AGO2 was trimmed more progressively and non-specifically than when loaded into wild-type AGO proteins (Figure 17C), without the accumulation of the characteristic 24 nt species observed *in vivo* and *in vitro* (Figures 13-17A). These results indicate that the 3′ trimming of miR-362-5p takes place within the miRISC and is influenced by the miRNA 3′ end-PAZ interaction. In summary, the distinguishing 3′ heterogeneity of miR-362-5p appears to result from the collaboration of multiple factors, including DICER, AGO, and an unknown “trimmer”.

Figure 15. Recapitulation of miR-362-5p biogenesis and 3′ heterogeneity.

(A) Recapitulation of miR-362-5p biogenesis in HEK293T cells. The cells were transfected with the indicated pri-miR-362 expression plasmid and the maturation of miR-362-5p was examined by small RNA northern blotting. U6 snRNA and 5S rRNA served as loading controls.

(B) The 3′ heterogeneity of miR-362-5p arises after DICER processing. The upper panel shows the structure of a miR-362 duplex, with the 2′-*O*-methyl-modified nucleotides in the mutant 5p strands indicated by arrows. Duplexes bearing wild-type (WT) or mutant 5p strands were individually introduced into HeLa S3 cells and the processing of ectopic miR-362-5p was investigated by small RNA northern blotting. U6 snRNA and 5S rRNA were used as loading controls.

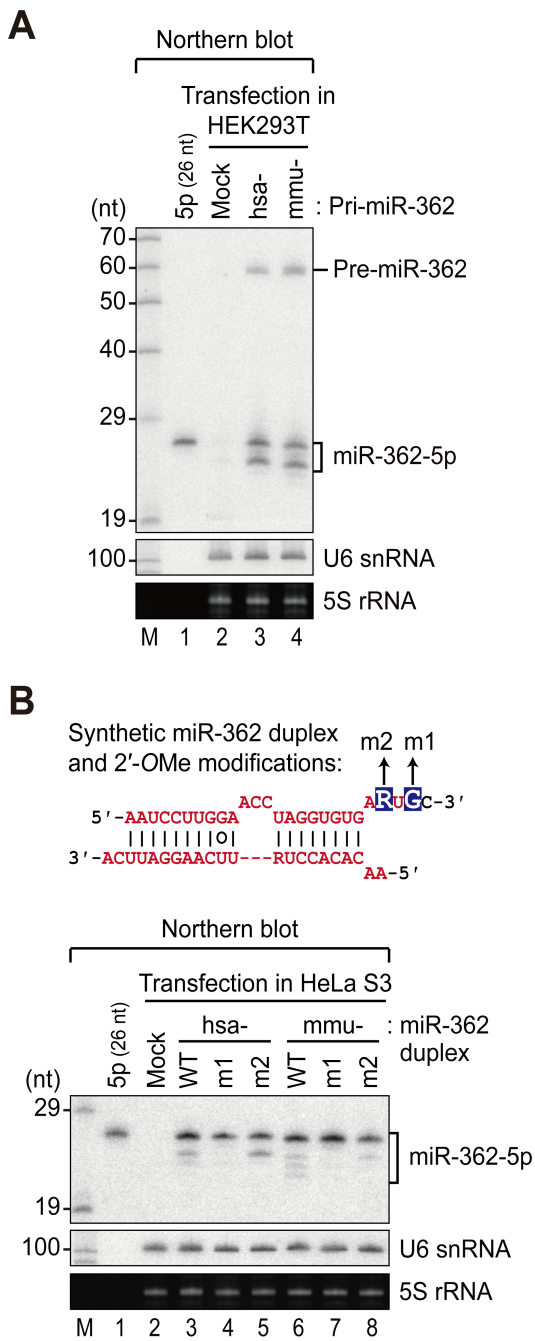
A
Northern blot
Transfection in HEK293T
5p (26 nt)
Mock
hsa-
mmu-
(nt)
: Pri-miR-362
70
60
50
40
29
19
100
Pre-miR-362
miR-362-5p
U6 snRNA
5S rRNA
M 1 2 3 4
B
Synthetic miR-362 duplex and 2′-OMe modifications:
m2 m1
5′-AAUCCUUGGA ACC UAGGUGUG AUC-3′
3′-ACUUAGGAACUU---RUCCACAC AA-5′
Northern blot
Transfection in HeLa S3
5p (26 nt)
Mock
hsa-
mmu-
WT
m1
m2
: miR-362 duplex
(nt)
29
19
100
miR-362-5p
U6 snRNA
5S rRNA
M 1 2 3 4 5 6 7 8

Figure 16. *In vitro* trimming of miR-362-5p loaded into AGO2.

(A) Schematic illustration of *in vitro* trimming assay. The miRNA duplex bearing 5′-labeled guide strand is incubated with cytoplasmic lysate from HEK293T cells overexpressing FLAG-AGO2. The resulting ribonucleoprotein complex is FLAG-immunopurified, extensively washed, and subjected to further incubation with HeLa S3 whole cell lysate.

(B) *In vitro* trimming of miR-362-5p loaded into AGO2. The indicated 5′-labeled 5p strand was used produce the miR-362 duplex. *In vitro* trimming was performed for the indicated time period.

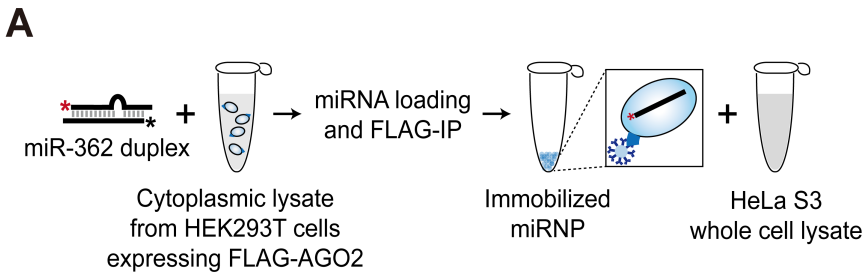
A
miR-362 duplex
miRNA loading
and FLAG-IP
Cytoplasmic lysate
from HEK293T cells
expressing FLAG-AGO2
Immobilized
miRNP
HeLa S3
whole cell lysate

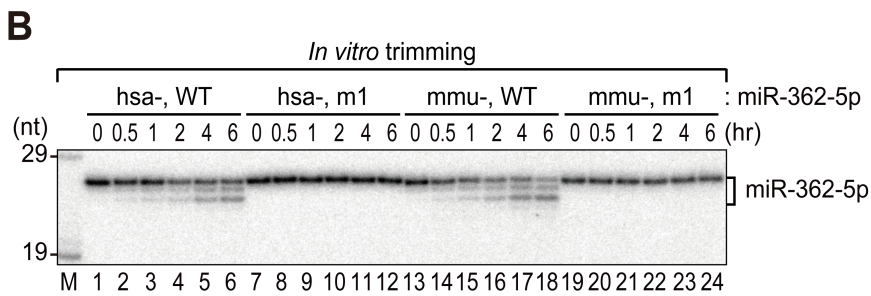
B
In vitro trimming
hsa-, WT
hsa-, m1
mmu-, WT
mmu-, m1
: miR-362-5p
(nt)
0 0.5 1 2 4 6 0 0.5 1 2 4 6 0 0.5 1 2 4 6 0 0.5 1 2 4 6 (hr)
29
19
miR-362-5p
M 1 2 3 4 5 6 7 8 9 10 11 12 13 14 15 16 17 18 19 20 21 22 23 24

Figure 17. *In vitro* trimming of miR-362-5p loaded into other AGO proteins and AGO2(Y311A).

(A) *In vitro* trimming of miR-362-5p loaded into other human AGO proteins (AGO1, AGO3, and AGO4). Trimming assays were performed essentially as in Figure 16, except for utilizing HEK293T lysate overexpressing the indicated FLAG-AGO protein for miR-362-5p loading.

(B) The 3′ end-binding pocket within the PAZ domain of human AGO2. The figure was adopted from a previous report (Park et al. 2017). The original structure is from elsewhere (PDB ID: 4W5N) (Schirle et al., 2014).

(C) *In vitro* trimming of miR-362-5p loaded into AGO2(Y311A).

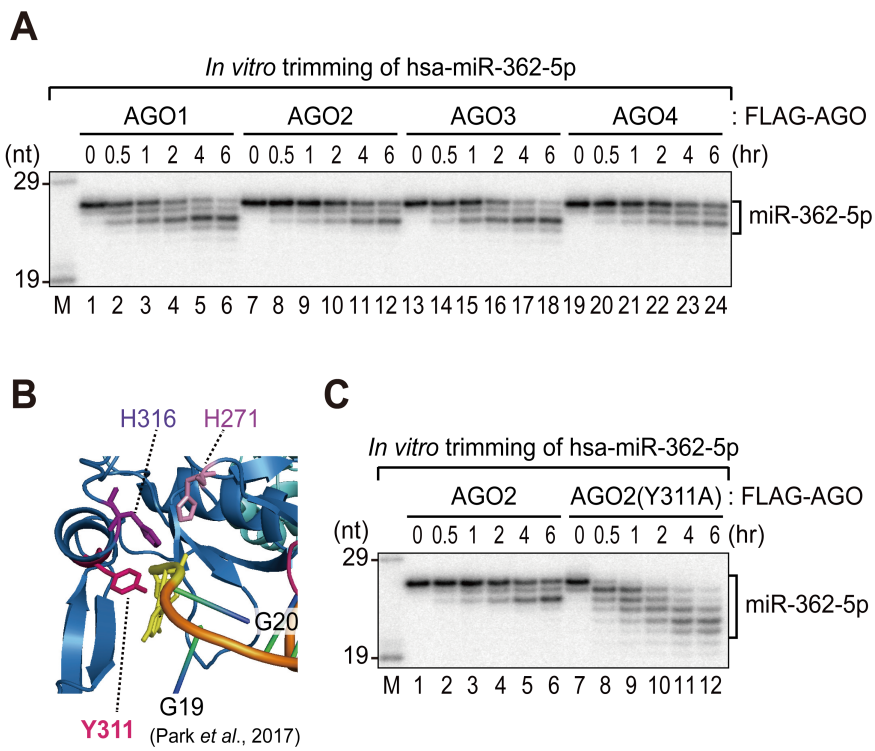
A
In vitro trimming of hsa-miR-362-5p
AGO1
AGO2
AGO3
AGO4
: FLAG-AGO
(nt)
0 0.5 1 2 4 6 0 0.5 1 2 4 6 0 0.5 1 2 4 6 0 0.5 1 2 4 6 (hr)
29
19
miR-362-5p
M 1 2 3 4 5 6 7 8 9 10 11 12 13 14 15 16 17 18 19 20 21 22 23 24
B
H316
H271
G20
G19
Y311
(Park et al., 2017)
C
In vitro trimming of hsa-miR-362-5p
AGO2
AGO2(Y311A)
: FLAG-AGO
(nt)
0 0.5 1 2 4 6 0 0.5 1 2 4 6 (hr)
29
19
miR-362-5p
M 1 2 3 4 5 6 7 8 9 10 11 12

PARN emerges as a miR-362-5p trimmer

To identify the miR-362-5p trimmer, several 3′-to-5′ exoribonucleases previously implicated in the miRNA pathway were individually depleted in HEK293T cells and the trimming of miR-362-5p was examined. Candidate genes included the catalytic subunits of the exosome complex that destructs miR-382 and defective pre-miRNAs (EXOSC10, DIS3, DIS3L) (Bail et al., 2010; Liu et al., 2014); a related but exosome-independent enzyme that trims miR-27 during TDMD and degrades oligo-uridylated pre-let-7 in embryonic stem cells (DIS3L2) (Chang et al., 2013; Haas et al., 2016); and two additional 3′-to-5′ exoribonucleases reportedly associated with small RNA biogenesis or turnover (PARN, ERI1) (Yoda et al., 2013; Boele et al., 2014; Thomas et al., 2014; Katoh et al., 2015). Notably, knockdown of PARN significantly decreased the fraction of the shorter miR-362-5p isoforms, while knockdown of other exoribonucleases did not obviously change the ratio between the two isoforms (Figure 18).

To rule out the possibility of off-target effects of RNAi, PARN-depleted HEK293T cells were rescued with an RNAi-resistant PARN expression plasmid. Complementation of PARN activity restored the normal isoform ratio, suggesting that PARN is indeed responsible for the 3′ trimming of miR-362-5p (Figure 19A; lanes 3-5 and 9-11). Increasing the amount of PARN plasmid promoted the generation of an even shorter isoform of ~22 nt (Figure 19A; lanes 6-8 and 12-14), which was evidently observed for endogenous mouse miR-362-5p (Figure 13A). Of note, overexpression of PARN above a certain level appeared to reduce the abundance of mature miR-362-5p (Figure 19A; compare lanes 3 and 8, or 9 and 14). However, this is unlikely to represent a true biological regulation by PARN and may reflect experimental artifacts associated with supra-physiological expression of the

enzyme, because miR-362-5p was not apparently stabilized upon PARN depletion (Figure 19A; lanes 3-4 and 9-10; discussed further below). To corroborate these results, a PARN mutant, D28A, was generated, in which one of the four catalytic residues was substituted with alanine. This mutant is catalytically deficient but still retains the ability to bind substrates, being expected to act as a *trans*-dominant negative mutant (Ren et al., 2002; Lai et al., 2003; Ren et al., 2004). As anticipated, overexpression of D28A PARN caused a shift in the isoform ratio toward the longer one, without altering the level of miR-362-5p (Figure 19B). These data clearly indicate that PARN functions as a key player in the 3′ end formation of miR-362-5p.

To address whether PARN trims the 3′ end of miR-362-5p after DICER processing, PARN was depleted in HeLa S3 cells and wild-type or m2 miR-362 duplexes were introduced. Consistent with the results obtained in HEK293T cells, the levels of shorter miR-362-5p isoforms were markedly diminished upon PARN knockdown (Figure 20). Of note, human and mouse miR-362-5p responded slightly differently to the reduction of PARN activity. For example, the 24 nt isoform of human miR-362-5p was barely produced in PARN-depleted cells (Figure 20; lanes 3-6), whereas the ~22-23 nt isoforms of mouse miR-362-5p were more prominently affected by PARN knockdown than the 24 nt isoform (Figure 20; lanes 7-10). Human and mouse miR-362-5p differ by only one nucleotide at the 23rd position (G and A in human and mouse, respectively; see Figure 10B). The nucleotide identity at this position may modulate PARN-mediated trimming in cells, leading to the differential trimming patterns observed in the two orthologous miRNAs.

Finally, the role of PARN as a miRNA trimmer was tested *in vitro*. To this end, miR-362-5p loaded into FLAG-AGO2 was incubated with lysates from HeLa S3 cells in which PARN was overexpressed or depleted (Figure 21A). Notably, the

3′ trimming of miR-362-5p was severely compromised when a lysate from PARN-depleted cells was used (Figure 21B; lanes 7-12), suggesting that PARN is largely responsible for the trimming activity present in HeLa whole cell lysate. On the other hand, a lysate containing an overexpressed PARN protein greatly accelerated the trimming (Figure 21B; lanes 13-18). In addition, recombinant PARN purified from *E. coli* to near homogeneity faithfully recapitulated the 3′ trimming of miR-362-5p (Figure 22), excluding the possibility that PARN may require essential co-factor(s) to execute miRNA trimming. These results collectively demonstrate that PARN is a *bona fide* trimmer acting on the 3′ end of miR-362-5p.

Figure 18. Identification of PARN as a miR-362-5p trimmer.

Several 3′-to-5′ exoribonucleases associated with the miRNA pathway were individually depleted in HEK293T cells and the maturation of ectopically expressed miR-362-5p was monitored by northern blotting. The fraction of the shorter miR-362-5p isoform (24 nt) was calculated by densitometry and is plotted below. Error bars represent standard error of the mean (SEM) from two biologically independent experiments and asterisks indicate statistical significance of the decrease in the fraction of the shorter isoform calculated by one-tailed paired *t*-test (** $p<0.01$). Knockdown efficiency for each enzyme determined by qRT-PCR is also provided.

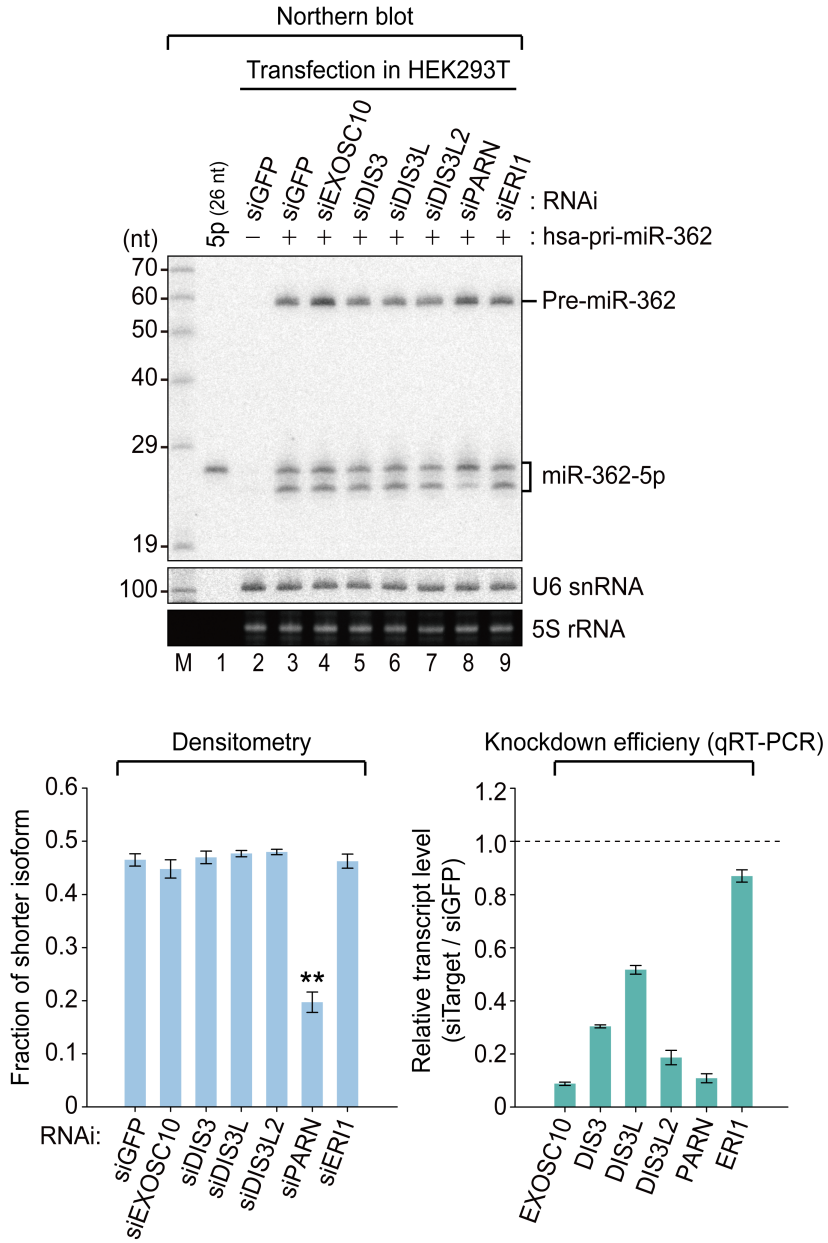
Northern blot
Transfection in HEK293T
5p (26 nt)
siGFP
siGFP
siEXOSC10
siDIS3
siDIS3L
siDIS3L2
siPARN
siERI1
: RNAi
: hsa-pri-miR-362
(nt)
70
60
50
40
29
19
100
Pre-miR-362
miR-362-5p
U6 snRNA
5S rRNA
M 1 2 3 4 5 6 7 8 9
Densitometry
Fraction of shorter isoform
0.6
0.5
0.4
0.3
0.2
0.1
0
**
RNAi:
siGFP
siEXOSC10
siDIS3
siDIS3L
siDIS3L2
siPARN
siERI1
Knockdown efficieny (qRT-PCR)
Relative transcript level
(siTarget / siGFP)
1.2
1.0
0.8
0.6
0.4
0.2
0
EXOSC10
DIS3
DIS3L
DIS3L2
PARN
ERI1

Figure 19. Complementation assay and overexpression of *trans*-dominant negative PARN mutant.

(A) Complementation of PARN activity restores the normal isoform ratio of miR-362-5p. HEK293T cells were first transfected with either siGFP (lanes 3 and 9) or siPARN (lanes 4-8 and 10-14). Twenty four hours after the first transfection, a fixed amount of the pri-miR-362 expression plasmid (1 μg per 35-mm dish) and variable amounts of the PARN expression plasmid (0.128 μg for lanes 5 and 11, 0.32 μg for lanes 6 and 12, 0.8 μg for lanes 7 and 13, and 2 μg for lanes 8 and 14) were introduced and further incubated for 48 hr. The amount of total plasmid DNA was adjusted with empty vector to 3 μg per 35-mm dish.

(B) Overexpression of D28A PARN interferes with the trimming of miR-362-5p by endogenous PARN. The fraction of the shorter miR-362-5p isoform (24 nt) is plotted on the right side. Error bars represent SEM from two biologically independent experiments and the asterisk indicates statistical significance of the decrease in the fraction of the shorter isoform calculated by one-tailed paired *t*-test (* $p<0.05$).

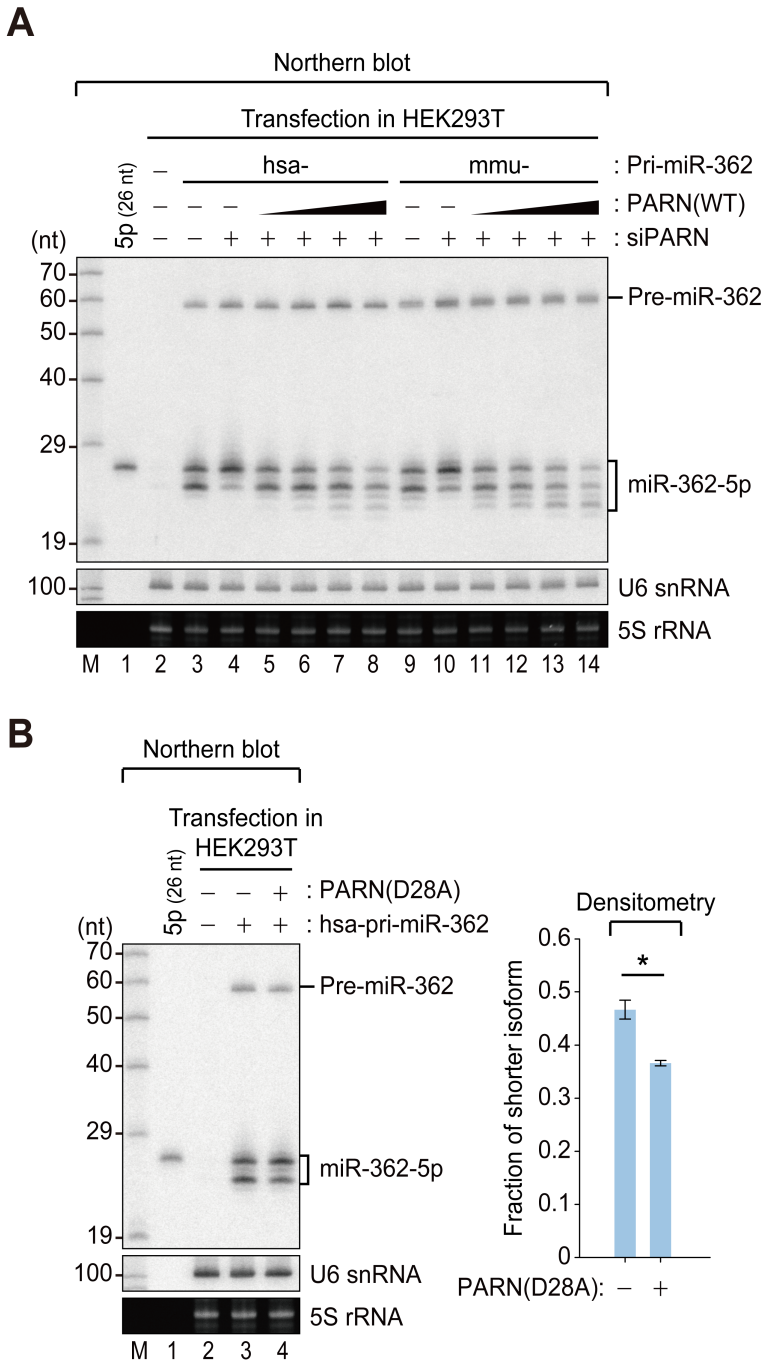
A
Northern blot
Transfection in HEK293T
hsa-
mmu-
: Pri-miR-362
: PARN(WT)
: siPARN
5p (26 nt)
(nt)
70
60
50
40
29
19
100
Pre-miR-362
miR-362-5p
U6 snRNA
5S rRNA
M 1 2 3 4 5 6 7 8 9 10 11 12 13 14
B
Northern blot
Transfection in HEK293T
: PARN(D28A)
: hsa-pri-miR-362
Densitometry
Fraction of shorter isoform
PARN(D28A):
*
Pre-miR-362
miR-362-5p
U6 snRNA
5S rRNA
M 1 2 3 4

Figure 20. The effects of PARN knockdown on miR-362-5p originating from the synthetic duplex.

PARN-mediated trimming takes place after DICER processing. The indicated miR-362 duplex was introduced into HeLa S3 cells pre-treated with siGFP or siPARN, and the 3′ processing of miR-362-5p was analyzed. Successful knockdown was confirmed by western blotting. The fraction of the shorter miR-362-5p isoforms (22-24 nt) is plotted below. Error bars represent SEM from two biologically independent experiments and asterisks indicate statistical significance of the decrease in the fraction of the shorter isoform calculated by one-tailed paired *t*-test (* $p<0.05$, *** $p<0.005$).

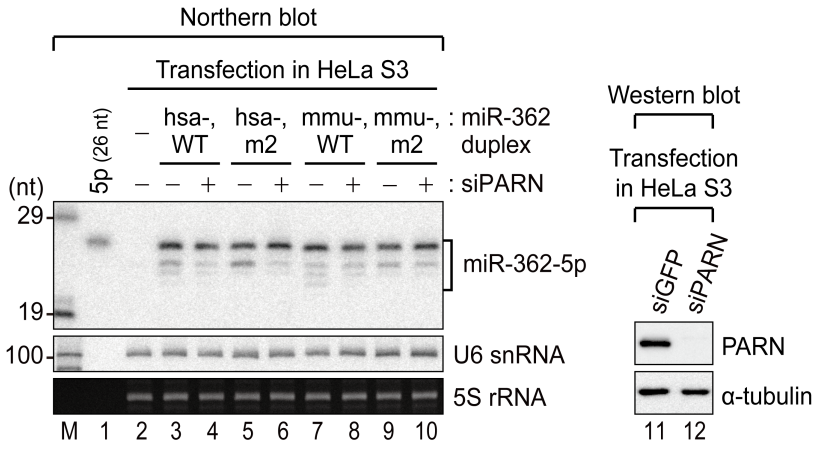
Northern blot
Transfection in HeLa S3
(nt)
5p (26 nt)
–
hsa-, WT
hsa-, m2
mmu-, WT
mmu-, m2
: miR-362 duplex
: siPARN
29
19
100
miR-362-5p
U6 snRNA
5S rRNA
M 1 2 3 4 5 6 7 8 9 10
Western blot
Transfection in HeLa S3
siGFP
siPARN
PARN
α-tubulin
11 12

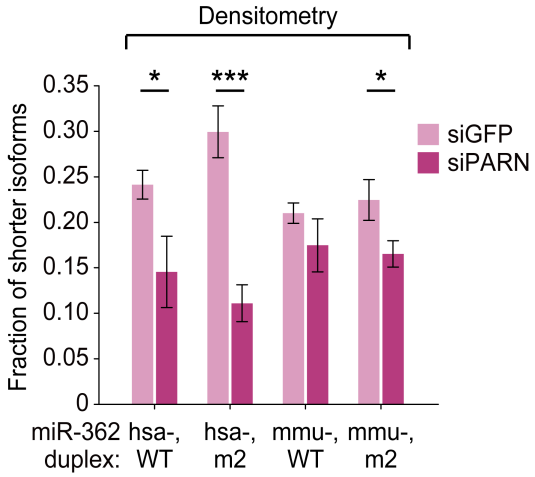
Densitometry
Fraction of shorter isoforms
0.35
0.30
0.25
0.20
0.15
0.10
0.05
0
*
***
*
siGFP
siPARN
miR-362 duplex:
hsa-, WT
hsa-, m2
mmu-, WT
mmu-, m2

Figure 21. *In vitro* trimming of AGO2-loaded miR-362-5p with lysates from HeLa S3 cells in which PARN expression was manipulated.

(A) Western blot analysis of lysates from HeLa S3 cells in which PARN was depleted or overexpressed. Alpha-tubulin served as a loading control.

(B) *In vitro* trimming of AGO2-loaded miR-362-5p with lysates from PARN-manipulated HeLa S3 cells. The fraction of trimmed species (~22-25 nt) was calculated by densitometry and is plotted below, with error bars representing SEM from two independent experiments.

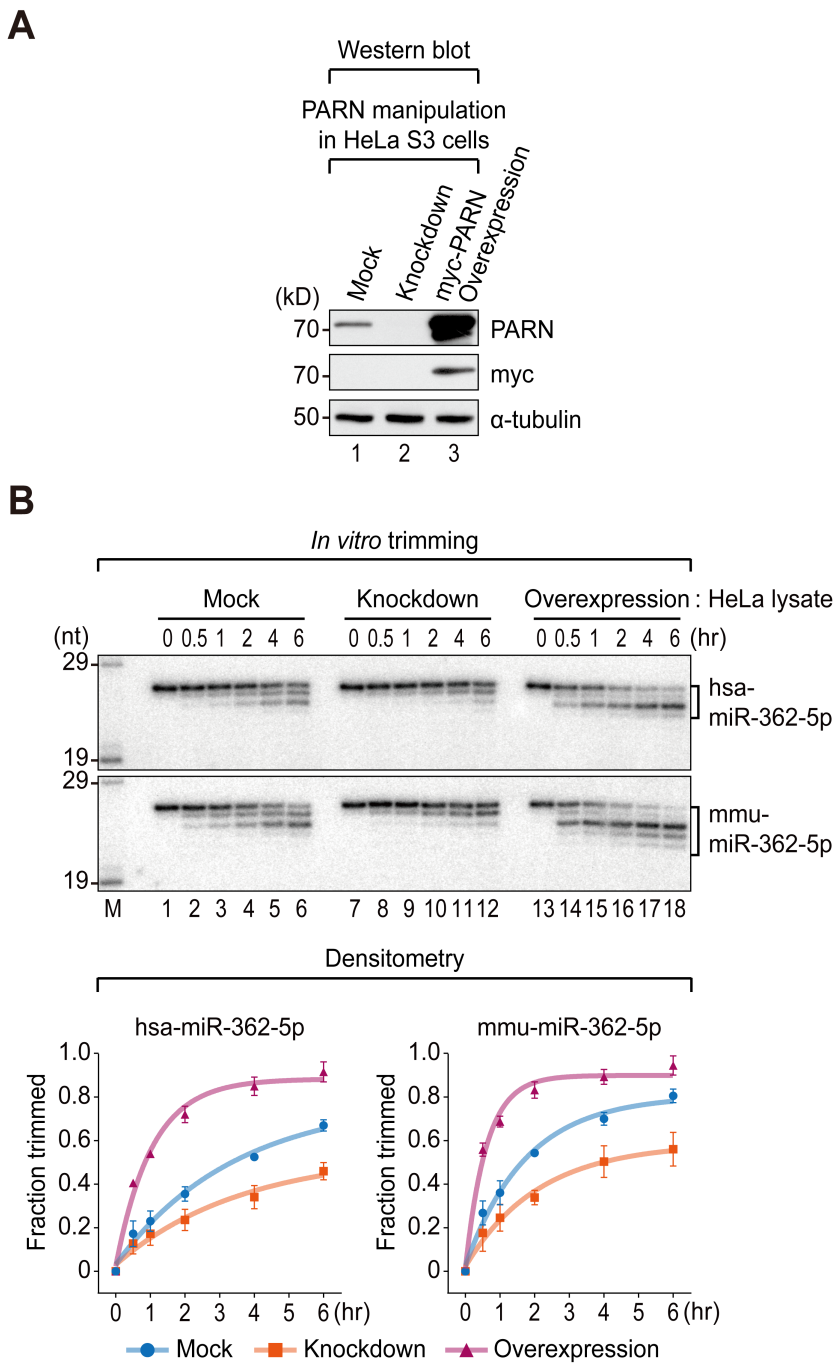
A
Western blot
PARN manipulation
in HeLa S3 cells
Mock
Knockdown
myc-PARN
Overexpression
(kD)
70
PARN
70
myc
50
α-tubulin
1 2 3
B
In vitro trimming
Mock
Knockdown
Overexpression : HeLa lysate
(nt)
0 0.5 1 2 4 6 0 0.5 1 2 4 6 0 0.5 1 2 4 6 (hr)
29
19
hsa-
miR-362-5p
29
19
mmu-
miR-362-5p
M 1 2 3 4 5 6 7 8 9 10 11 12 13 14 15 16 17 18
Densitometry
hsa-miR-362-5p
mmu-miR-362-5p
Fraction trimmed
1.0
0.8
0.6
0.4
0.2
0
0 1 2 3 4 5 6 (hr)
Mock
Knockdown
Overexpression

Figure 22. *In vitro* trimming of AGO2-loaded miR-362-5p with recombinant PARN purified from *E. coli*.

(A) Coomassie brilliant blue (CBB) staining of recombinant GST-PARN produced in and purified from *E. coli*.

(B) *In vitro* trimming of AGO2-loaded miR-362-5p with recombinant GST-PARN. The fraction of trimmed species (~21-25 nt) was calculated by densitometry and is plotted below, with error bars representing SEM from two independent experiments.

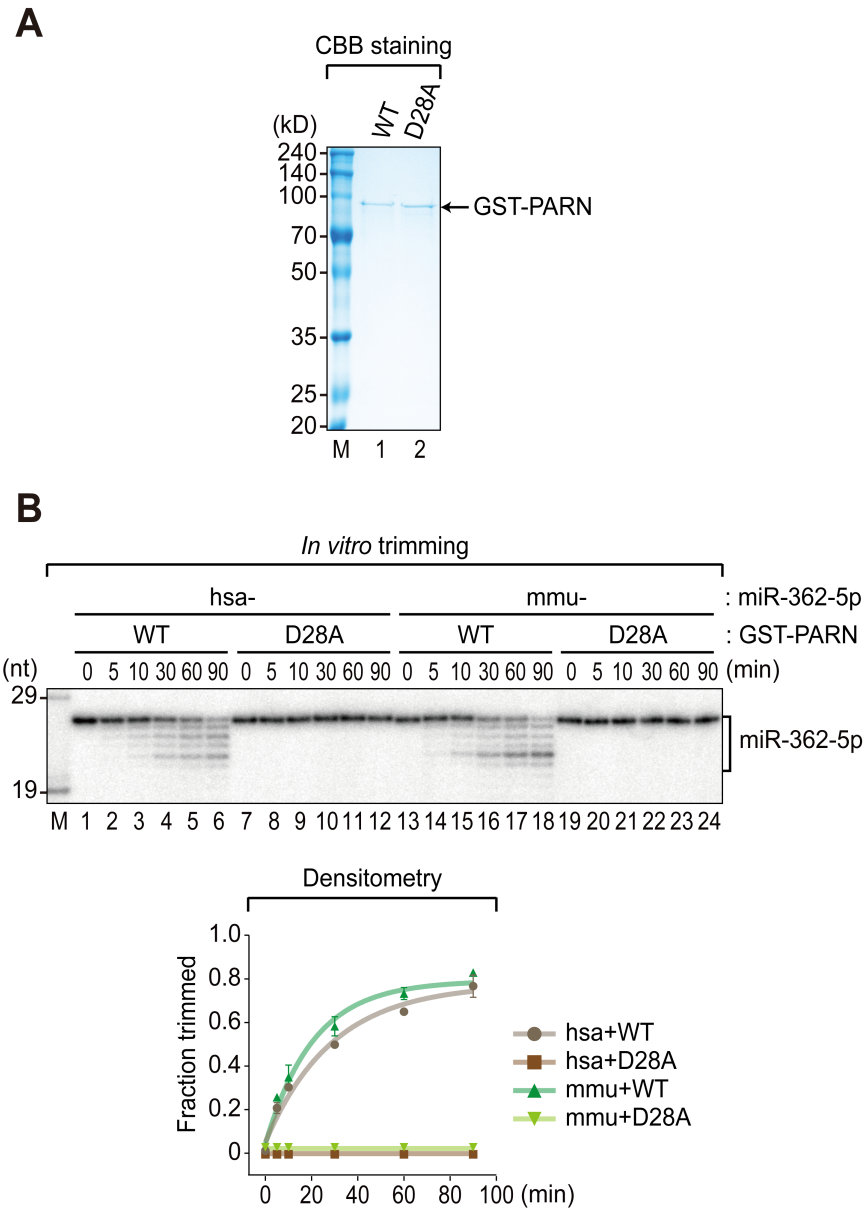
A
CBB staining
WT
D28A
(kD)
240
140
100
70
50
35
25
20
GST-PARN
M 1 2
B
In vitro trimming
hsa-
mmu-
: miR-362-5p
WT
D28A
WT
D28A
: GST-PARN
(nt)
0 5 10 30 60 90 0 5 10 30 60 90 0 5 10 30 60 90 0 5 10 30 60 90 (min)
29
19
miR-362-5p
M 1 2 3 4 5 6 7 8 9 10 11 12 13 14 15 16 17 18 19 20 21 22 23 24
Densitometry
Fraction trimmed
1.0
0.8
0.6
0.4
0.2
0
0 20 40 60 80 100 (min)
hsa+WT
hsa+D28A
mmu+WT
mmu+D28A

The impact of PARN on the miRNAome

PARN is involved in the biogenesis of miR-451, an atypical miRNA whose precursor bypasses DICER processing (Figure 5) (Yoda et al., 2013). Notably, my findings as well as recent reports on two model miRNAs (Boele et al., 2014; Katoh et al., 2015) suggest that small RNA substrates of PARN may not be limited to ac-pre-miR-451, but may also broadly include canonical miRNAs (Figures 18-22). The proposed outcomes of PARN-mediated trimming diverged across miRNAs (Figure 9), either triggering the degradation for miR-21 and miR-122 (Boele et al., 2014; Katoh et al., 2015) or finalizing the maturation without altering the steady-state levels for miR-451 (Yoda et al., 2013) and miR-362-5p (Figures 18-22). To comprehensively examine the impact of PARN on the mammalian miRNAome, *PARN* knockout (KO) HeLa S3 cells were generated using CRISPR/Cas9 technology. For this purpose, a guide RNA was designed to target the second coding exon of the human *PARN* gene (Figure 23A), and the resulting gene editing construct was introduced into HeLa S3 cells. Following clonal selection, two independent clones with a complete absence of the PARN protein were obtained (Figure 23B). Sequencing-based genotyping confirmed the presence of frame-shifting indels on the targeted locus (Figure 23C). *PARN* KO cells exhibited slightly retarded proliferation (data not shown) but were still viable throughout multiple passages, suggesting that the activity of PARN is not essential, at least in cultured cells.

Next, small RNA deep sequencing was performed on ~18-30 nt RNA isolated from parental cells and individual *PARN* KO clones. First, the length distribution of miRNAs in each sample was analyzed, with the idea that PARN-mediated trimming of 3′ ends would reduce the size of miRNAs. Notably, the distribution was shifted by ~1 nt toward longer species upon ablation of *PARN*, such that the length of

miRNAs from *PARN* KO cells peaked at 23 nt rather than 22 nt (Figure 24A). On the other hand, the steady-state levels of miRNAs were not altered apparently in *PARN* KO cells (Figure 24B), suggesting that PARN regulates the length, but not the abundance, of mature miRNAs on a global scale.

Figure 23. Generation of *PARN* KO HeLa S3 cells.

(A) Domain architecture of human PARN. The red scissors mark the position of the site targeted by CRISPR/Cas9 nuclease.

(B) Western blot analysis of lysates from parental HeLa S3 cells and two independent *PARN* KO clones. Alpha-tubulin and beta-actin served as loading controls.

(C) PCR-based genotyping of the targeted locus in *PARN* KO cells. Exonic and intronic sequences are indicated by black uppercase and gray lowercase letters, respectively. The nucleotide sequence complementary to the guide RNA and the protospacer adjacent motif are shown in red and blue, respectively. The type and frequency of indels identified by Sanger sequencing is indicated on the right side.

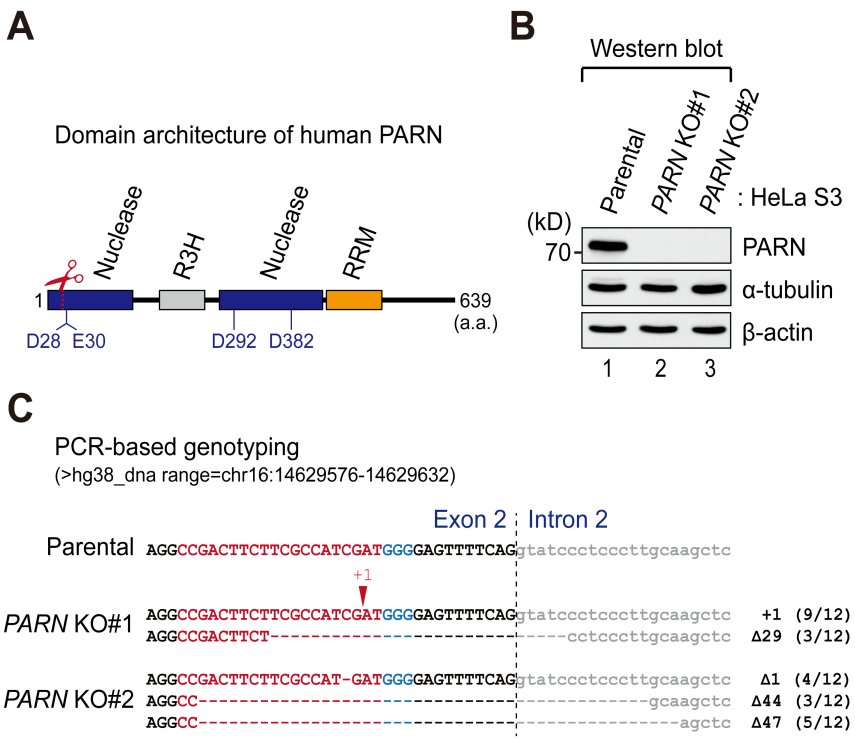
A
Domain architecture of human PARN
Nuclease
R3H
Nuclease
RRM
1
639
(a.a.)
D28 E30
D292 D382
B
Western blot
Parental
PARN KO#1
PARN KO#2
: HeLa S3
(kD)
70
PARN
α-tubulin
β-actin
1 2 3
C
PCR-based genotyping
(>hg38_dna range=chr16:14629576-14629632)
Exon 2
Intron 2
Parental
AGGCCGACTTCTTCGCCATCGATGGGGAGTTTTCAGgtatccctcccttgcaagctc
+1
PARN KO#1
AGGCCGACTTCTTCGCCATCGATGGGGAGTTTTCAGgtatccctcccttgcaagctc +1 (9/12)
AGGCCGACTTCT----------cctcccttgcaagctc Δ29 (3/12)
PARN KO#2
AGGCCGACTTCTTCGCCAT-GATGGGGAGTTTTCAGgtatccctcccttgcaagctc Δ1 (4/12)
AGGCC----------gcaagctc Δ44 (3/12)
AGGCC----------agctc Δ47 (5/12)

Figure 24. The impact of PARN on the HeLa miRNAome.

(A) PARN reduces the length of mature miRNAs. The length distribution of total small RNA sequencing reads mapped to the miRNA loci is presented.

(B) PARN does not affect the abundance of mature miRNAs. Normalized read counts for individual miRNAs in each cell line, presented as reads per 30 million (RP30M), were compared. The boundaries for two-fold expression changes are indicated by red dashed lines.

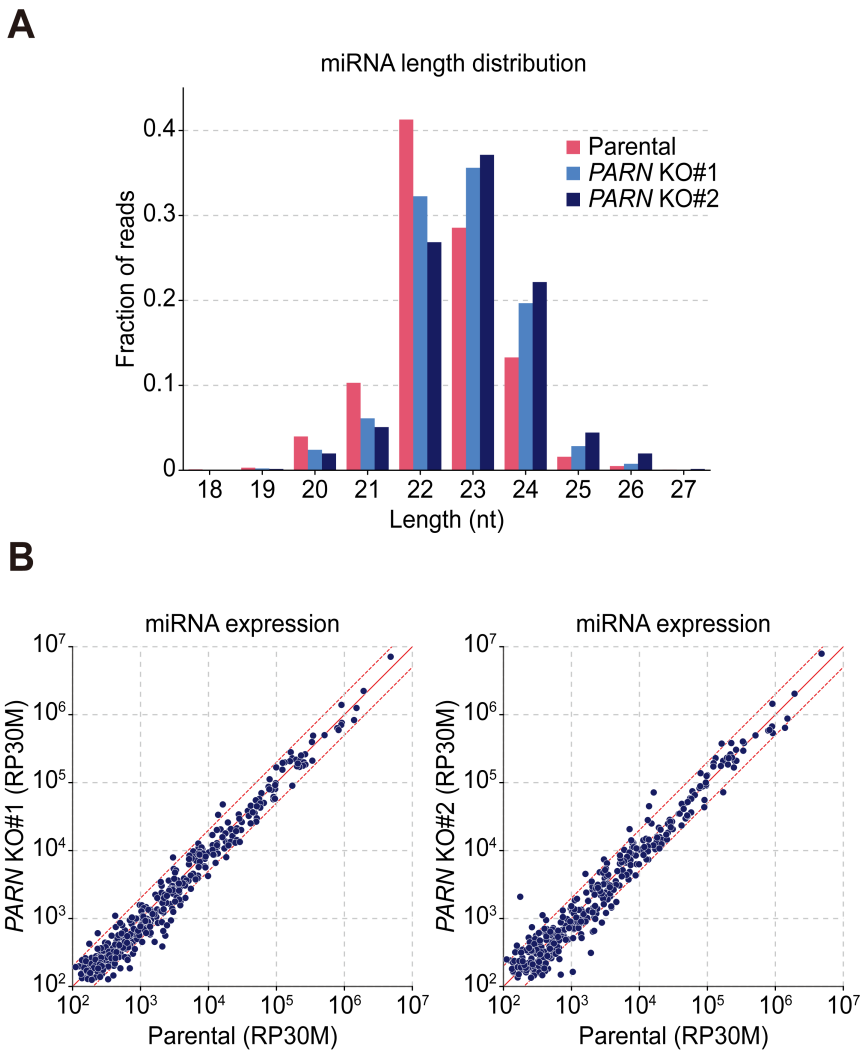
A
miRNA length distribution
Fraction of reads
0.4
0.3
0.2
0.1
0
Parental
PARN KO#1
PARN KO#2
18
19
20
21
22
23
24
25
26
27
Length (nt)
B
miRNA expression
PARN KO#1 (RP30M)
Parental (RP30M)
miRNA expression
PARN KO#2 (RP30M)
Parental (RP30M)

Mechanisms of PARN-mediated miRNA shortening

My data from biochemical and cell-based assays suggest a model for the biogenesis of miR-362-5p: DICER cleaves pre-miR-362 asymmetrically, perhaps because of the internal tri-nucleotide bulge (Figure 10), such that the resulting miRNA duplex contains the 26 nt 5p strand (Figure 12). Once selected by AGO proteins, this strand is subsequently trimmed at the 3′ end by PARN to generate the ~22-24 nt isoforms (Figures 18-22). Thus, although their upstream effectors are quite different, the genome-matching portions of both miR-451 and miR-362-5p are actively digested by PARN (Yoda et al., 2013). On the other hand, PARN is known to remove post-transcriptionally added mono or oligo(A) tails from miR-21 and miR-122 to promote their destabilization (Boele et al., 2014; Katoh et al., 2015).

Based on these observations, it was hypothesized that PARN may shorten the length of miRNAs by two distinct modes, depending on the origin of the nucleotide being resected. PARN may function as a "trimmer" to nibble the portion of miRNA sequence encoded by the genome, and/or as a "de-tailor" to erase untemplated nucleotide addition (Figure 25). To investigate whether both modes do indeed operate, small RNA sequencing reads were divided into two categories: genome-matching reads and prefix-matching reads (Figure 26A). Prefix-matching reads refer to those containing one or more non-genome-matching nucleotides at the 3′ end (Reimao-Pinto et al., 2015), and are therefore expected to represent unambiguous 3′ nucleotide addition events. Approximately 14% of total reads from parental HeLa S3 cells fell into this category (discussed below), reaffirming widespread 3′ modification of miRNAs by untemplated nucleotide addition. Next, the length distribution of reads from each category was individually examined, with the idea that the lengthening of miRNAs upon *PARN* deletion should be observed only in one

category if one of the two modes dominates. This was not the case, however, because the lengths of both the genome-matching reads and the prefix-matching reads were elongated in *PARN* KO cells to a similar extent (Figure 26B). These data indicate that PARN functions as both a trimmer and a de-tailor in miRNA metabolism.

Figure 25. Two distinct modes of PARN-mediated miRNA shortening.

Illustration of the roles of PARN as a “trimmer” and a “de-tailor” in miRNA metabolism. The dominantly abundant miRNA isoform in cells, which would therefore be the probable sequence annotated by sequencing-based databases, is shown in red. As a trimmer, PARN digests the genome-encoded 3′ extensions of miRNAs such that the shorter species occasionally becomes most abundant. As a de-tailor, PARN removes untemplated nucleotides from the 3′ end of miRNAs.

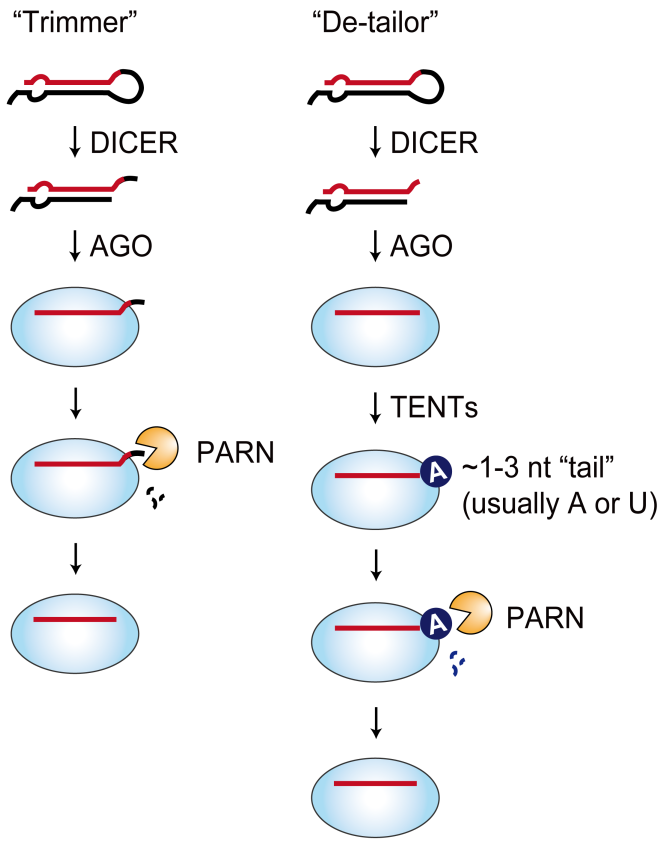
“Trimmer”
“De-tailor”
DICER
DICER
AGO
AGO
TENTs
PARN
~1-3 nt “tail”
(usually A or U)
A
A
PARN

Figure 26. PARN as both a trimmer and a de-tailor.

(A) Separation of small RNA sequencing reads into two categories. Genome-matching reads refer to those that are perfectly and contiguously mapped to the genome. Prefix-matching reads indicate those containing one or more non-genome-matching nucleotides at the 3′ end. The terms (“genome-matching” and “prefix-matching”) and the illustration for each category were adopted or modified from a previous report (Reimao-Pinto et al., 2015).

(B) PARN functions as both a trimmer and a de-tailor. The length distributions of genome-matching and prefix-matching reads are presented.

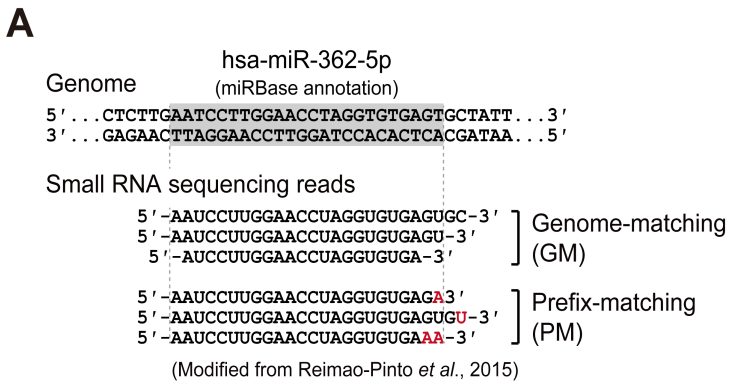
A
hsa-miR-362-5p
(miRBase annotation)
Genome
5′...CTCTTGAATCCTTGGAACCTAGGTGTGAGTGCTATT...3′
3′...GAGAACTTAGGAACCTTGGATCCACACTCACGATAA...5′
Small RNA sequencing reads
5′-AAUCCUUGGAACCUAGGUGUGAGUGC-3′
5′-AAUCCUUGGAACCUAGGUGUGAGU-3′
5′-AUCCUUGGAACCUAGGUGUGA-3′
Genome-matching
(GM)
5′-AAUCCUUGGAACCUAGGUGUGAGA3′
5′-AAUCCUUGGAACCUAGGUGUGAGUGU-3′
5′-AAUCCUUGGAACCUAGGUGUGAAA-3′
Prefix-matching
(PM)
(Modified from Reimao-Pinto et al., 2015)

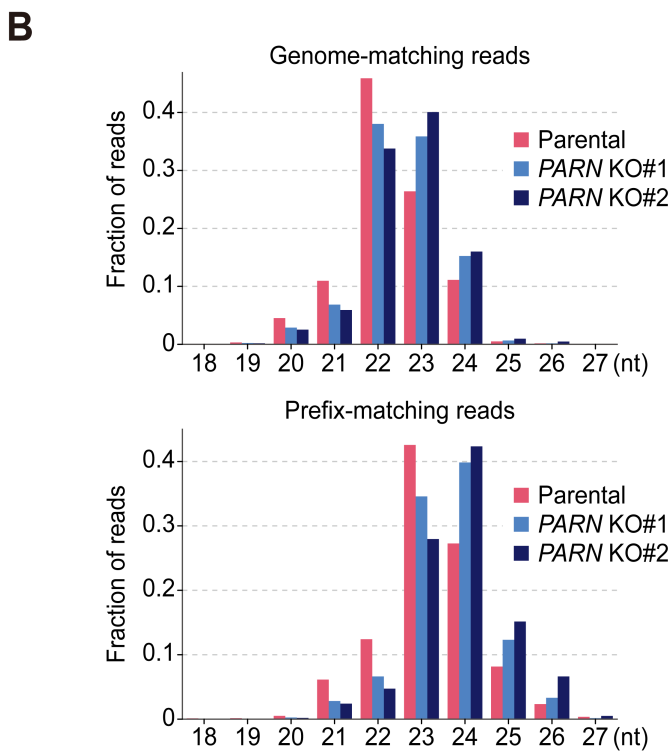
B
Genome-matching reads
Fraction of reads
0.4
0.3
0.2
0.1
0
18 19 20 21 22 23 24 25 26 27 (nt)
Parental
PARN KO#1
PARN KO#2
Prefix-matching reads
Fraction of reads
0.4
0.3
0.2
0.1
0
18 19 20 21 22 23 24 25 26 27 (nt)
Parental
PARN KO#1
PARN KO#2

PARN as a general miRNA trimmer

To investigate the role of PARN as a miRNA trimmer in more detail, the fraction of genome-matching reads that have extensions beyond the 3′ end of the reference sequence annotated in miRBase (designated “Fraction +1”) was calculated for each miRNA (Figure 27). Because miRbase entries are deposited mainly on the basis of high-throughput sequencing, it is likely that the miRBase sequence would represent miRNA species that had undergone post-processing modifications such as 3′ trimming, as illustrated by the case of miR-362-5p (Figure 10). Keeping this in mind, it was examined how the fraction of 3′-extended reads changed in *PARN* KO cells, with the expectation that the difference would reflect the extent to which a given miRNA is subjected to PARN-mediated trimming. For example, 1,892 genome-matching reads were obtained for miR-362-5p in parental HeLa S3 cells (despite the failure to detect it with northern blotting; see Figures 15B and 20) and 441 of them were longer than 24 nt, the length of the miRBase sequence for this miRNA: thus, “Fraction +1” for miR-362-5p in parental cells was calculated as 441/1,892 = ~23.3%. On the other hand, “Fraction +1” for the same miRNA in *PARN* KO cells turned out to be ~42.5% and ~78.3% in clones #1 and #2, respectively. Here, the arithmetic difference of “Fraction +1” between parental and *PARN* KO cells was taken as a measure of PARN-mediated trimming for this miRNA: for example, (~78.3%)−(~23.3%) = ~55 percent points were assigned to miR-362-5p in the comparison between parental and *PARN* KO#2 cells.

Strikingly, among the 247 miRNAs examined, 179 (~72%) were more frequently 3′-extended in both *PARN* KO clones than in parental cells, and 77 (~31%) exhibited average changes in the 3′-extended fraction of more than 5 percent points, demonstrating widespread PARN-mediated trimming of miRNAs (Figure 28). Both

5p and 3p miRNAs were lengthened at their 3′ ends in *PARN* KO cells (Figure 28), supporting the notion that PARN trims mature miRNAs liberated by DICER processing (Figure 25). Some miRNAs appeared to be efficiently trimmed by PARN, with the changes in the 3′-extended fraction even exceeding 25 percent points, as exemplified by miR-425-5p, miR-361-3p, miR-182-5p, miR-301a-3p, and my experimental model miRNA, miR-362-5p (Figure 28). Next, analysis was extended to the genome-matching reads containing *two* or more nucleotides at the 3′ end ("Fraction +2"), because some miRNAs could potentially be missing from the current analysis if their PARN-mediated trimming mostly occurred outside of the reference sequence. As one such miRNA, miR-224-5p ranked 92nd in the first analysis with an average change of ~2.8 percent points, but ranked 1st in the second analysis with an average change of ~40 percent points (Figures 28 and 29). The reference sequence of miR-224-5p is 21 nt in length, but this miRNA existed in two dominantly abundant isoforms of 22 nt and 24 nt in parental cells, the latter of which was likely trimmed by PARN to generate the former (Figure 29). The fraction of reads with *three* or more genome-matching nucleotides ("Fraction +3") was generally low across most miRNAs and barely changed upon *PARN* deletion, except for miR-224-5p (Figures 28 and 29), suggesting that PARN tailors miRNAs to the reference sequence by trimming their 3′ ends by ~1-2 nt.

To validate the analysis, small RNA northern blotting was performed with total RNA prepared from parental and *PARN* KO cells. Trimming was clearly manifested by the shift of miRNA isoforms toward ~1-2 nt longer species in *PARN* KO cells, which was in good agreement with the observed changes in the length distribution of sequencing reads for individual miRNAs (Figure 30). One prominent example was miR-182-5p, the dominantly abundant isoform of which was 24 nt in

parental cells but became 26 nt in both *PARN* KO clones. To address whether PARN-mediated trimming of miRNAs operates in other cell types, PARN was depleted in four different human cell lines and changes in the isoform distribution of miRNAs were monitored by northern blotting. Notably, the miRNAs that were trimmed in HeLa S3 cells were also consistently trimmed in all cell lines tested (Figure 31), suggesting that PARN-mediated trimming of a specific miRNA is an inherent feature of its maturation rather than a cell-type-specific event. It is noteworthy that the composition of genome-matching 3′ nucleotides resected by PARN is surprisingly diverse and is not particularly enriched for A (Figure 32), the nucleotide most preferred by PARN *in vitro* (Henriksson et al., 2010). The steady-state levels of all miRNAs examined were comparable in control and PARN-depleted cells (Figures 30 and 31), reaffirming that PARN-mediated trimming does not generally lead to changes in miRNA stability (Figure 24B).

To examine whether untrimmed miRNAs in *PARN* KO cells associate with AGO proteins as efficiently as trimmed miRNAs in parental cells, peptide-based affinity purification of AGO proteins (termed “AGO-APP”) was utilized to isolate endogenous miRISC from HeLa whole cell lysate (Hauptmann et al., 2015). A small peptide derived from the AGO-binding domain of human TNRC6B (T6B) was fused to GST and used as a bait for AGO affinity purification (Figures 33A and 33B). As previously reported (Hauptmann et al., 2015), GST-T6B was capable of precipitating all human AGO proteins (AGO1-4) exogenously expressed in HEK293T cells (Figure 33C), and isolating the endogenous pool of AGO proteins equipped with miRNAs from HeLa S3 lysate (Figure 33D). Notably, AGO-APP from parental or *PARN* KO cells enriched the miRNAs to a similar extent, without altering the overall length distribution of the miRNA isoforms (Figure 34), suggesting that PARN-

mediated trimming does not affect the interaction of miRNAs with AGO proteins.

To address whether 3′ trimming affects miRNA-mediated gene silencing, miR-182-5p was chosen as a model miRNA, because it was one of the miRNAs most efficiently trimmed by PARN in HeLa S3 cells (Figures 28 and 30). The regulatory activity of miR-182-5p was abolished in mock- or PARN-depleted HeLa S3 cells by introducing 2′-*O*Me-modified anti-miR-182-5p (Figure 35A), and the level of one of its target mRNAs, *FRS2*, was measured, which contains four canonical target sites for miR-182-5p in its 3′-UTR (Agarwal et al., 2015). The *FRS2* mRNA level was significantly increased upon transfection of anti-miR-182-5p, but the extent of its derepression was comparable in mock- and PARN-depleted cells (Figure 35B). A similar trend was observed for the expression of a luminescence-based reporter bearing one of the miR-182-5p target sites (Figures 35C), suggesting that PARN-mediated trimming is dispensable for miRNA-mediated regulation, at least in HeLa S3 cells. Given that miRNA-mediated repression of mRNAs involves deadenylation followed by destabilization (Jonas and Izaurralde, 2015), these results are in part consistent with the recent findings that downregulation of PARN causes no evident change in the poly(A) tail length or abundance of mRNAs (Moon et al., 2015; Son et al., 2018; Yi et al., 2018).

Figure 27. Definition of "Fraction *n*".

For each miRNA, "Fraction +1" was defined by the fraction of reads that contain *one* or more additional nucleotides at the 3′ end, compared with the reference sequence annotated in miRBase. "Fraction +2" and "Fraction +3" were defined similarly, by the fraction of reads that contain *two* or more and *three* or more nucleotides at the 3′ end, respectively. Note that only genome-matching reads were considered in these analyses for simplicity.

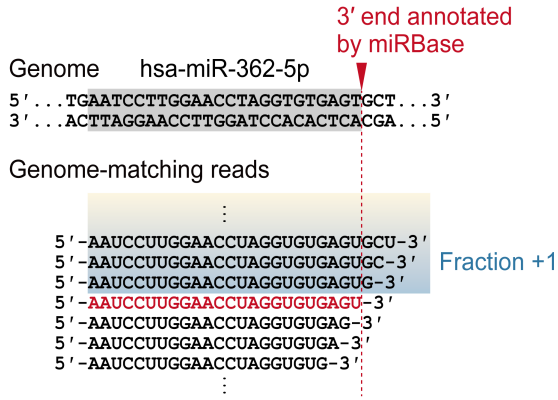
3′ end annotated
by miRBase
Genome
hsa-miR-362-5p
5′...TGAATCCTTGGAACCTAGGTGTGAGTGCT...3′
3′...ACTTAGGAACCTTGGATCCACACTCACGA...5′
Genome-matching reads
5′-AAUCCUUGGAACCUAGGUGUGAGUGCU-3′
5′-AAUCCUUGGAACCUAGGUGUGAGUGC-3′
5′-AAUCCUUGGAACCUAGGUGUGAGUG-3′
5′-AAUCCUUGGAACCUAGGUGUGAGU-3′
5′-AAUCCUUGGAACCUAGGUGUGAG-3′
5′-AAUCCUUGGAACCUAGGUGUGA-3′
5′-AAUCCUUGGAACCUAGGUGUG-3′
Fraction +1

Figure 28. PARN as a general miRNA trimmer.

(A) The fraction of 3′-extended miRNA isoforms upon *PARN* ablation. For 247 miRNAs whose genome-matching counts exceed 1,000 in parental HeLa S3 cells, “Fraction +1”, “Fraction +2”, and “Fraction +3” were calculated individually in parental and *PARN* KO cells. The 5p and 3p miRNAs are shown in blue and turquoise, respectively.

(B) Changes in “Fraction +1”, “Fraction +2”, and “Fraction +3” upon *PARN* deletion were calculated for each miRNA by *subtracting* the fraction in parental cells from the fraction in each *PARN* KO clone. The miRNAs with more than 25 percent point changes on average in the 3′-extended fraction are shown in red.

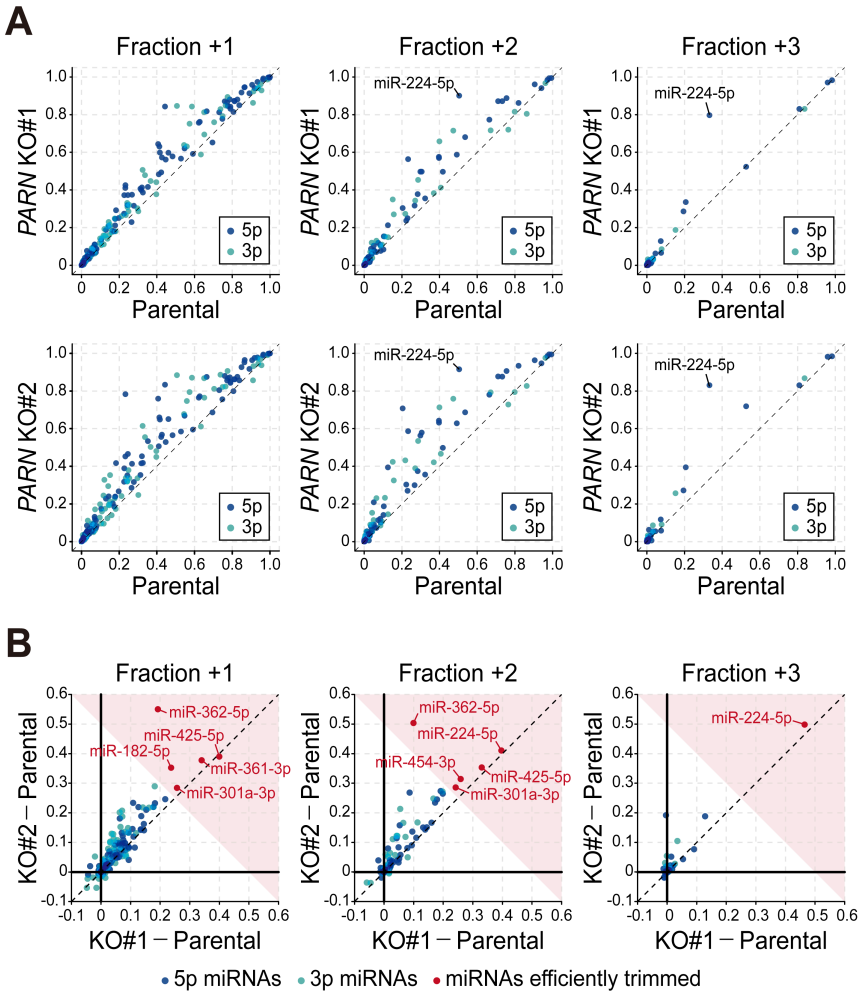
A
Fraction +1
Fraction +2
Fraction +3
PARN KO#1
PARN KO#2
Parental
5p
3p
miR-224-5p
B
KO#2 − Parental
KO#1 − Parental
miR-362-5p
miR-425-5p
miR-182-5p
miR-361-3p
miR-301a-3p
miR-224-5p
miR-454-3p
5p miRNAs
3p miRNAs
miRNAs efficiently trimmed

Figure 29. Changes in the 3′-extended fraction of miR-224-5p upon *PARN* ablation.

The miRBase sequence of miR-224-5p is 21 nt in length, but PARN trims this miRNA from 24 nt to 22 nt, rather than to 21 nt, such that the vast majority of miR-224-5p isoforms are longer than 21 nt. This explains the little change in “Fraction +1” of miR-224 upon *PARN* deletion, despite its high sensitivity to PARN, and rationalizes extending the analysis to “Fraction +2” and “Fraction +3”.

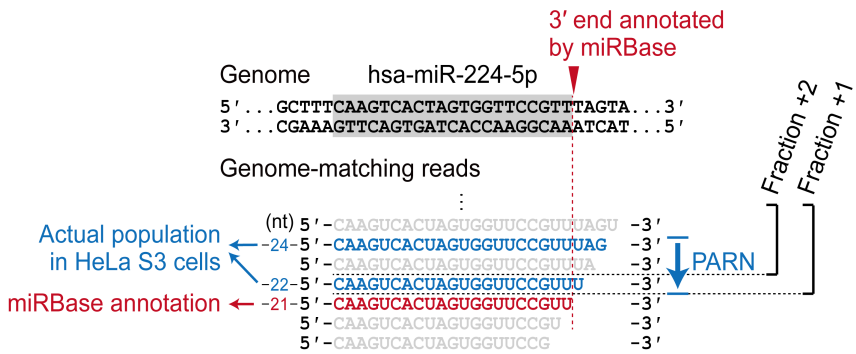

	Parental	*PARN* KO (mean)	Change in fraction (*PARN* KO − Parental)
Fraction +1	0.965	0.993	0.028
Fraction +2	0.504	0.908	0.403

Figure 30. Validation of PARN-mediated miRNA trimming.

The expression and length distribution was examined by small RNA northern blotting for six miRNAs that exhibited significant changes in the 3′-extended fraction (miR-224-5p, miR-182-5p, miR-425-5p, miR-361-3p, miR-301a-3p, and miR-454-3p; see Figure 28) and two miRNAs with negligible changes (miR-16-5p and miR-27a-3p). For miRNAs trimmed by PARN, the length distribution of sequencing reads for each miRNA in parental and *PARN* KO#2 cells is shown on the right side of the blot image. U1 snRNA, U6 snRNA, lysyl tRNA ($tRNA^{Lys}$), and 5S rRNA served as loading controls.

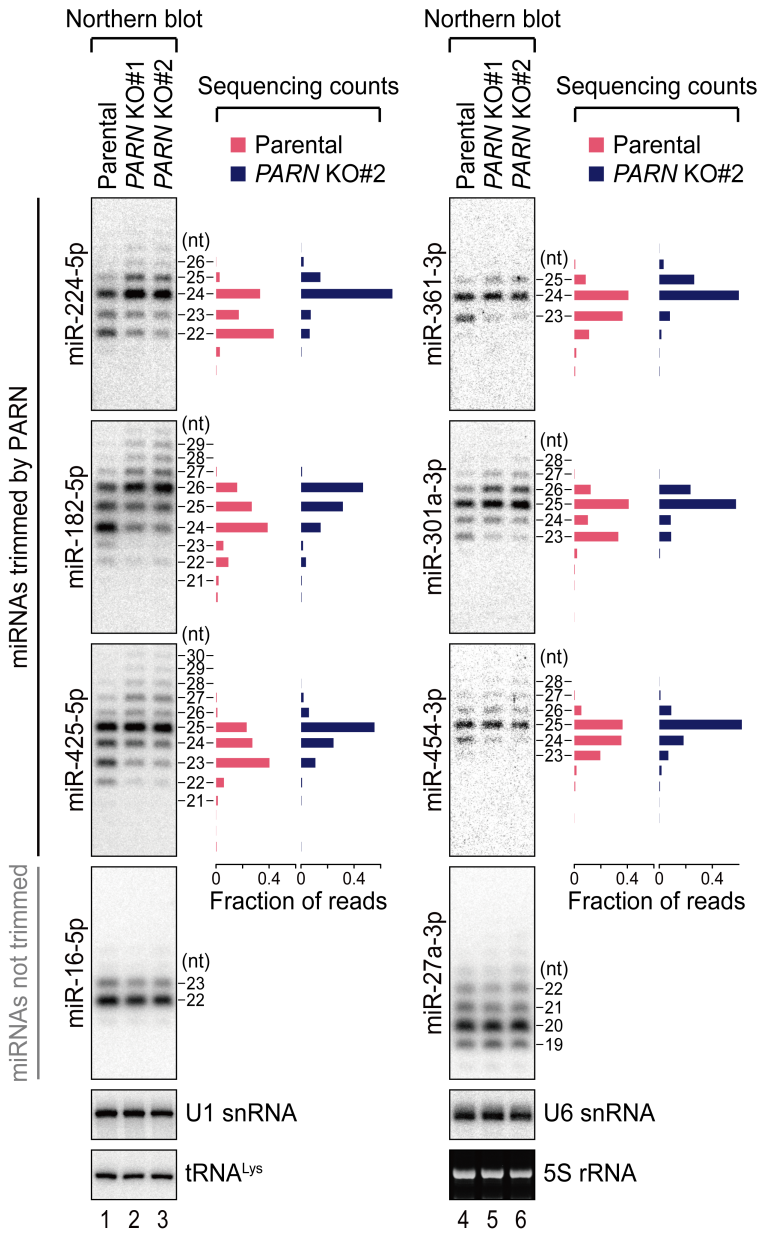
Northern blot
Parental
PARN KO#1
PARN KO#2
Sequencing counts
Parental
PARN KO#2
miRNAs trimmed by PARN
miRNAs not trimmed
miR-224-5p
miR-182-5p
miR-425-5p
miR-16-5p
miR-361-3p
miR-301a-3p
miR-454-3p
miR-27a-3p
(nt)
Fraction of reads
U1 snRNA
tRNALys
U6 snRNA
5S rRNA
1 2 3
4 5 6

Figure 31. PARN-mediated miRNA trimming in other cell lines.

PARN was depleted in four different human cell lines and the expression of miRNAs that were efficiently trimmed by PARN in HeLa S3 cells was examined by northern blot analysis. Knockdown efficiency was confirmed by western blotting (the last two rows). The purple bars indicate the shorter miRNA isoforms plausibly generated by PARN, the fraction of which was calculated for each miRNA and is plotted on the right side. Error bars and asterisks represent SEM and statistical significance from two independent experiments, respectively (* $p<0.05$, *** $p<0.005$, one-tailed paired *t*-test).

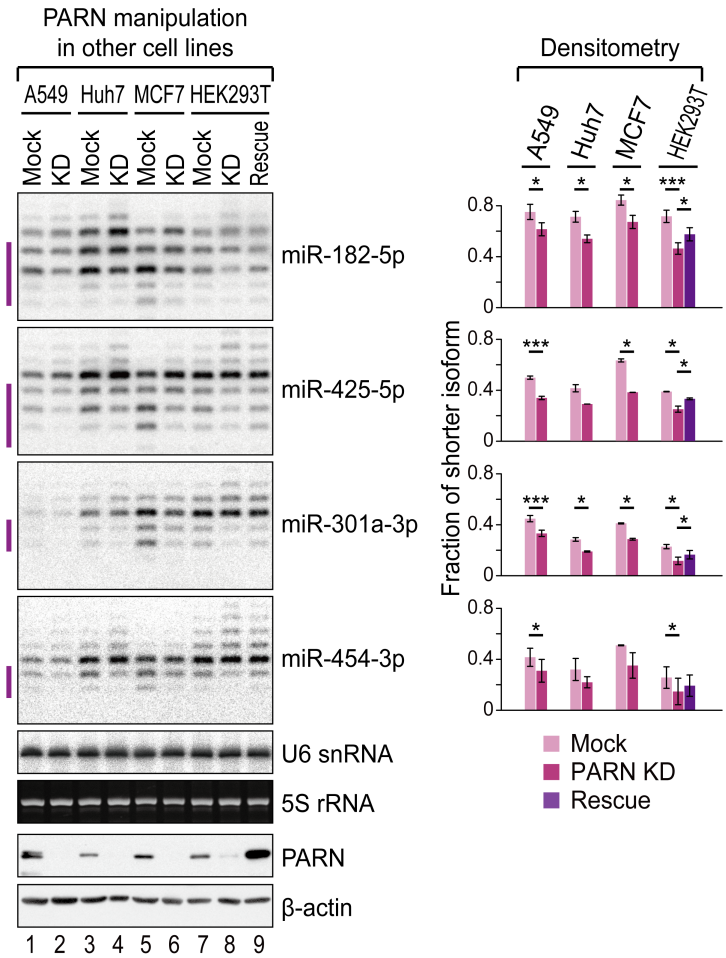
PARN manipulation
in other cell lines
A549
Huh7
MCF7
HEK293T
Mock
KD
Mock
KD
Mock
KD
Mock
KD
Rescue
miR-182-5p
miR-425-5p
miR-301a-3p
miR-454-3p
U6 snRNA
5S rRNA
PARN
β-actin
1 2 3 4 5 6 7 8 9
Densitometry
A549
Huh7
MCF7
HEK293T
Fraction of shorter isoform
0.8
0.4
0
Mock
PARN KD
Rescue

Figure 32. The composition of nucleotides trimmed by PARN.

The sequences of human miRNAs that undergo efficient 3′ trimming by PARN are presented. For each miRNA, the reference sequence annotated by miRBase is shown in red. With the exception of miR-451, which is not expressed in HeLa S3 cells, these miRNAs were selected based on a cutoff of 20 percent point mean changes in any of three 3′-extended fractions. The nucleotides resected by PARN, deduced from the changes in length distribution of isoforms in sequencing libraries, are indicated with blue shading.

Human miRNAs efficiently trimmed by PARN

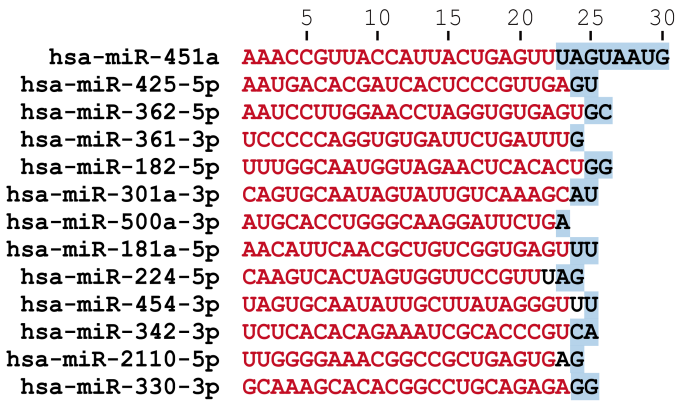

Figure 33. AGO affinity purification by peptides (AGO-APP).

(A) Schematic illustration of AGO-TNRC6 interactions. TNRC6 proteins contain a tryptophan-rich AGO-binding domain. In AGO-APP, a small peptide corresponding to the AGO-binding domain of human TNRC6B (residues 599-683; designated T6B) is fused to GST and used as a bait for pan-AGO affinity purification.

(B) CBB staining of the recombinant proteins used in AGO-APP.

(C) AGO-APP precipitates all human AGO proteins to a comparable efficiency. HEK293T cytoplasmic lysate containing the indicated FLAG-AGO protein was incubated with GST-T6B or GST immobilized on glutathione-agarose beads. After washing, co-purifying proteins were eluted and subjected to western blot analysis. Alpha-tubulin served as a loading control for input lysates and a negative control for AGO-APP.

(D) AGO-APP is capable of isolating endogenous miRISC. Whole cell lysate from untreated HeLa S3 cells was subjected to AGO-APP and co-purifying RNAs were extracted. Enrichment of selected miRNAs in the AGO-APP precipitate was examined by TaqMan MicroRNA assays. U6 snRNA served as a negative control for AGO-APP.

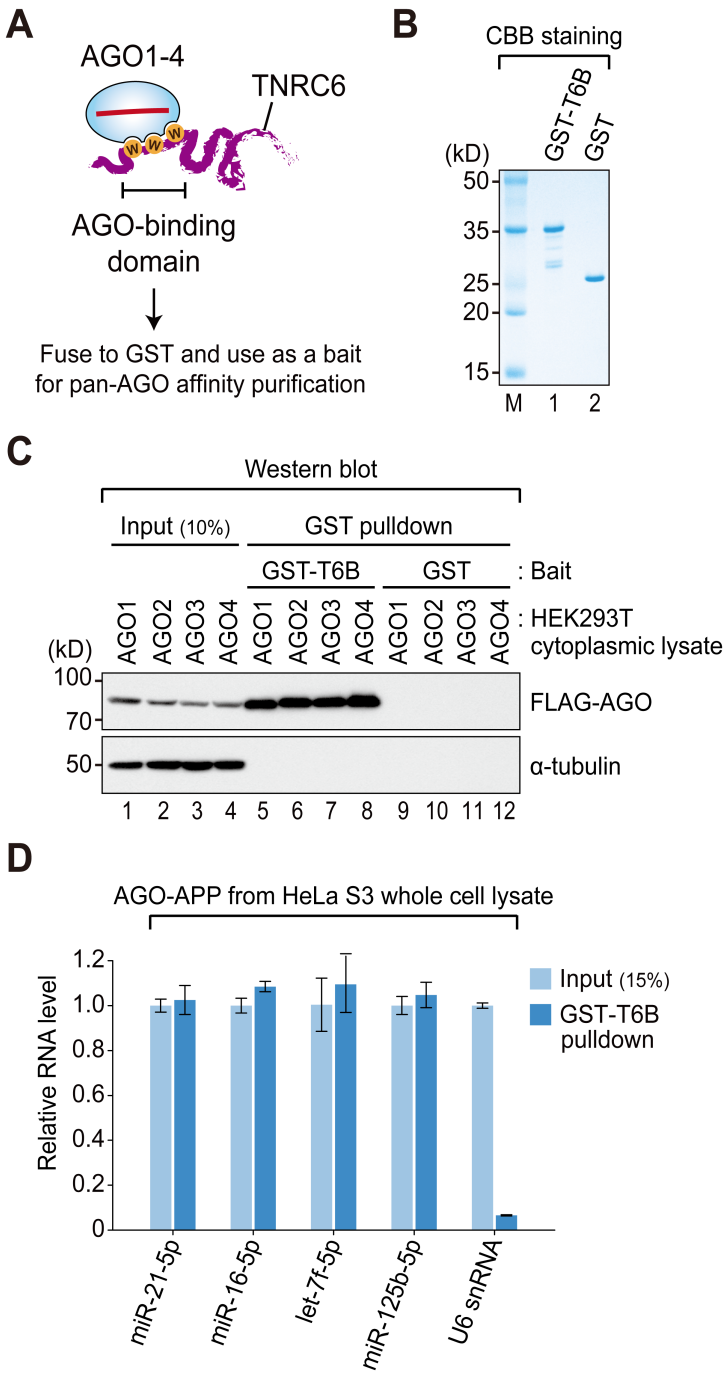
A
AGO1-4
TNRC6
AGO-binding domain
Fuse to GST and use as a bait for pan-AGO affinity purification
B
CBB staining
GST-T6B
GST
(kD)
50
35
25
20
15
M 1 2
C
Western blot
Input (10%)
GST pulldown
GST-T6B
GST
: Bait
AGO1 AGO2 AGO3 AGO4 AGO1 AGO2 AGO3 AGO4 AGO1 AGO2 AGO3 AGO4
: HEK293T cytoplasmic lysate
(kD)
100
70
50
FLAG-AGO
α-tubulin
1 2 3 4 5 6 7 8 9 10 11 12
D
AGO-APP from HeLa S3 whole cell lysate
Relative RNA level
1.2
1.0
0.8
0.6
0.4
0.2
0
Input (15%)
GST-T6B pulldown
miR-21-5p
miR-16-5p
let-7f-5p
miR-125b-5p
U6 snRNA

Figure 34. PARN-mediated trimming and miRNA-AGO interactions.

Endogenous miRISC was purified from lysates of parental or *PARN* KO#2 cells by AGO-APP and the enrichment and length distribution of co-purifying miRNAs was examined by northern blotting. $tRNA^{Lys}$ and 5S rRNA served as loading controls for input lysates and negative controls for AGO-APP.

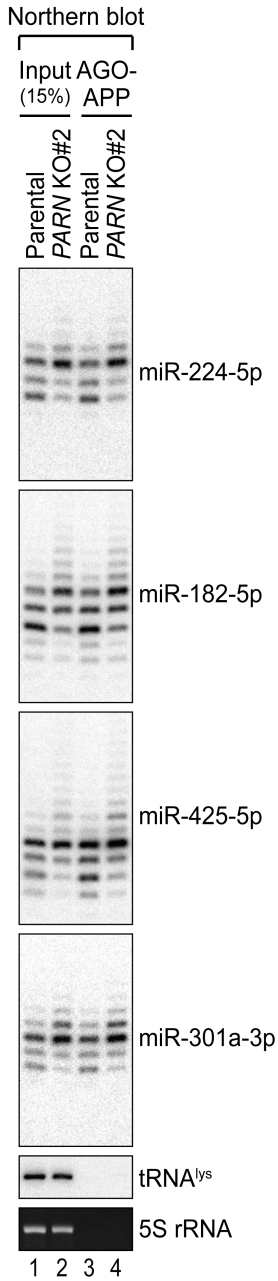
Northern blot
Input (15%)
AGO-APP
Parental
PARN KO#2
Parental
PARN KO#2
miR-224-5p
miR-182-5p
miR-425-5p
miR-301a-3p
tRNA^lys
5S rRNA
1 2 3 4

Figure 35. PARN-mediated trimming and miRNA targeting.

(A) Northern blot analysis of total RNAs from manipulated HeLa S3 cells. HeLa S3 cells pre-treated with control siRNA (siGFP) or siPARN were transfected with anti-miR-182-5p or anti-miR-1-3p. anti-miR-1-3p was used as a negative control because the cognate miRNA, miR-1-3p, is not expressed in HeLa S3 cells. The fraction of the shorter miR-182-5p isoforms in anti-miR-1-3p-treated cells was calculated as in Figure 31 and is plotted on the right side. Error bars represent SEM from three biologically independent experiments and asterisks indicate statistical significance of the decrease in the fraction of the shorter isoforms calculated by one-tailed paired *t*-test (*** $p<0.005$).

(B)(C) Derepression of *FRS2* mRNA or luciferase reporter bearing one of the miR-182-5p target sites within the *FRS2* 3′ UTR upon blocking miR-182-5p activity. The relative abundance of the *FRS2* mRNA in each sample was measured by qRT-PCR. Error bars represent SEM from three biologically independent experiments and asterisks indicate statistical significance of the increase in the relative *FRS2* mRNA level or reporter gene activity calculated by one-tailed paired *t*-test (** $p<0.01$, *** $p<0.005$). There were no significant differences in the extent of derepression between mock- and PARN-depleted cells (see dashed arrows; n.s., not significant, two-tailed paired *t*-test).

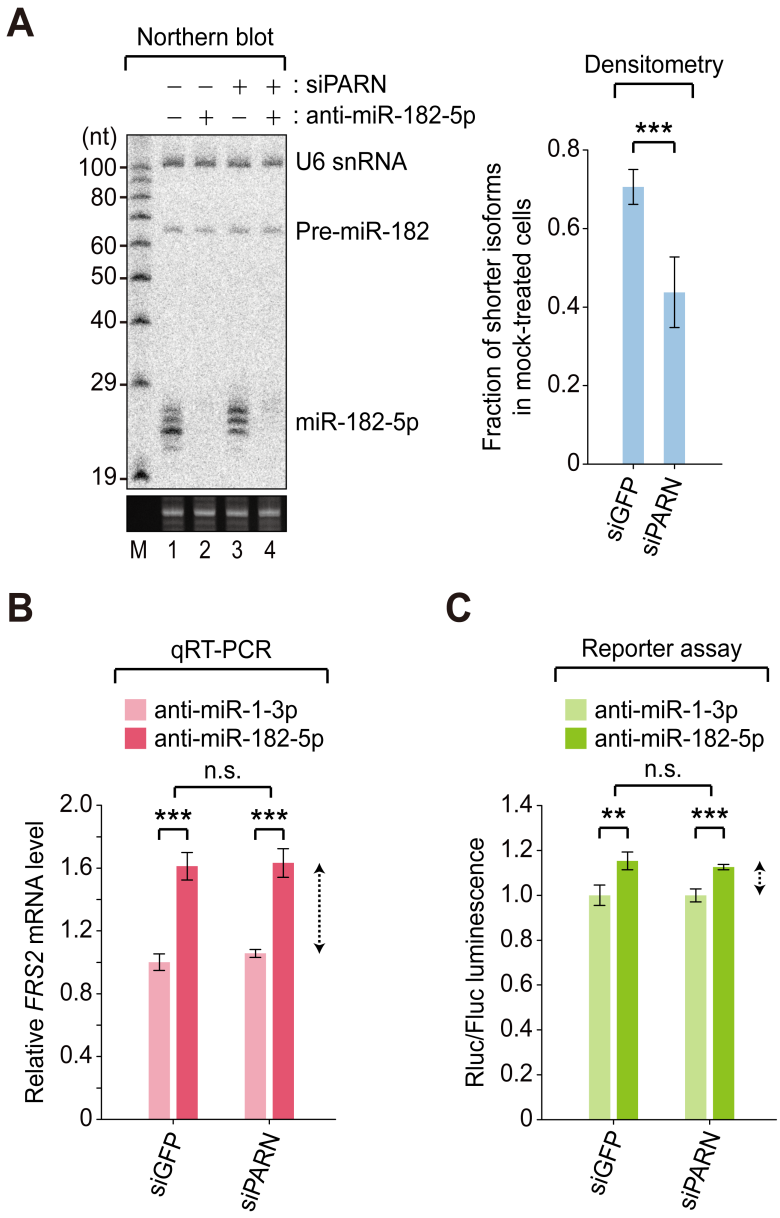
A
Northern blot
− − + + : siPARN
− + − + : anti-miR-182-5p
(nt)
100
80
60
50
40
29
19
U6 snRNA
Pre-miR-182
miR-182-5p
M 1 2 3 4
Densitometry
***
Fraction of shorter isoforms in mock-treated cells
0.8
0.6
0.4
0.2
0
siGFP
siPARN
B
qRT-PCR
anti-miR-1-3p
anti-miR-182-5p
n.s.
***
***
Relative FRS2 mRNA level
2.0
1.6
1.2
0.8
0.4
0
siGFP
siPARN
C
Reporter assay
anti-miR-1-3p
anti-miR-182-5p
n.s.
**
***
Rluc/Fluc luminescence
1.4
1.2
1.0
0.8
0.6
0.4
0.2
0
siGFP
siPARN

PARN as a miRNA de-tailor

The 3′ ends of miRNAs are extensively modified by the action of TENTs (Burroughs et al., 2010; Chiang et al., 2010; Wyman et al., 2011; Thornton et al., 2014). However, it is unclear whether such "tailing" is a biologically reversible process. Notably, ablation of *PARN* markedly increased the fraction of prefix-matching reads in small RNA sequencing libraries (Figure 36A), which represent miRNA species that are unambiguously modified at their 3′ ends by one or more non-genome-matching nucleotides (Figure 26A). Concurrent with the elevated tailing frequency, the overall length of miRNA tails also increased in the absence of PARN (Figure 36B). The mRNA levels of TENTs were comparable in parental and *PARN* KO cells (data not shown), excluding the possibility of their potential upregulation by *PARN* deletion. These findings suggest that PARN may be responsible for the reversal of untemplated nucleotide addition to miRNAs.

The frequency of untemplated nucleotide addition varies among miRNAs, with some miRNAs being much more frequently modified than others (Burroughs et al., 2010; Chiang et al., 2010; Wyman et al., 2011; Thornton et al., 2014). Furthermore, two miRNAs previously reported to be de-tailed and destructed by PARN, miR-21 and miR-122 (Boele et al., 2014; Katoh et al., 2015), tend to be expressed at high levels in their respective niches (Chang et al., 2004; Mccall et al., 2017). To examine whether the observed increase in the fraction of prefix-matching reads in *PARN* KO cells is mostly accounted for by de-tailing of such few miRNAs that are abundant and/or highly modified, the fraction of tailed species for each miRNA was calculated in parental and *PARN* KO cells. Notably, 229 of 267 miRNAs (~86%) were more frequently tailed in both *PARN* KO clones than in parental cells (Figure 37), demonstrating that PARN-mediated de-tailing is not confined to the few,

but is pervasive across most miRNAs. Of note, the *PARN* KO#2 clone exhibited stronger molecular phenotypes than the KO#1 clone throughout small RNA sequencing analyses (Figures 36 and 37).

To characterize the role of PARN as a miRNA de-tailor in more detail, it was examined how the composition of miRNA tails changed in *PARN* KO cells. In agreement with previous reports (Burroughs et al., 2010; Chiang et al., 2010; Wyman et al., 2011), mono-adenylation and mono-uridylation were the two most frequent types of modification, the combined reads of which comprised more than 70% of prefix-matching reads in parental HeLa S3 cells (~6.7% and ~2.9% of total reads, respectively; Figure 38). Remarkably, the frequency of mono-adenylation was substantially elevated in *PARN* KO cells (~6.7% in parental cells to ~9.8% in KO#1 cells and ~12% in KO#2 cells), while those of mono-uridylation and mono-cytidylation remained largely unaffected (Figure 38). Interestingly, the frequency of mono-guanylation was also elevated by *PARN* ablation, with a similar fold increase as that of mono-adenylation, but still remained low compared with those of other types of modification (~0.22% in parental cells to ~0.32% in KO#1 cells and ~0.40% in KO#2 cells; Figure 38). Next, analysis was extended to the composition of di-nucleotide miRNA tails. Although di-nucleotide addition appeared fairly a rare event (~2.6% of total reads in parental cells), a preference of PARN for A was clearly observed, such that all seven types of di-nucleotide tails containing at least one A (AA, AC, AG, AU, CA, GA, and UA) were more frequently added to miRNAs in both *PARN* KO clones than in parental cells (Figure 38). Examination of the modification status of individual miRNAs corroborated these results, with the frequency of mono-adenylation, but not that of mono-uridylation, being prominently increased in the absence of PARN (Figure 39). To validate the analysis, the isoform

distribution of members of the miR-17~92a cluster was investigated, which were previously reported to undergo TENT2-catalyzed adenylation (Burroughs et al., 2010), and appeared effectively deadenylated by PARN in HeLa S3 cells (Figure 40A). Northern blot analysis indeed demonstrated the appearance of high-molecular-weight species of these miRNAs in *PARN* KO cells, which were barely or not visible in parental cells (Figure 40B). Collectively, these findings suggest that PARN exhibits a degree of nucleotide preference in the de-tailing of miRNAs.

PARN catalyzes the shortening of untemplated oligo(A) tails in diverse types of non-coding RNA transcripts (Berndt et al., 2012; Moon et al., 2015; Nguyen et al., 2015a; Tseng et al., 2015; Boyraz et al., 2016; Son et al., 2018). To address whether PARN similarly modulates the length of adenosine tails in miRNAs, the frequencies of mono-, di-, and tri-adenylation were examined in parental and *PARN* KO cells. Notably, the frequencies of di- and tri-adenylation were more prominently affected than that of mono-adenylation, such that miRNAs acquired longer adenosine tails in *PARN* KO cells (Figure 41). On the other hand, the uridylation frequencies remained stable or slightly decreased upon *PARN* deletion (Figure 41). To be certain that PARN globally shortens the adenosine tails of miRNAs, the mean tail length of individual miRNAs was calculated based on the frequencies of mono-, di-, and tri-nucleotide addition. The adenosine tails, but not the uridine tails, were significantly lengthened in *PARN* KO cells (Figure 42), suggesting that PARN does indeed play a pivotal role in shaping the length distribution of miRNA adenosine tails. To illustrate these findings, miR-186-5p was chosen as a model miRNA, the adenosine tail of which was extensively deadenylated by PARN (mean adenosine tail length of ~1.31 nt in parental cells to ~1.59 nt in KO#1 cells and ~1.75 nt in KO#2 cells; Figure 42). Northern blotting and examination of sequencing reads clearly

demonstrated the accumulation of miRNA species harboring longer adenosine tails in *PARN* KO cells (Figure 43). Taken together, these results add miRNAs to the rapidly expanding list of non-coding RNAs whose 3′ adenosine tails are targeted and regulated by PARN activity.

Figure 36. PARN as a miRNA de-tailor.

(A) Fraction of genome-matching (GM) and prefix-matching reads (PM) in the small RNA libraries of parental and *PARN* KO cells.

(B) Changes in the length of miRNA tails upon *PARN* deletion.

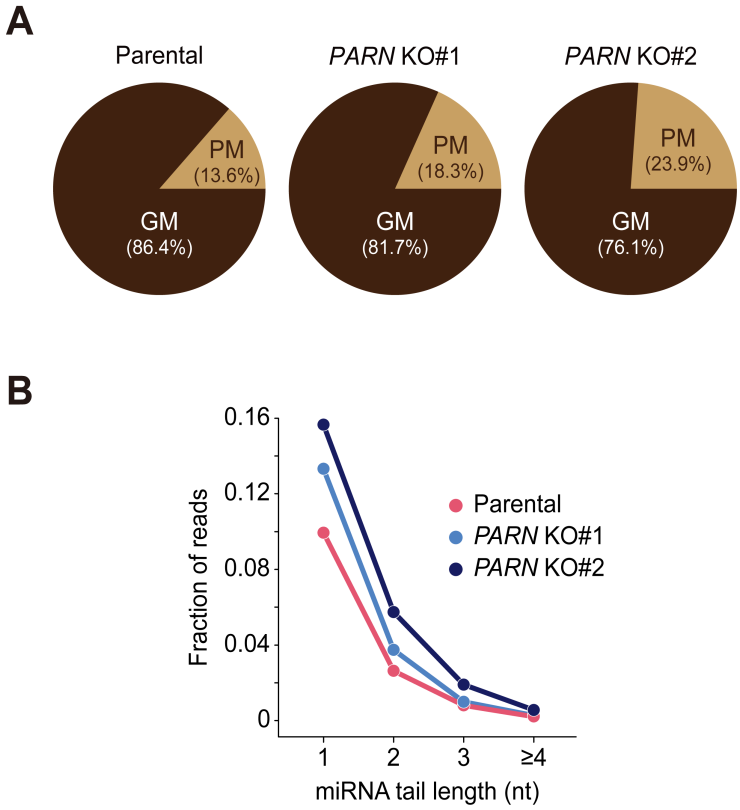
A
Parental
PM
(13.6%)
GM
(86.4%)
PARN KO#1
PM
(18.3%)
GM
(81.7%)
PARN KO#2
PM
(23.9%)
GM
(76.1%)
B
0.16
0.12
0.08
0.04
0
Fraction of reads
Parental
PARN KO#1
PARN KO#2
1
2
3
≥4
miRNA tail length (nt)

Figure 37. Changes in the tailing frequency of individual miRNAs upon *PARN* ablation.

(A) Tailing frequency of individual miRNAs in parental and *PARN* KO cells. The fraction of prefix-matching reads was calculated for the 267 miRNAs with total read counts exceeding 1,000 in parental cells. The 5p and 3p miRNAs are colored blue and turquoise, respectively.

(B) Elevated miRNA tailing frequency in *PARN* KO cells. Changes in the tailing frequency upon *PARN* deletion were calculated for each miRNA by *subtracting* the fraction in parental cells from the fraction in each *PARN* KO clone.

A

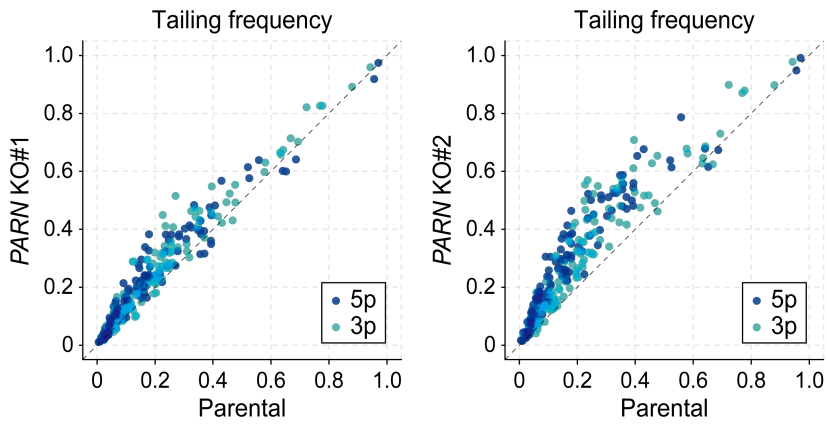
Tailing frequency
PARN KO#1
Parental
5p
3p
Tailing frequency
PARN KO#2
Parental
5p
3p

B

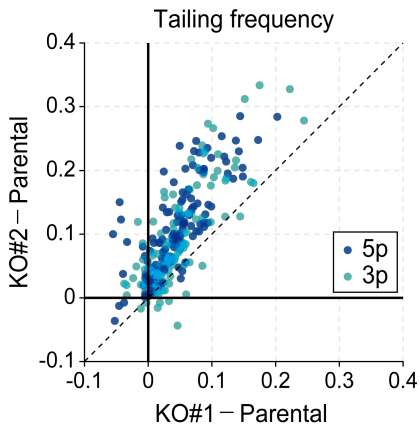
Tailing frequency
KO#2 − Parental
KO#1 − Parental
5p
3p

Figure 38. Nucleotide composition of mono-nucleotide and di-nucleotide miRNA tails in parental and *PARN* KO cells.

For eight types of di-nucleotide tails whose frequencies were lower than 0.025% in parental cells (CU, CA, UG, UC, CC, GC, GG, CG), the frequencies were combined altogether and presented as “etc”.

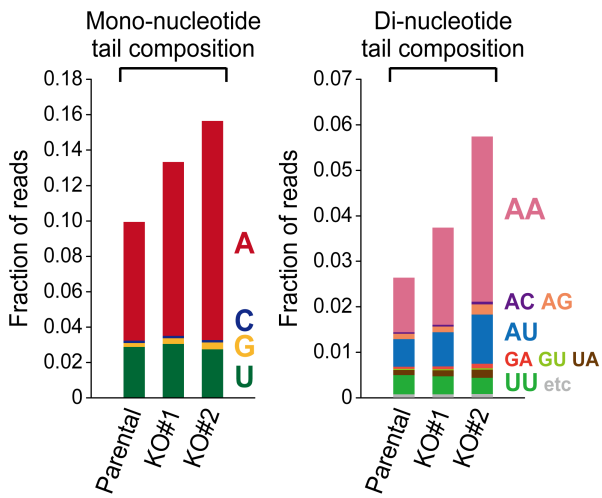
Mono-nucleotide
tail composition
Fraction of reads
0.18
0.16
0.14
0.12
0.10
0.08
0.06
0.04
0.02
0
A
C
G
U
Parental
KO#1
KO#2
Di-nucleotide
tail composition
Fraction of reads
0.07
0.06
0.05
0.04
0.03
0.02
0.01
0
AA
AC AG
AU
GA GU UA
UU etc
Parental
KO#1
KO#2

Figure 39. Changes in the frequencies of mono-adenylation and mono-uridylation upon *PARN* ablation.

(A)(B) The frequencies of mono-adenylation and mono-uridylation of individual miRNAs in parental and *PARN* KO cells. Modification frequency was calculated for the 267 miRNAs used in Figure 37, as the fraction of reads containing the indicated untemplated nucleotide addition. The 5p and 3p miRNAs are colored blue and turquoise, respectively.

(C) Changes in the frequencies of mono-adenylation and mono-uridylation upon *PARN* deletion were calculated for each miRNA by *subtracting* the fraction in parental cells from the fraction in each *PARN* KO clone. The miRNAs with more than 5 percent point changes on average in the modification frequency are indicated with brown shading.

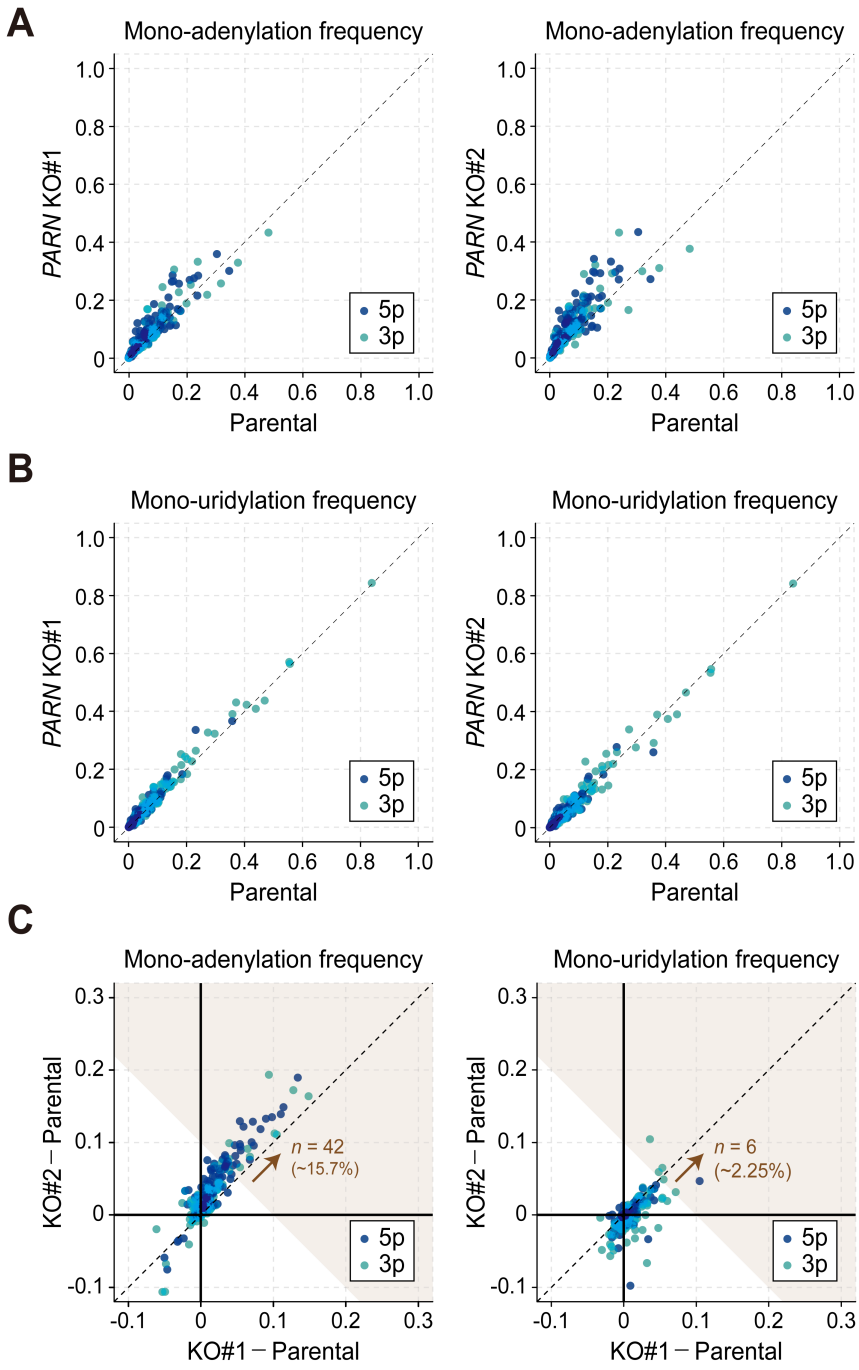
A
Mono-adenylation frequency
PARN KO#1
Parental
5p
3p
Mono-adenylation frequency
PARN KO#2
Parental
5p
3p
B
Mono-uridylation frequency
PARN KO#1
Parental
5p
3p
Mono-uridylation frequency
PARN KO#2
Parental
5p
3p
C
Mono-adenylation frequency
KO#2 − Parental
KO#1 − Parental
n = 42
(~15.7%)
5p
3p
Mono-uridylation frequency
KO#2 − Parental
KO#1 − Parental
n = 6
(~2.25%)
5p
3p

Figure 40. Deadenylation of the miR-17~92a cluster miRNAs by PARN.

(A) Mono-adenylation frequency of the members of the miR-17~92a cluster in parental and *PARN* KO cells.

(B) Northern blot analysis of miR-17/20a, miR-18a, and miR-19a/b. For simultaneous detection of paralogous miRNAs with nearly identical sequences (miR-17-5p and miR-20a, and miR-19a-3p and miR-19b-3p), degenerated oligonucleotides were used as hybridization probes. See Table 1.

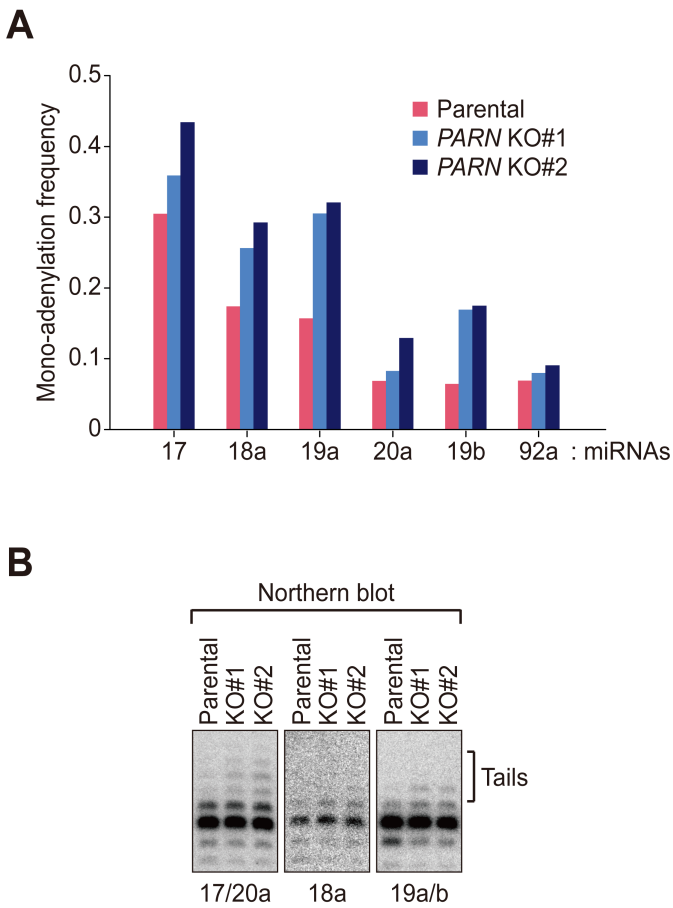
A
Mono-adenylation frequency
0.5
0.4
0.3
0.2
0.1
0
Parental
PARN KO#1
PARN KO#2
17
18a
19a
20a
19b
92a
: miRNAs
B
Northern blot
Parental
KO#1
KO#2
Parental
KO#1
KO#2
Parental
KO#1
KO#2
Tails
17/20a
18a
19a/b

Figure 41. Changes in the frequencies of six types of modification (A, AA, AAA, U, UU, UUU) upon *PARN* ablation.

The fold increases in the modification frequency are shown on the right side.

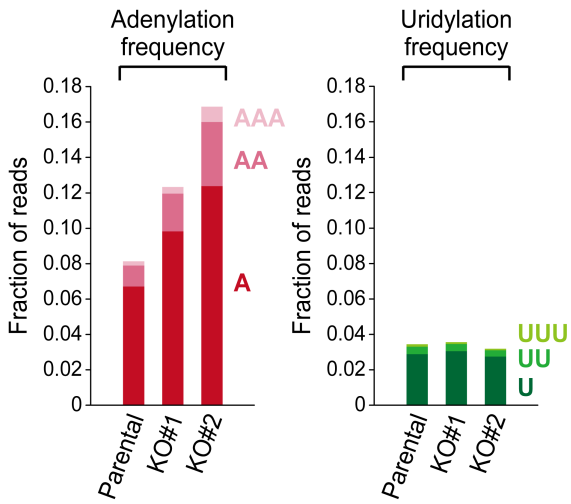

	Fold increase (KO/Parental)	
Tail	KO#1	KO#2
A	1.466	1.848
AA	1.778	3.025
AAA	1.658	3.872
U	1.059	0.950
UU	0.952	0.862
UUU	0.846	0.687

Figure 42. Changes in the mean length of adenosine tails and uridine tails upon *PARN* ablation.

(A)(B) The mean length of adenosine or uridine tails in parental and *PARN* KO cells. For each type of tail, miRNAs with mono-nucleotide-added read counts exceeding 100 in parental cells were used for the analysis (n = 198 for adenosine tails and n = 190 for uridine tails). The mean tail length was calculated based on the frequencies of mono-, di-, and tri-nucleotide addition, because the fraction of reads containing four or more untemplated nucleotides was very low across all small RNA libraries (Figure 36B).

(C) Boxplots depicting changes in the mean tail length of individual miRNAs upon *PARN* deletion. Upper and lower bounds of the box indicate the first and third quartiles, respectively, and an internal bar represents the median.

(D) Changes in the length of adenosine tails upon *PARN* deletion were calculated for each miRNA by *subtracting* the mean length in parental cells from the mean length in each *PARN* KO clone. The miRNAs with more than 0.3 nt changes on average in the mean adenosine tail length are indicated with red shading.

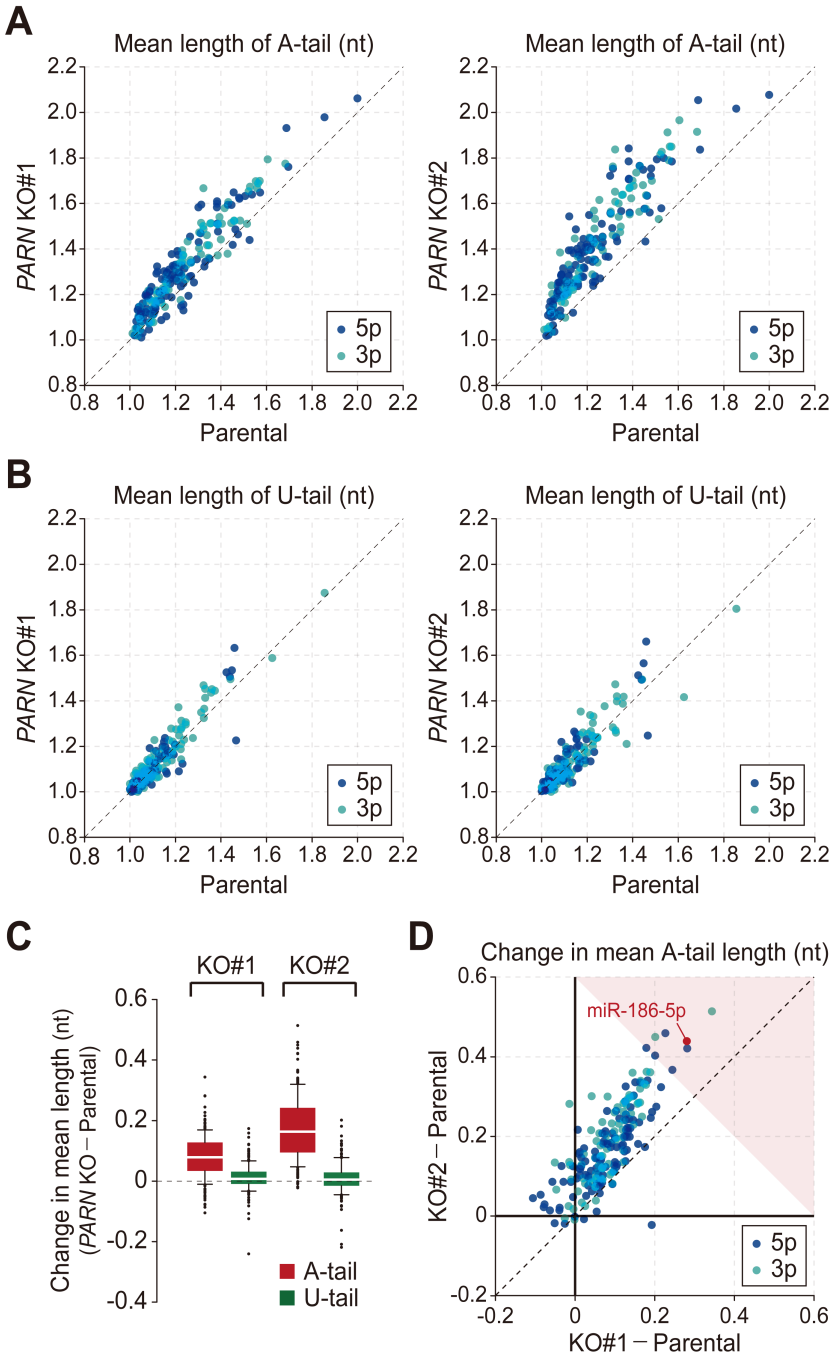
A
Mean length of A-tail (nt)
PARN KO#1
Parental
5p
3p
Mean length of A-tail (nt)
PARN KO#2
Parental
5p
3p
B
Mean length of U-tail (nt)
PARN KO#1
Parental
5p
3p
Mean length of U-tail (nt)
PARN KO#2
Parental
5p
3p
C
KO#1
KO#2
Change in mean length (nt)
(PARN KO − Parental)
A-tail
U-tail
D
Change in mean A-tail length (nt)
miR-186-5p
KO#2 − Parental
KO#1 − Parental
5p
3p

Figure 43. Modulation of adenosine tail length of miR-186-5p by PARN.

The expression, length distribution, and adenylation status of miR-186-5p in parental and *PARN* KO cells was examined by small RNA northern blotting and sequencing reads. SNORA63, a known substrate of PARN (Berndt et al. 2012; Son et al. 2018), served as a positive control for PARN deletion.

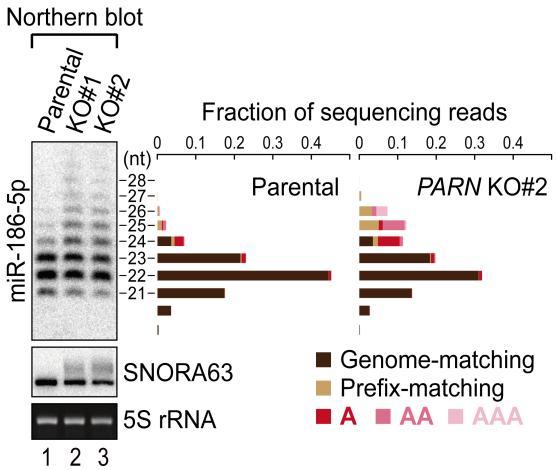
Northern blot
Parental
KO#1
KO#2
miR-186-5p
(nt)
28
27
26
25
24
23
22
21
SNORA63
5S rRNA
1 2 3
Fraction of sequencing reads
0 0.1 0.2 0.3 0.4
0 0.1 0.2 0.3 0.4
Parental
PARN KO#2
Genome-matching
Prefix-matching
A AA AAA

DISCUSSION

In this study, I report that the 3′-to-5′ exoribonuclease PARN sculpts the 3′ ends of miRNAs in human cells. I find that some canonical miRNAs are represented in cells with the sequences shorter at the 3′ ends than those defined by the core RNase III enzymes and link this discrepancy to the 3′ trimming of such miRNAs by PARN (Figures 10-22). By generating *PARN* KO cells and characterizing their miRNAome, I demonstrate that PARN-mediated shortening is pervasive across miRNAs and involves two distinct modes, “trimming” and “de-tailing”, depending on whether the nucleotide being resected by PARN is encoded by the genome or acquired post-transcriptionally (Figures 23-43).

Although the biochemical properties of PARN were extensively studied over the three decades since its initial identification (Balatsos et al., 2012; Virtanen et al., 2013), comprehensive characterization of its *in vivo* targets began to emerge only recently (Berndt et al., 2012; Moon et al., 2015; Nguyen et al., 2015a; Tseng et al., 2015; Boyraz et al., 2016; Shukla et al., 2016; Shukla and Parker, 2017). Curiously, these studies have primarily associated PARN with the biogenesis and 3′ end formation of a wide variety of non-coding RNAs, which is unexpected given its preference for a long stretch of adenosines and the m^7G cap structure (Korner and Wahle, 1997; Korner et al., 1998; Dehlin et al., 2000; Gao et al., 2000; Martinez et al., 2000; Martinez et al., 2001), the two hallmarks of a eukaryotic mRNA. My current study further expands the repertoire of non-coding RNA substrates for PARN to many canonical miRNAs. Despite a certain degree of nucleotide preference (Figures 38, 39, 41, and 42), PARN is versatile enough to digest the 3′ extensions of

miRNAs derived from the genome (Figures 28-32), which is consistent with its ability to process the highly GC-rich segment of 18S pre-rRNA (Ishikawa et al., 2017; Montellese et al., 2017).

Previously, three miRNAs have been reported as PARN substrates, including ac-pre-miR-451 (Yoda et al., 2013), miR-21 (Boele et al., 2014), and miR-122 (Katoh et al., 2015). To reconcile these studies with my findings, I focused on miR-21, because neither miR-451 nor miR-122 are expressed in HeLa S3 cells. Boele and colleagues claimed that DICER processing of pre-miR-21 releases miR-21+C, a 23 nt species, which is mono-adenylated by TENT4B and subsequently trimmed by PARN into the 22 nt reference sequence of miR-21 (Figure 44A) (Boele et al., 2014). Indeed, I found that both "Fraction +1" and the mono-adenylation frequency of miR-21 increased in both *PARN* KO clones (~78% in parental cells to ~85% in KO#1 cells and ~87% in KO#2 cells for "Fraction +1"; ~5.4% in parental cells to ~13% in KO#1 cells and ~15% in KO#2 cells for the adenylation frequency; Figure 44B). Of note, the authors defined the ratio of the miR-21 count to the miR-21+C count as the "degradation ratio" to conclude that PARN promotes decay of this specific miRNA (Figure 44A) (Boele et al., 2014). However, there were no significant changes in the steady-state levels of the vast majority of miRNAs upon *PARN* ablation, including those more efficiently trimmed by PARN than miR-21 (Figures 24B, 30, 31). My data suggest that PARN-mediated 3′ trimming likely operates in the maturation pathway of miRNAs rather than in the decay pathway, at least in HeLa S3 cells.

PARN is conserved among most eukaryotes, with the notable exception of the two model organisms, *Drosophila melanogaste*r and *Saccharomyces cerevisiae* (Parker and Song, 2004; Opyrchal et al., 2005; Goldstrohm and Wickens, 2008). In *Drosophila*, Nibbler, a 3′-to-5′ exoribonuclease distinct from PARN, appears to have

largely substituted for the role of PARN in miRNA metabolism (Han et al., 2011; Liu et al., 2011). To gain insights into the evolutionary conservation of PARN-mediated miRNA trimming, I focused on miR-182-5p, a miRNA that is efficiently trimmed by PARN (Figures 28, 30, and 31) and is broadly found in the genomes of bilaterian organisms (Dambal et al., 2015). The primary sequence and secondary structure of pre-miR-182 was strikingly similar among the vertebrate orthologues (Figure 45A) (Kozomara and Griffiths-Jones, 2014; Fromm et al., 2015), plausibly suggesting that they may undergo conserved DICER processing. Next, the length distributions of miR-182-5p sequencing reads obtained from a panel of vertebrate species (Fromm et al., 2015) were compared with those obtained from HeLa S3 small RNA libraries. *PARN* ablation in HeLa S3 cells caused a shift in the length of the most abundant miR-182-5p isoform from 24 nt to 26 nt, suggesting that the last two nucleotides of the 26 nt isoform are subjected to PARN-mediated trimming (Figures 30 and 32). Notably, in all species examined, the dominantly abundant isoform of miR-182-5p was shorter than 26 nt in length (25 nt in mouse, 24 nt in chicken and frog, and 22 nt in zebrafish; Figure 45B). Given that the miR-182-5p orthologues in these species possess nearly identical sequences to human miR-182-5p (Figure 45A), it is tempting to speculate that PARN may contribute to the 3′ end formation of this specific miRNA, and possibly other miRNAs, in vertebrates.

The degree of PARN-mediated trimming varied among miRNAs (Figures 28, 30, and 31). Then, what specifies the trimming of a specific miRNA? I failed to find common sequence motifs or compositional biases among the miRNAs experiencing efficient trimming in HeLa S3 cells (Figure 32). However, I noticed that they were slightly longer than the typical size of miRNAs of ~22 nt, ranging from 24 nt to 26 nt in length (Figures 32 and 46A). Furthermore, PARN failed to trim the miRNAs to

less than a certain size *in vitro* and in cells, which was ~22 nt in the case of miR-362-5p (Figures 19A, 21, and 22). Perhaps the longer miRNAs readily dissociate their 3′ ends from the PAZ domain and PARN trims them to the sizes that perfectly fit in and fully protected by AGO proteins. Notably, similar observations were made in previous studies of Nibbler-mediated miRNA trimming in *Drosophila* (Han et al., 2011; Liu et al., 2011), suggesting that the length of miRNAs may play a role in specifying exoribonuclease-directed 3′ trimming in both human and *Drosophila*. Nevertheless, miRNA length is apparently not the sole determinant of trimming: for example, miR-182-5p is trimmed by PARN from 26 nt to 24 nt, which is the size of untrimmed miR-224-5p (Figures 30 and 32). miR-186-5p, one of the miRNAs that are highly deadenylated by PARN, also undergoes a degree of trimming, from 22 nt to 21 nt (Figure 43). These observations suggest the existence of more complicated determinant(s) of PARN-mediated trimming beyond the length of miRNAs.

A previous study emphasized the role of the RNA-binding protein, CUGBP1, in guiding PARN to its substrate miRNAs for destruction (Katoh et al., 2015). However, overexpression or knockdown of CUGBP1 did not obviously affect the 3′ trimming of miR-362-5p in HEK293T cells (Figure 46B). Furthermore, recombinant PARN produced in *E. coli* effectively trimmed the 3′ end of AGO-loaded miR-362-5p *in vitro* (Figure 22), which, together with an earlier report (Yoda et al., 2013), suggests that PARN does not require any co-factor(s) to execute miRNA trimming. Nevertheless, I do not exclude the possibility that some *trans*-acting factor(s) may modulate the activity of PARN in miRNA metabolism, for example, in a cell-type-specific manner, because the degree of trimming of a specific miRNA varied across multiple cell types (Figure 31). Another appealing possibility for the specificity of PARN-mediated miRNA trimming *in vivo* is “tailing”. Some non-coding RNA

substrates of PARN, including snoRNAs and TERC, are primed with oligo(A) tails by the action of TENTs prior to being trimmed (Berndt et al., 2012; Moon et al., 2015; Nguyen et al., 2015a; Tseng et al., 2015; Boyraz et al., 2016; Son et al., 2018), and similar mechanisms were suggested to operate in the cases of miR-21 and miR-122 (Boele et al., 2014; Katoh et al., 2015). Indeed, many miRNAs subjected to a high degree of trimming also acquired longer tails upon PARN deletion (Figures 30 and 31). However, the adenylation frequency of these miRNAs was not particularly prominent compared with those for other miRNAs (Figures 39, 42, and 46C), making it difficult to generalize the association of this type of modification with PARN-mediated trimming. Considering these observations, I speculate that whether a given miRNA is trimmed by PARN, and if so, to what extent, may be determined by a combination of multiple factors, including the length, nucleotide composition, and/or modification status of the miRNA and *trans*-acting factor(s), if any, modulating PARN activity.

PARN-mediated shortening of miRNA 3′ ends changes neither the seed nucleotides nor the stability of miRNAs and is therefore not expected to substantially influence the vast majority of canonical targeting events relying on the miRNA seed (Figure 35). This, together with the notable conservation of a similar process in *Drosophila* (Han et al., 2011; Liu et al., 2011), raises the question as to why some miRNAs have evolved to be trimmed by these 3′-to-5′ exoribonucleases (Figure 47). I speculate that PARN-mediated trimming may prove its relevance at a minority of target sites, which extend pairing to the 3′ region of the miRNA to enhance the specificity of miRNA-target interaction (3′-supplementary sites) or to compensate for imperfect pairing to the seed (3′-compensatory sites) (Figure 2) (Bartel, 2009). Alternatively, but not mutually exclusively, trimming may differentially contribute

to the fate of miRNAs in a spatiotemporal manner or in response to external cues. For example, non-canonical target RNAs that lack pairing to the seed are known to promote the degradation of the cognate miRNA through releasing it from and/or destabilizing its 3′ end within AGO proteins (De et al., 2013; Park et al., 2017). Given its ability to trim most miRNAs (Figure 28), PARN may be the culprit enzyme that destructs free miRNAs released from AGO proteins or destabilizes AGO-bound miRNAs in this context. It will be of interest to investigate the role of PARN in a larger paradigm of TDMD, in which the 3′ region of miRNAs plays a key role in specifying and eliciting regulatory effects (Fuchs Wightman et al., 2018). Finally, I point out that PARN-mediated 3′ trimming may influence the recently discovered length-related functions of miRNAs. For example, longer 3′ isoforms of miR-122, resulting from either untemplated nucleotide addition or lack of 3′ trimming, interact with the genomic RNA of hepatitis C virus more efficiently than the reference species (Yamane et al., 2017). Similarly, 3′ heterogeneity of miR-222 appears to have functional consequences, with longer 3′ isoforms exhibiting increased apoptotic activity and nuclear enrichment in a length-dependent manner (Yu et al., 2017). It will be interesting to investigate whether such length-related effects are regulated by PARN-mediated trimming. In conclusion, further studies are required to uncover the full extent and the biological relevance of PARN-mediated miRNA shortening, and its possible contribution to human pathologies related to *PARN* mutations.

Figure 44. PARN-mediated trimming and de-tailing of miR-21.

(A) A model for post-processing modifications of miR-21 proposed by Boele and colleagues (Boele et al., 2014). They suggested that DICER processing of pre-miR-21 releases miR-21+C, a 23 nt species, which is first mono-adenylated by TENT4B and subsequently trimmed by PARN to produce the 22 nt mature miR-21. The "degradation ratio" they defined is also shown.

(B) "Fraction +1" and the mono-adenylation frequency of miR-21 in parental and *PARN* KO cells are shown on the left side. The result of northern blot analysis of miR-21 is shown on the right side.

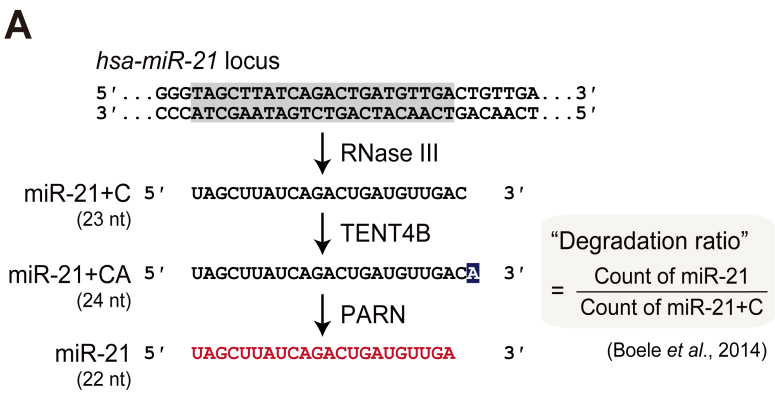
A
hsa-miR-21 locus
5′...GGGTAGCTTATCAGACTGATGTTGACTGTTGA...3′
3′...CCCATCGAATAGTCTGACTACAACTGACAACT...5′
RNase III
miR-21+C 5′ UAGCUUAUCAGACUGAUGUUGAC 3′
(23 nt)
TENT4B
miR-21+CA 5′ UAGCUUAUCAGACUGAUGUUGACA 3′
(24 nt)
PARN
miR-21 5′ UAGCUUAUCAGACUGAUGUUGA 3′
(22 nt)
"Degradation ratio"
= Count of miR-21 / Count of miR-21+C
(Boele et al., 2014)

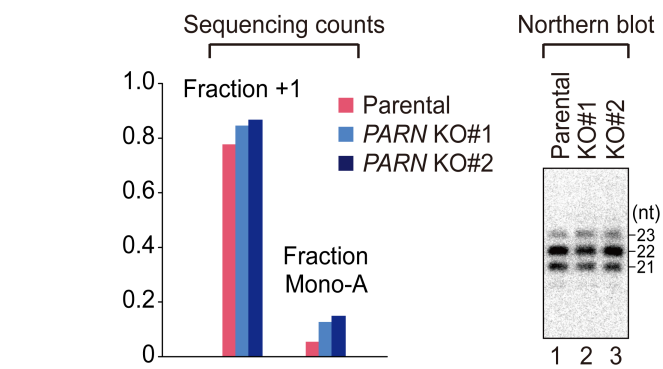
B
Sequencing counts
Northern blot
Fraction +1
Parental
PARN KO#1
PARN KO#2
1.0
0.8
0.6
0.4
0.2
0
Fraction
Mono-A
Parental
KO#1
KO#2
(nt)
23
22
21
1 2 3

Figure 45. Possible evolutionary conservation of PARN-mediated miRNA trimming in vertebrates.

(A) The sequences of bilaterian pre-miR-182 orthologues. Note that the remarkable sequence homology of pre-miR-182 does not extend beyond vertebrates. The 25th and 26th nucleotides of miR-182-5p, which are subjected to PARN-meditated trimming in human cells, are highly conserved among vertebrate orthologues (blue shading).

(B) The length distribution of miR-182-5p sequencing reads in selected vertebrate species. The reads from *Mus musculus*, *Gallus gallus*, *Xenopus tropicalis*, and *Danio rerio* were obtained from miRGeneDB2.0 (http://mirgenedb.org/) with default options (Fromm et al., 2015).

A

Primary sequences of pre-miR-182 orthologues

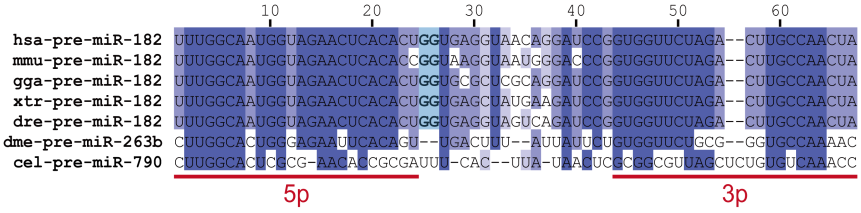

B

Length distribution of miR-182-5p sequencing reads (Fromm *et al.*, 2015)

Figure 46. Possible determinants of PARN-mediated miRNA trimming.

(A) Mean lengths of seven efficiently trimmed miRNAs (miR-224-5p, miR-182-5p, miR-425-5p, miR-361-3p, miR-301a-3p, miR-454-3p, miR-362-5p) in *PARN* KO#2 cells.

(B) Effects of CUGBP1 on miR-362-5p trimming in HEK293T cells. CUGBP1 was overexpressed (left side) or depleted (right side) in HEK293T cells and the maturation of ectopically expressed miR-362-5p was monitored by northern blotting. Overexpression and depletion of CUGBP1 were confirmed by western blot analysis and qRT-PCR, respectively. Note that the blot presented on the right side is the same as that presented in Figure 18. Dashed lines indicate discontinuous lanes from the same gel.

(C) Boxplots depicting modification frequencies of twelve efficiently trimmed miRNAs (see Figure 32) in *PARN* KO#2 cells. Upper and lower bounds of the box indicate the first and third quartiles, respectively, and an internal bar represents the median.

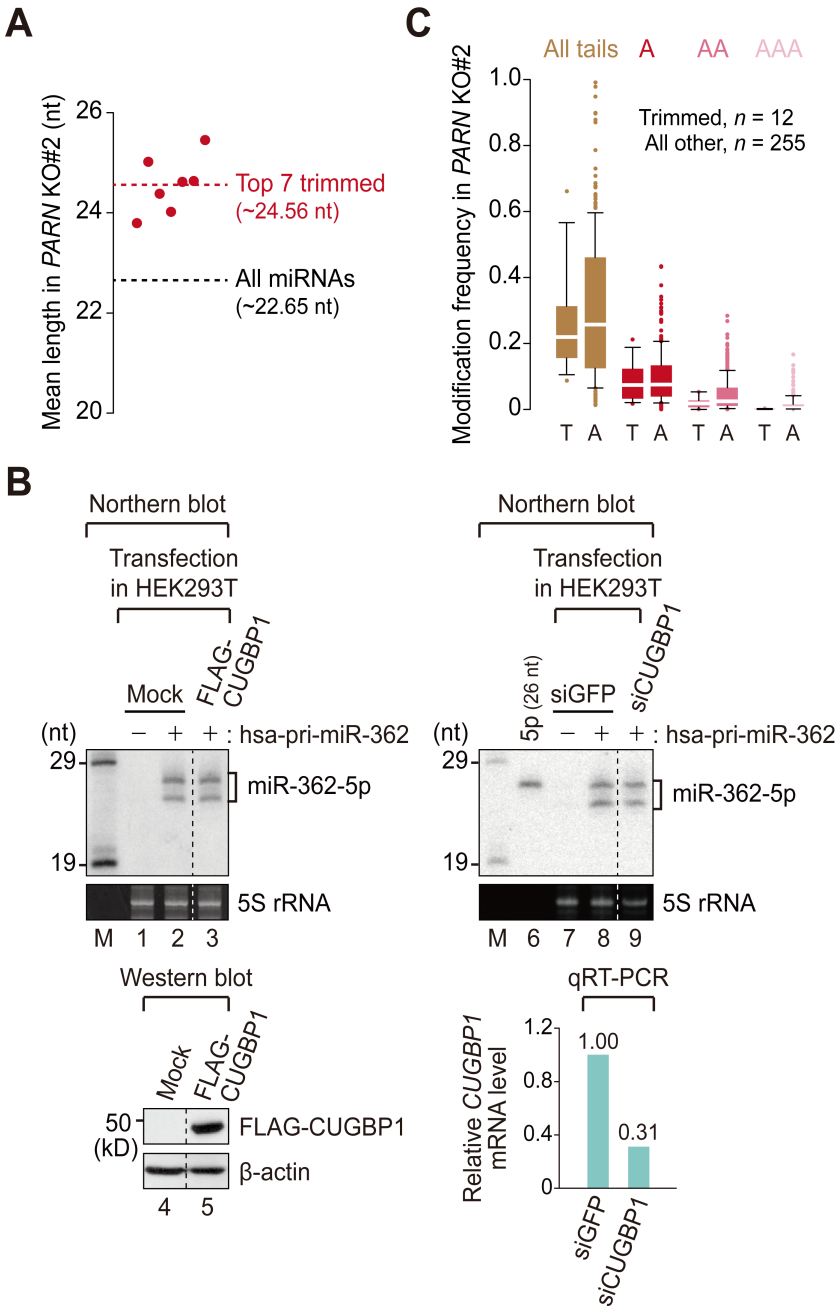
A
Mean length in PARN KO#2 (nt)
26
24
22
20
Top 7 trimmed
(~24.56 nt)
All miRNAs
(~22.65 nt)
C
All tails
A
AA
AAA
Modification frequency in PARN KO#2
1.0
0.8
0.6
0.4
0.2
0
Trimmed, n = 12
All other, n = 255
T A T A T A T A
B
Northern blot
Transfection
in HEK293T
Mock
FLAG-CUGBP1
(nt)
– + + : hsa-pri-miR-362
29
19
miR-362-5p
5S rRNA
M 1 2 3
Northern blot
Transfection
in HEK293T
siGFP
siCUGBP1
5p (26 nt)
(nt)
– + + : hsa-pri-miR-362
29
19
miR-362-5p
5S rRNA
M 6 7 8 9
Western blot
Mock
FLAG-CUGBP1
50
(kD)
FLAG-CUGBP1
β-actin
4 5
qRT-PCR
Relative CUGBP1
mRNA level
1.2
0.8
0.4
0
1.00
0.31
siGFP
siCUGBP1

Figure 47. Exoribonuclease-mediated trimming of a conserved miRNA in vertebrates and *Drosophila*.

miR-182-5p is broadly conserved in bilaterian organisms and its orthologues miRNA is annotated as miR-263b-5p in *Drosophila* (Figure 45). Possessing nearly identical seed sequences, they are known to play roles in similar biological pathways in their hosts, for example, in sensory organ development (Dambal et al., 2015). Curiously, both miR-182-5p and miR-263b-5p are trimmed by two distantly related 3′-to-5′ exoribonucleases, PARN and Nibbler, in vertebrates and *Drosophila*, respectively. Ramifications of such a highly conserved modification process are currently unclear.

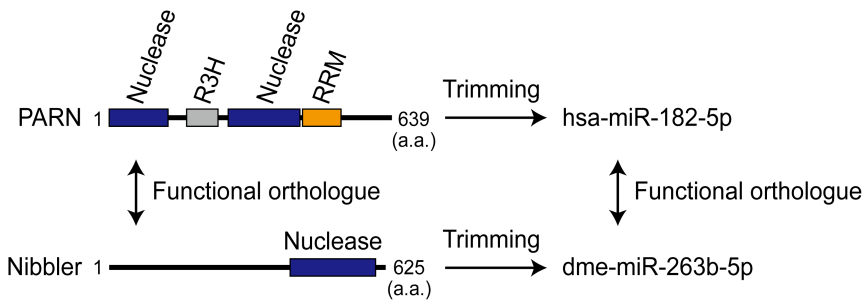
Nuclease
R3H
Nuclease
RRM
PARN
1
639
(a.a.)
Trimming
hsa-miR-182-5p
Functional orthologue
Functional orthologue
Nuclease
Nibbler
1
625
(a.a.)
Trimming
dme-miR-263b-5p

CONCLUSION

The frequent 3′ heterogeneity of miRNAs was first recognized more than a decade ago (Morin et al., 2008). Much is now known how the 3′ ends of metazoan miRNAs are extended, with multiple TENTs responsible for "tailing" having been identified and characterized in detail by several transcriptome-wide studies (Burroughs et al., 2010; Chiang et al., 2010; Wyman et al., 2011; Thornton et al., 2014). On the contrary, how the shorter 3′ isoforms of miRNAs are generated has been obscure, especially in vertebrates: to my knowledge, they have never been characterized comprehensively, nor has it been thoroughly investigated whether they represented naturally occurring isoforms or decay intermediates. In line with this, how the tailing by TENTs is reversed has not been addressed.

Here, I identify PARN as a catalytic entity that pervasively shortens miRNAs in human cells. First, I rigorously reaffirm the notion that the "cellular definition" of a miRNA does not necessarily coincide with the definition made by the core RNase III enzymes DROSHA and DICER. I find that 3′-to-5′ exoribonuclease-mediated trimming contributes to such discrepancy and identify PARN as the culprit miRNA "trimmer". By generating *PARN* KO cells and characterizing their miRNAs by high-throughput sequencing, I demonstrate that PARN-mediated miRNA shortening is widespread across miRNAs and involves two distinct modes, depending on the origin of the nucleotide being resected. As a "trimmer", PARN digests the 3′ genomic extensions of miRNAs that are supposedly longer than the average, and as a "de-tailor", PARN erases or reduces the size of miRNA tails attached by TENTs. Surprisingly, PARN-mediated shortening has little impact on miRNA stability,

suggesting that this process likely operates to finalize miRNA maturation, rather than to initiate miRNA decay.

In a miRNA point of view, my findings provide a comprehensive perspective on the role of 3′-to-5′ exoribonuclease in diversifying miRNA sequence in vertebrates. Considering previous studies of miRNA shortening in *Drosophila*, PARN appears to be the functional orthologue of Nibbler. Why such a highly conserved modification process has evolved is currently unclear, given that the 3′ region of metazoan miRNAs plays a minor role in miRNA-mediated repression. Furthermore, PARN-mediated shortening does not apparently alter the stability of miRNAs or their association with AGO proteins. Thus, further studies are definitely needed to unveil the full extent and biological significance of this process that comes with seemingly neutral consequences. Another important question to be addressed is how the specificity of trimming is achieved and how and when these nucleases recognize the 3′ ends of miRNAs that are normally buried within and protected by AGO proteins. In a PARN point of view, miRNAs are an unexpected class of its substrates, because they possess neither the long adenosine tails nor the m^7G cap, the features preferred by PARN. Furthermore, the nucleotides trimmed by PARN are surprisingly diverse in their composition and are not particularly enriched for adenosine. It will be interesting to investigate whether PARN employs distinct catalytic mechanisms for different substrates: for example, PARN may remove short nucleotide sequences of miRNAs in a distributive rather than a processive manner.

In summary, my findings provide insights into how the 3′ ends of miRNAs are sculpted and diversified by 3′-to-5′ exoribonuclease activities by adding these tiny regulators to the growing list of non-coding RNA substrates of PARN.

REFERENCES

Abbott AL, Alvarez-Saavedra E, Miska EA, Lau NC, Bartel DP, Horvitz HR et al. (2005) The let-7 MicroRNA family members mir-48, mir-84, and mir-241 function together to regulate developmental timing in Caenorhabditis elegans. *Dev Cell* 9, 403-414.

Agarwal V, Bell GW, Nam JW and Bartel DP (2015) Predicting effective microRNA target sites in mammalian mRNAs. *Elife* 4.

Ameres SL, Horwich MD, Hung JH, Xu J, Ghildiyal M, Weng ZP et al. (2010) Target RNA-directed trimming and tailing of small silencing RNAs. *Science* 328, 1534-1539.

Ameres SL, Martinez J and Schroeder R (2007) Molecular basis for target RNA recognition and cleavage by human RISC. *Cell* 130, 101-112.

Ameres SL and Zamore PD (2013) Diversifying microRNA sequence and function. *Nat Rev Mol Cell Biol* 14, 475-488.

Andersson MG, Haasnoot PC, Xu N, Berenjian S, Berkhout B and Akusjarvi G (2005) Suppression of RNA interference by adenovirus virus-associated RNA. *J Virol* 79, 9556-9565.

Ashkenazy H, Abadi S, Martz E, Chay O, Mayrose I, Pupko T et al. (2016) ConSurf 2016: an improved methodology to estimate and visualize evolutionary conservation in macromolecules. *Nucleic Acids Res* 44, W344-350.

Astrom J, Astrom A and Virtanen A (1991) In vitro deadenylation of mammalian mRNA by a HeLa cell 3' exonuclease. *EMBO J* 10, 3067-3071.

Astrom J, Astrom A and Virtanen A (1992) Properties of a HeLa cell 3' exonuclease specific for degrading poly(A) tails of mammalian mRNA. *J Biol Chem* 267, 18154-18159.

Auyeung VC, Ulitsky I, Mcgeary SE and Bartel DP (2013) Beyond secondary structure: primary-sequence determinants license pri-miRNA hairpins for processing. *Cell* 152, 844-858.

Azuma-Mukai A, Oguri H, Mituyama T, Qian ZR, Asai K, Siomi H et al. (2008) Characterization of endogenous human Argonautes and their miRNA partners in RNA silencing. *Proc Natl Acad Sci U S A* 105, 7964-7969.

Babiarz JE, Ruby JG, Wang Y, Bartel DP and Blelloch R (2008) Mouse ES cells express endogenous shRNAs, siRNAs, and other Microprocessor-independent, Dicer-dependent small RNAs. *Genes Dev* 22, 2773-2785.

Baek D, Villen J, Shin C, Camargo FD, Gygi SP and Bartel DP (2008) The impact of microRNAs on protein output. *Nature* 455, 64-71.

Bail S, Swerdel M, Liu HD, Jiao XF, Goff LA, Hart RP et al. (2010) Differential regulation of microRNA stability. *RNA* 16, 1032-1039.

Balatsos NA, Maragozidis P, Anastasakis D and Stathopoulos C (2012) Modulation of poly(A)-specific ribonuclease (PARN): current knowledge and perspectives. *Curr Med Chem* 19, 4838-4849.

Balatsos NA, Nilsson P, Mazza C, Cusack S and Virtanen A (2006) Inhibition of mRNA deadenylation by the nuclear cap binding complex (CBC). *J Biol Chem* 281, 4517-4522.

Bartel DP (2009) MicroRNAs: target recognition and regulatory functions. *Cell* 136, 215-233.

Bartel DP (2018) Metazoan microRNAs. *Cell* 173, 20-51.

Behm-Ansmant I, Rehwinkel J, Doerks T, Stark A, Bork P and Izaurralde E (2006) mRNA degradation by miRNAs and GW182 requires both CCR4:NOT deadenylase and DCP1:DCP2 decapping complexes. *Genes Dev* 20, 1885-1898.

Bellutti F, Kauer M, Kneidinger D, Lion T and Klein R (2015) Identification of RISC-associated adenoviral microRNAs, a subset of their direct targets, and global changes in the targetome upon lytic adenovirus 5 infection. *J Virol* 89, 1608-1627.

Bentwich I, Avniel A, Karov Y, Aharonov R, Gilad S, Barad O et al. (2005) Identification of hundreds of conserved and nonconserved human microRNAs. *Nat Genet* 37, 766-770.

Berezikov E, Chung WJ, Willis J, Cuppen E and Lai EC (2007) Mammalian mirtron genes. *Mol Cell* 28, 328-336.

Berndt H, Harnisch C, Rammelt C, Stohr N, Zirkel A, Dohm JC et al. (2012) Maturation of mammalian H/ACA box snoRNAs: PAPD5-dependent adenylation and PARN-dependent trimming. *RNA* 18, 958-972.

Bernstein E, Caudy AA, Hammond SM and Hannon GJ (2001) Role for a bidentate ribonuclease in the initiation step of RNA interference. *Nature* 409, 363-366.

Bernstein E, Kim SY, Carmell MA, Murchison EP, Alcorn H, Li MZ et al. (2003) Dicer is essential for mouse development. *Nat Genet* 35, 215-217.

Blow MJ, Grocock RJ, Van Dongen S, Enright AJ, Dicks E, Futreal PA et al. (2006) RNA editing of human microRNAs. *Genome Biol* 7, R27.

Boele J, Persson H, Shin JW, Ishizu Y, Newie IS, Sokilde R et al. (2014) PAPD5-mediated 3' adenylation and subsequent degradation of miR-21 is disrupted in proliferative disease. *Proc Natl Acad Sci U S A* 111, 11467-11472.

Bohnsack MT, Czaplinski K and Gorlich D (2004) Exportin 5 is a RanGTP-dependent dsRNA-binding protein that mediates nuclear export of pre-miRNAs. *RNA* 10, 185-191.

Boyraz B, Moon DH, Segal M, Muosieyiri MZ, Aykanat A, Tai AK et al. (2016) Posttranscriptional manipulation of TERC reverses molecular hallmarks of telomere disease. *J Clin Invest* 126, 3377-3382.

Braun JE, Huntzinger E, Fauser M and Izaurralde E (2011) GW182 proteins directly recruit cytoplasmic deadenylase complexes to miRNA targets. *Mol Cell* 44, 120-133.

Braun JE, Truffault V, Boland A, Huntzinger E, Chang CT, Haas G et al. (2012) A direct interaction between DCP1 and XRN1 couples mRNA decapping to 5' exonucleolytic degradation. *Nat Struct Mol Biol* 19, 1324-1331.

Brennecke J, Stark A, Russell RB and Cohen SM (2005) Principles of microRNA-target recognition. *PLoS Biol* 3, e85.

Brummelkamp TR, Bernards R and Agami R (2002) A system for stable expression of short interfering RNAs in mammalian cells. *Science* 296, 550-553.

Burroughs AM, Ando Y, De Hoon MJ, Tomaru Y, Nishibu T, Ukekawa R et al. (2010) A comprehensive survey of 3' animal miRNA modification events and a possible role for 3' adenylation in modulating miRNA targeting effectiveness. *Genome Res* 20, 1398-1410.

Burroughs AM, Ando Y, De Hoon MJ, Tomaru Y, Suzuki H, Hayashizaki Y et al. (2011) Deep-sequencing of human Argonaute-associated small RNAs provides insight into miRNA sorting and reveals Argonaute association with RNA fragments of diverse origin. *RNA Biol* 8, 158-177.

Cevher MA, Zhang X, Fernandez S, Kim S, Baquero J, Nilsson P et al. (2010) Nuclear

deadenylation/polyadenylation factors regulate 3' processing in response to DNA damage. *EMBO J* 29, 1674-1687.
Chakravarthy S, Sternberg SH, Kellenberger CA and Doudna JA (2010) Substrate-specific kinetics of Dicer-catalyzed RNA processing. *J Mol Biol* 404, 392-402.
Chandradoss SD, Schirle NT, Szczepaniak M, Macrae IJ and Joo C (2015) A dynamic search process underlies microRNA targeting. *Cell* 162, 96-107.
Chang H, Lim J, Ha M and Kim VN (2014) TAIL-seq: genome-wide determination of poly(A) tail length and 3' end modifications. *Mol Cell* 53, 1044-1052.
Chang HM, Triboulet R, Thornton JE and Gregory RI (2013) A role for the Perlman syndrome exonuclease Dis3l2 in the Lin28-let-7 pathway. *Nature* 497, 244-248.
Chang J, Nicolas E, Marks D, Sander C, Lerro A, Buendia MA et al. (2004) miR-122, a mammalian liver-specific microRNA, is processed from hcr mRNA and may downregulate the high affinity cationic amino acid transporter CAT-1. *RNA Biol* 1, 106-113.
Chekulaeva M, Mathys H, Zipprich JT, Attig J, Colic M, Parker R et al. (2011) miRNA repression involves GW182-mediated recruitment of CCR4-NOT through conserved W-containing motifs. *Nat Struct Mol Biol* 18, 1218-1226.
Cheloufi S, Dos Santos CO, Chong MM and Hannon GJ (2010) A dicer-independent miRNA biogenesis pathway that requires Ago catalysis. *Nature* 465, 584-589.
Chen CY, Zheng D, Xia Z and Shyu AB (2009) Ago-TNRC6 triggers microRNA-mediated decay by promoting two deadenylation steps. *Nat Struct Mol Biol* 16, 1160-1166.
Chen YW, Song S, Weng R, Verma P, Kugler JM, Buescher M et al. (2014) Systematic study of Drosophila microRNA functions using a collection of targeted knockout mutations. *Dev Cell* 31, 784-800.
Chendrimada TP, Gregory RI, Kumaraswamy E, Norman J, Cooch N, Nishikura K et al. (2005) TRBP recruits the Dicer complex to Ago2 for microRNA processing and gene silencing. *Nature* 436, 740-744.
Chiang HR, Schoenfeld LW, Ruby JG, Auyeung VC, Spies N, Baek D et al. (2010) Mammalian microRNAs: experimental evaluation of novel and previously annotated genes. *Genes Dev* 24, 992-1009.
Chong MM, Zhang G, Cheloufi S, Neubert TA, Hannon GJ and Littman DR (2010) Canonical and alternate functions of the microRNA biogenesis machinery. *Genes Dev* 24, 1951-1960.
Cifuentes D, Xue H, Taylor DW, Patnode H, Mishima Y, Cheloufi S et al. (2010) A novel miRNA processing pathway independent of Dicer requires Argonaute2 catalytic activity. *Science* 328, 1694-1698.
Copeland PR and Wormington M (2001) The mechanism and regulation of deadenylation: identification and characterization of Xenopus PARN. *RNA* 7, 875-886.
Court DL, Gan J, Liang YH, Shaw GX, Tropea JE, Costantino N et al. (2013) RNase III: Genetics and function; structure and mechanism. *Annu Rev Genet* 47, 405-431.
D'ambrogio A, Gu W, Udagawa T, Mello CC and Richter JD (2012) Specific miRNA stabilization by Gld2-catalyzed monoadenylation. *Cell Rep* 2, 1537-1545.
Dambal S, Shah M, Mihelich B and Nonn L (2015) The microRNA-183 cluster: the family that plays together stays together. *Nucleic Acids Res* 43, 7173-7188.
Das SK, Sokhi UK, Bhutia SK, Azab B, Su ZZ, Sarkar D et al. (2010) Human polynucleotide phosphorylase selectively and preferentially degrades microRNA-221 in human melanoma cells. *Proc Natl Acad Sci U S A* 107, 11948-11953.

De La Mata M, Gaidatzis D, Vitanescu M, Stadler MB, Wentzel C, Scheiffele P et al. (2015) Potent degradation of neuronal miRNAs induced by highly complementary targets. *EMBO Rep* 16, 500-511.

De N, Young L, Lau PW, Meisner NC, Morrissey DV and Macrae IJ (2013) Highly complementary target RNAs promote release of guide RNAs from human Argonaute2. *Mol Cell* 50, 344-355.

De Pietri Tonelli D, Pulvers JN, Haffner C, Murchison EP, Hannon GJ and Huttner WB (2008) miRNAs are essential for survival and differentiation of newborn neurons but not for expansion of neural progenitors during early neurogenesis in the mouse embryonic neocortex. *Development* 135, 3911-3921.

Dehlin E, Wormington M, Korner CG and Wahle E (2000) Cap-dependent deadenylation of mRNA. *EMBO J* 19, 1079-1086.

Denli AM, Tops BB, Plasterk RH, Ketting RF and Hannon GJ (2004) Processing of primary microRNAs by the Microprocessor complex. *Nature* 432, 231-235.

Deutscher MP and Li ZW (2001) Exoribonucleases and their multiple roles in RNA metabolism. *Prog Nucleic Acid Res Mol Biol* 66, 67-105.

Devany E, Zhang X, Park JY, Tian B and Kleiman FE (2013) Positive and negative feedback loops in the p53 and mRNA 3' processing pathways. *Proc Natl Acad Sci U S A* 110, 3351-3356.

Dhanraj S, Gunja SM, Deveau AP, Nissbeck M, Boonyawat B, Coombs AJ et al. (2015) Bone marrow failure and developmental delay caused by mutations in poly(A)-specific ribonuclease (PARN). *J Med Genet* 52, 738-748.

Ding L, Spencer A, Morita K and Han M (2005) The developmental timing regulator AIN-1 interacts with miRISCs and may target the argonaute protein ALG-1 to cytoplasmic P bodies in C. elegans. *Mol Cell* 19, 437-447.

Dueck A, Ziegler C, Eichner A, Berezikov E and Meister G (2012) microRNAs associated with the different human Argonaute proteins. *Nucleic Acids Res* 40, 9850-9862.

Eichhorn SW, Guo H, Mcgeary SE, Rodriguez-Mias RA, Shin C, Baek D et al. (2014) mRNA destabilization is the dominant effect of mammalian microRNAs by the time substantial repression ensues. *Mol Cell* 56, 104-115.

Elkayam E, Kuhn CD, Tocilj A, Haase AD, Greene EM, Hannon GJ et al. (2012) The structure of human Argonaute-2 in complex with miR-20a. *Cell* 150, 100-110.

Fabian MR, Cieplak MK, Frank F, Morita M, Green J, Srikumar T et al. (2011) miRNA-mediated deadenylation is orchestrated by GW182 through two conserved motifs that interact with CCR4-NOT. *Nat Struct Mol Biol* 18, 1211-1217.

Fang W and Bartel DP (2015) The menu of features that define primary microRNAs and enable de novo design of microRNA genes. *Mol Cell* 60, 131-145.

Fareh M, Yeom KH, Haagsma AC, Chauhan S, Heo I and Joo C (2016) TRBP ensures efficient Dicer processing of precursor microRNA in RNA-crowded environments. *Nat Commun* 7, 13694.

Fernandez-Valverde SL, Taft RJ and Mattick JS (2010) Dynamic isomiR regulation in Drosophila development. *RNA* 16, 1881-1888.

Fernandez N, Cordiner RA, Young RS, Hug N, Macias S and Caceres JF (2017) Genetic variation and RNA structure regulate microRNA biogenesis. *Nat Commun* 8, 15114.

Filippov V, Solovyev V, Filippova M and Gill SS (2000) A novel type of RNase III family proteins in eukaryotes. *Gene* 245, 213-221.

Ford LP, Watson J, Keene JD and Wilusz J (1999) ELAV proteins stabilize deadenylated

intermediates in a novel in vitro mRNA deadenylation/degradation system. *Genes Dev* 13, 188-201.
Forstemann K, Tomari Y, Du T, Vagin VV, Denli AM, Bratu DP et al. (2005) Normal microRNA maturation and germ-line stem cell maintenance requires Loquacious, a double-stranded RNA-binding domain protein. *PLoS Biol* 3, e236.
Frank F, Sonenberg N and Nagar B (2010) Structural basis for 5'-nucleotide base-specific recognition of guide RNA by human AGO2. *Nature* 465, 818-822.
Friedman RC, Farh KK, Burge CB and Bartel DP (2009) Most mammalian mRNAs are conserved targets of microRNAs. *Genome Res* 19, 92-105.
Fromm B, Billipp T, Peck LE, Johansen M, Tarver JE, King BL et al. (2015) A uniform system for the annotation of vertebrate microRNA genes and the evolution of the human microRNAome. *Annu Rev Genet* 49, 213-242.
Fuchs Wightman F, Giono LE, Fededa JP and De La Mata M (2018) Target RNAs strike back on microRNAs. *Front Genet* 9, 435.
Fukunaga R, Han BW, Hung JH, Xu J, Weng Z and Zamore PD (2012) Dicer partner proteins tune the length of mature miRNAs in flies and mammals. *Cell* 151, 533-546.
Gao M, Fritz DT, Ford LP and Wilusz J (2000) Interaction between a poly(A)-specific ribonuclease and the 5' cap influences mRNA deadenylation rates in vitro. *Mol Cell* 5, 479-488.
Gebert LFR and Macrae IJ (2019) Regulation of microRNA function in animals. *Nat Rev Mol Cell Biol* 20, 21-37.
Gherzi R, Lee KY, Briata P, Wegmuller D, Moroni C, Karin M et al. (2004) A KH domain RNA binding protein, KSRP, promotes ARE-directed mRNA turnover by recruiting the degradation machinery. *Mol Cell* 14, 571-583.
Giraldez AJ, Mishima Y, Rihel J, Grocock RJ, Van Dongen S, Inoue K et al. (2006) Zebrafish MiR-430 promotes deadenylation and clearance of maternal mRNAs. *Science* 312, 75-79.
Goldstrohm AC and Wickens M (2008) Multifunctional deadenylase complexes diversify mRNA control. *Nat Rev Mol Cell Biol* 9, 337-344.
Gregory RI, Chendrimada TP, Cooch N and Shiekhattar R (2005) Human RISC couples microRNA biogenesis and posttranscriptional gene silencing. *Cell* 123, 631-640.
Gregory RI, Yan KP, Amuthan G, Chendrimada T, Doratotaj B, Cooch N et al. (2004) The Microprocessor complex mediates the genesis of microRNAs. *Nature* 432, 235-240.
Grimson A, Farh KK, Johnston WK, Garrett-Engele P, Lim LP and Bartel DP (2007) MicroRNA targeting specificity in mammals: determinants beyond seed pairing. *Mol Cell* 27, 91-105.
Grishok A, Pasquinelli AE, Conte D, Li N, Parrish S, Ha I et al. (2001) Genes and mechanisms related to RNA interference regulate expression of the small temporal RNAs that control C. elegans developmental timing. *Cell* 106, 23-34.
Gu S, Jin L, Zhang Y, Huang Y, Zhang F, Valdmanis PN et al. (2012) The loop position of shRNAs and pre-miRNAs is critical for the accuracy of dicer processing in vivo. *Cell* 151, 900-911.
Guo H, Ingolia NT, Weissman JS and Bartel DP (2010) Mammalian microRNAs predominantly act to decrease target mRNA levels. *Nature* 466, 835-840.
Gutierrez-Vazquez C, Enright AJ, Rodriguez-Galan A, Perez-Garcia A, Collier P, Jones MR et al. (2017) 3' Uridylation controls mature microRNA turnover during CD4 T-cell activation. *RNA* 23, 882-891.

Ha M and Kim VN (2014) Regulation of microRNA biogenesis. *Nat Rev Mol Cell Biol* 15, 509-524.

Haas G, Cetin S, Messmer M, Chane-Woon-Ming B, Terenzi O, Chicher J et al. (2016) Identification of factors involved in target RNA-directed microRNA degradation. *Nucleic Acids Res* 44, 2873-2887.

Haase AD, Jaskiewicz L, Zhang H, Laine S, Sack R, Gatignol A et al. (2005) TRBP, a regulator of cellular PKR and HIV-1 virus expression, interacts with Dicer and functions in RNA silencing. *EMBO Rep* 6, 961-967.

Haley B and Zamore PD (2004) Kinetic analysis of the RNAi enzyme complex. *Nat Struct Mol Biol* 11, 599-606.

Han BW, Hung JH, Weng Z, Zamore PD and Ameres SL (2011) The 3'-to-5' exoribonuclease Nibbler shapes the 3' ends of microRNAs bound to Drosophila Argonaute1. *Curr Biol* 21, 1878-1887.

Han J, Lee Y, Yeom KH, Kim YK, Jin H and Kim VN (2004) The Drosha-DGCR8 complex in primary microRNA processing. *Genes Dev* 18, 3016-3027.

Han J, Lee Y, Yeom KH, Nam JW, Heo I, Rhee JK et al. (2006) Molecular basis for the recognition of primary microRNAs by the Drosha-DGCR8 complex. *Cell* 125, 887-901.

Hauptmann J, Schraivogel D, Bruckmann A, Manickavel S, Jakob L, Eichner N et al. (2015) Biochemical isolation of Argonaute protein complexes by Ago-APP. *Proc Natl Acad Sci U S A* 112, 11841-11845.

He GJ and Yan YB (2014) Self-association of poly(A)-specific ribonuclease (PARN) triggered by the R3H domain. *Biochim Biophys Acta* 1844, 2077-2085.

He GJ, Zhang A, Liu WF, Cheng Y and Yan YB (2009) Conformational stability and multistate unfolding of poly(A)-specific ribonuclease. *FEBS J* 276, 2849-2860.

He GJ, Zhang A, Liu WF and Yan YB (2013) Distinct roles of the R3H and RRM domains in poly(A)-specific ribonuclease structural integrity and catalysis. *Biochim Biophys Acta* 1834, 1089-1098.

Hendrickson DG, Hogan DJ, Mccullough HL, Myers JW, Herschlag D, Ferrell JE et al. (2009) Concordant regulation of translation and mRNA abundance for hundreds of targets of a human microRNA. *PLoS Biol* 7, e1000238.

Henriksson N, Nilsson P, Wu M, Song H and Virtanen A (2010) Recognition of adenosine residues by the active site of poly(A)-specific ribonuclease. *J Biol Chem* 285, 163-170.

Heo I, Joo C, Cho J, Ha M, Han J and Kim VN (2008) Lin28 mediates the terminal uridylation of let-7 precursor MicroRNA. *Mol Cell* 32, 276-284.

Heo I, Joo C, Kim YK, Ha M, Yoon MJ, Cho J et al. (2009) TUT4 in concert with Lin28 suppresses microRNA biogenesis through pre-microRNA uridylation. *Cell* 138, 696-708.

Houseley J, Lacava J and Tollervey D (2006) RNA-quality control by the exosome. *Nat Rev Mol Cell Biol* 7, 529-539.

Hutvagner G, Mclachlan J, Pasquinelli AE, Balint E, Tuschl T and Zamore PD (2001) A cellular function for the RNA-interference enzyme Dicer in the maturation of the let-7 small temporal RNA. *Science* 293, 834-838.

Hutvagner G and Zamore PD (2002) A microRNA in a multiple-turnover RNAi enzyme complex. *Science* 297, 2056-2060.

Im HI and Kenny PJ (2012) MicroRNAs in neuronal function and dysfunction. *Trends*

Neurosci 35, 325-334.
Ishikawa H, Yoshikawa H, Izumikawa K, Miura Y, Taoka M, Nobe Y et al. (2017) Poly(A)-specific ribonuclease regulates the processing of small-subunit rRNAs in human cells. *Nucleic Acids Res* 45, 3437-3447.
Iwasaki S, Kobayashi M, Yoda M, Sakaguchi Y, Katsuma S, Suzuki T et al. (2010) Hsc70/Hsp90 chaperone machinery mediates ATP-dependent RISC loading of small RNA duplexes. *Mol Cell* 39, 292-299.
Jiang F, Ye X, Liu X, Fincher L, Mckearin D and Liu Q (2005) Dicer-1 and R3D1-L catalyze microRNA maturation in Drosophila. *Genes Dev* 19, 1674-1679.
Johanson TM, Keown AA, Cmero M, Yeo JH, Kumar A, Lew AM et al. (2015) Drosha controls dendritic cell development by cleaving messenger RNAs encoding inhibitors of myelopoiesis. *Nat Immunol* 16, 1134-1141.
Jonas S and Izaurralde E (2015) Towards a molecular understanding of microRNA-mediated gene silencing. *Nat Rev Genet* 16, 421-433.
Jones-Rhoades MW, Bartel DP and Bartel B (2006) MicroRNAs and their regulatory roles in plants. *Annu Rev Plant Biol* 57, 19-53.
Jones MR, Quinton LJ, Blahna MT, Neilson JR, Fu S, Ivanov AR et al. (2009) Zcchc11-dependent uridylation of microRNA directs cytokine expression. *Nat Cell Biol* 11, 1157-1163.
Juvvuna PK, Khandelia P, Lee LM and Makeyev EV (2012) Argonaute identity defines the length of mature mammalian microRNAs. *Nucleic Acids Res* 40, 6808-6820.
Kanellopoulou C, Muljo SA, Kung AL, Ganesan S, Drapkin R, Jenuwein T et al. (2005) Dicer-deficient mouse embryonic stem cells are defective in differentiation and centromeric silencing. *Genes Dev* 19, 489-501.
Karginov FV, Cheloufi S, Chong MM, Stark A, Smith AD and Hannon GJ (2010) Diverse endonucleolytic cleavage sites in the mammalian transcriptome depend upon microRNAs, Drosha, and additional nucleases. *Mol Cell* 38, 781-788.
Kataoka Y, Takeichi M and Uemura T (2001) Developmental roles and molecular characterization of a Drosophila homologue of Arabidopsis Argonaute1, the founder of a novel gene superfamily. *Genes Cells* 6, 313-325.
Katoh T, Hojo H and Suzuki T (2015) Destabilization of microRNAs in human cells by 3' deadenylation mediated by PARN and CUGBP1. *Nucleic Acids Res* 43, 7521-7534.
Katoh T, Sakaguchi Y, Miyauchi K, Suzuki T, Kashiwabara S, Baba T et al. (2009) Selective stabilization of mammalian microRNAs by 3' adenylation mediated by the cytoplasmic poly(A) polymerase GLD-2. *Genes Dev* 23, 433-438.
Kawahara Y, Megraw M, Kreider E, Iizasa H, Valente L, Hatzigeorgiou AG et al. (2008) Frequency and fate of microRNA editing in human brain. *Nucleic Acids Res* 36, 5270-5280.
Kawahara Y, Zinshteyn B, Sethupathy P, Iizasa H, Hatzigeorgiou AG and Nishikura K (2007) Redirection of silencing targets by adenosine-to-inosine editing of miRNAs. *Science* 315, 1137-1140.
Kawamata T, Seitz H and Tomari Y (2009) Structural determinants of miRNAs for RISC loading and slicer-independent unwinding. *Nat Struct Mol Biol* 16, 953-960.
Ketting RF, Fischer SE, Bernstein E, Sijen T, Hannon GJ and Plasterk RH (2001) Dicer functions in RNA interference and in synthesis of small RNA involved in developmental timing in C. elegans. *Genes Dev* 15, 2654-2659.
Khvorova A, Reynolds A and Jayasena SD (2003) Functional siRNAs and miRNAs exhibit

strand bias. *Cell* 115, 209-216.
Kim B, Jeong K and Kim VN (2017) Genome-wide mapping of DROSHA cleavage sites on primary microRNAs and noncanonical substrates. *Mol Cell* 66, 258-269 e255.
Kim JH and Richter JD (2006) Opposing polymerase-deadenylase activities regulate cytoplasmic polyadenylation. *Mol Cell* 24, 173-183.
Kim K, Nguyen TD, Li S and Nguyen TA (2018) SRSF3 recruits DROSHA to the basal junction of primary microRNAs. *RNA* 24, 892-898.
Kim Y, Yeo J, Lee JH, Cho J, Seo D, Kim JS et al. (2014) Deletion of human tarbp2 reveals cellular microRNA targets and cell-cycle function of TRBP. *Cell Rep* 9, 1061-1074.
Kim YK, Kim B and Kim VN (2016) Re-evaluation of the roles of DROSHA, Exportin 5, and DICER in microRNA biogenesis. *Proc Natl Acad Sci U S A* 113, E1881-1889.
Kiss T and Filipowicz W (1993) Small nucleolar RNAs encoded by introns of the human cell cycle regulatory gene RCC1. *EMBO J* 12, 2913-2920.
Kiss T and Filipowicz W (1995) Exonucleolytic processing of small nucleolar RNAs from pre-mRNA introns. *Genes Dev* 9, 1411-1424.
Klum SM, Chandradoss SD, Schirle NT, Joo C and Macrae IJ (2018) Helix-7 in Argonaute2 shapes the microRNA seed region for rapid target recognition. *EMBO J* 37, 75-88.
Korner CG and Wahle E (1997) Poly(A) tail shortening by a mammalian poly(A)-specific 3'-exoribonuclease. *J Biol Chem* 272, 10448-10456.
Korner CG, Wormington M, Muckenthaler M, Schneider S, Dehlin E and Wahle E (1998) The deadenylating nuclease (DAN) is involved in poly(A) tail removal during the meiotic maturation of Xenopus oocytes. *EMBO J* 17, 5427-5437.
Kozomara A and Griffiths-Jones S (2014) miRBase: annotating high confidence microRNAs using deep sequencing data. *Nucleic Acids Res* 42, D68-73.
Krek A, Grun D, Poy MN, Wolf R, Rosenberg L, Epstein EJ et al. (2005) Combinatorial microRNA target predictions. *Nat Genet* 37, 495-500.
Kropski JA, Reiss S, Markin C, Brown KK, Schwartz DA, Schwarz MI et al. (2017) Rare genetic variants in PARN are associated with pulmonary fibrosis in families. *Am J Respir Crit Care Med* 196, 1481-1484.
Krupp G (1988) RNA synthesis: strategies for the use of bacteriophage RNA polymerases. *Gene* 72, 75-89.
Krutzfeldt J, Rajewsky N, Braich R, Rajeev KG, Tuschl T, Manoharan M et al. (2005) Silencing of microRNAs in vivo with 'antagomirs'. *Nature* 438, 685-689.
Kwon SC, Nguyen TA, Choi YG, Jo MH, Hohng S, Kim VN et al. (2016) Structure of human DROSHA. *Cell* 164, 81-90.
Lagos-Quintana M, Rauhut R, Lendeckel W and Tuschl T (2001) Identification of novel genes coding for small expressed RNAs. *Science* 294, 853-858.
Lai WS, Kennington EA and Blackshear PJ (2003) Tristetraprolin and its family members can promote the cell-free deadenylation of AU-rich element-containing mRNAs by poly(A) ribonuclease. *Mol Cell Biol* 23, 3798-3812.
Langmead B and Salzberg SL (2012) Fast gapped-read alignment with Bowtie 2. *Nat Methods* 9, 357-359.
Lau NC, Lim LP, Weinstein EG and Bartel DP (2001) An abundant class of tiny RNAs with probable regulatory roles in Caenorhabditis elegans. *Science* 294, 858-862.
Lazarus HM and Sporin MB (1967) Purification and properties of a nuclear exoribonuclease from Ehrlich ascites tumor cells. *Proc Natl Acad Sci U S A* 57, 1386-1393.
Lee HY and Doudna JA (2012) TRBP alters human precursor microRNA processing in vitro.

RNA 18, 2012-2019.
Lee HY, Zhou K, Smith AM, Noland CL and Doudna JA (2013) Differential roles of human Dicer-binding proteins TRBP and PACT in small RNA processing. *Nucleic Acids Res* 41, 6568-6576.
Lee JE, Lee JY, Trembly J, Wilusz J, Tian B and Wilusz CJ (2012) The PARN deadenylase targets a discrete set of mRNAs for decay and regulates cell motility in mouse myoblasts. *PLoS Genet* 8, e1002901.
Lee LW, Zhang SL, Etheridge A, Ma L, Martin D, Galas D et al. (2010) Complexity of the microRNA repertoire revealed by next-generation sequencing. *RNA* 16, 2170-2180.
Lee M, Choi Y, Kim K, Jin H, Lim J, Nguyen TA et al. (2014) Adenylation of maternally inherited microRNAs by Wispy. *Mol Cell* 56, 696-707.
Lee RC and Ambros V (2001) An extensive class of small RNAs in Caenorhabditis elegans. *Science* 294, 862-864.
Lee RC, Feinbaum RL and Ambros V (1993) The C. elegans heterochronic gene lin-4 encodes small RNAs with antisense complementarity to lin-14. *Cell* 75, 843-854.
Lee Y, Ahn C, Han J, Choi H, Kim J, Yim J et al. (2003) The nuclear RNase III Drosha initiates microRNA processing. *Nature* 425, 415-419.
Lee Y, Hur I, Park SY, Kim YK, Suh MR and Kim VN (2006) The role of PACT in the RNA silencing pathway. *EMBO J* 25, 522-532.
Lee Y, Kim M, Han J, Yeom KH, Lee S, Baek SH et al. (2004) MicroRNA genes are transcribed by RNA polymerase II. *EMBO J* 23, 4051-4060.
Lejeune F, Li X and Maquat LE (2003) Nonsense-mediated mRNA decay in mammalian cells involves decapping, deadenylating, and exonucleolytic activities. *Mol Cell* 12, 675-687.
Leuschner PJ, Ameres SL, Kueng S and Martinez J (2006) Cleavage of the siRNA passenger strand during RISC assembly in human cells. *EMBO Rep* 7, 314-320.
Lewis BP, Burge CB and Bartel DP (2005) Conserved seed pairing, often flanked by adenosines, indicates that thousands of human genes are microRNA targets. *Cell* 120, 15-20.
Lewis BP, Shih IH, Jones-Rhoades MW, Bartel DP and Burge CB (2003) Prediction of mammalian microRNA targets. *Cell* 115, 787-798.
Li H and Durbin R (2009) Fast and accurate short read alignment with Burrows-Wheeler transform. *Bioinformatics* 25, 1754-1760.
Liang YH, Lavoie M, Comeau MA, Abou Elela S and Ji X (2014) Structure of a eukaryotic RNase III postcleavage complex reveals a double-ruler mechanism for substrate selection. *Mol Cell* 54, 431-444.
Lim LP, Lau NC, Garrett-Engele P, Grimson A, Schelter JM, Castle J et al. (2005) Microarray analysis shows that some microRNAs downregulate large numbers of target mRNAs. *Nature* 433, 769-773.
Lim LP, Lau NC, Weinstein EG, Abdelhakim A, Yekta S, Rhoades MW et al. (2003) The microRNAs of Caenorhabditis elegans. *Genes Dev* 17, 991-1008.
Lin S and Gregory RI (2015) MicroRNA biogenesis pathways in cancer. *Nat Rev Cancer* 15, 321-333.
Lin WJ, Duffy A and Chen CY (2007) Localization of AU-rich element-containing mRNA in cytoplasmic granules containing exosome subunits. *J Biol Chem* 282, 19958-19968.
Liu B, Childs-Disney JL, Znosko BM, Wang D, Fallahi M, Gallo SM et al. (2016) Analysis of secondary structural elements in human microRNA hairpin precursors. *BMC*

Bioinformatics 17.
Liu J, Carmell MA, Rivas FV, Marsden CG, Thomson JM, Song JJ et al. (2004) Argonaute2 is the catalytic engine of mammalian RNAi. *Science* 305, 1437-1441.
Liu J, Rivas FV, Wohlschlegel J, Yates JR, 3rd, Parker R and Hannon GJ (2005) A role for the P-body component GW182 in microRNA function. *Nat Cell Biol* 7, 1261-1266.
Liu N, Abe M, Sabin LR, Hendriks GJ, Naqvi AS, Yu Z et al. (2011) The exoribonuclease Nibbler controls 3' end processing of microRNAs in Drosophila. *Curr Biol* 21, 1888-1893.
Liu Q, Rand TA, Kalidas S, Du F, Kim HE, Smith DP et al. (2003) R2D2, a bridge between the initiation and effector steps of the Drosophila RNAi pathway. *Science* 301, 1921-1925.
Liu WF, Zhang A, Cheng Y, Zhou HM and Yan YB (2009) Allosteric regulation of human poly(A)-specific ribonuclease by cap and potassium ions. *Biochem Biophys Res Commun* 379, 341-345.
Liu WF, Zhang A, He GJ and Yan YB (2007) The R3H domain stabilizes poly(A)-specific ribonuclease by stabilizing the RRM domain. *Biochem Biophys Res Commun* 360, 846-851.
Liu X, Jin DY, Mcmanus MT and Mourelatos Z (2012) Precursor microRNA-programmed silencing complex assembly pathways in mammals. *Mol Cell* 46, 507-517.
Liu XH, Zheng Q, Vrettos N, Maragkakis M, Alexiou P, Gregory BD et al. (2014) A microRNA precursor surveillance system in quality control of microRNA synthesis. *Mol Cell* 55, 868-879.
Liu Z, Wang J, Cheng H, Ke X, Sun L, Zhang QC et al. (2018) Cryo-EM structure of human Dicer and its complexes with a pre-miRNA substrate. *Cell* 173, 1191-1203 e1112.
Luciano DJ, Mirsky H, Vendetti NJ and Maas S (2004) RNA editing of a miRNA precursor. *RNA* 10, 1174-1177.
Lujambio A and Lowe SW (2012) The microcosmos of cancer. *Nature* 482, 347-355.
Lund E, Guttinger S, Calado A, Dahlberg JE and Kutay U (2004) Nuclear export of microRNA precursors. *Science* 303, 95-98.
Ma H, Wu Y, Choi JG and Wu H (2013) Lower and upper stem-single-stranded RNA junctions together determine the Drosha cleavage site. *Proc Natl Acad Sci U S A* 110, 20687-20692.
Ma JB, Ye K and Patel DJ (2004) Structural basis for overhang-specific small interfering RNA recognition by the PAZ domain. *Nature* 429, 318-322.
Macrae IJ, Ma E, Zhou M, Robinson CV and Doudna JA (2008) In vitro reconstitution of the human RISC-loading complex. *Proc Natl Acad Sci U S A* 105, 512-517.
Macrae IJ, Zhou K and Doudna JA (2007) Structural determinants of RNA recognition and cleavage by Dicer. *Nat Struct Mol Biol* 14, 934-940.
Macrae IJ, Zhou K, Li F, Repic A, Brooks AN, Cande WZ et al. (2006) Structural basis for double-stranded RNA processing by Dicer. *Science* 311, 195-198.
Maniataki E and Mourelatos Z (2005) A human, ATP-independent, RISC assembly machine fueled by pre-miRNA. *Genes Dev* 19, 2979-2990.
Martin M (2011) Cutadapt removes adapter sequences from high-throughput sequencing reads. *EMBnet.journal* 17, 3.
Martinez J, Ren YG, Nilsson P, Ehrenberg M and Virtanen A (2001) The mRNA cap structure stimulates rate of poly(A) removal and amplifies processivity of degradation. *J Biol Chem* 276, 27923-27929.

Martinez J, Ren YG, Thuresson AC, Hellman U, Astrom J and Virtanen A (2000) A 54-kDa fragment of the Poly(A)-specific ribonuclease is an oligomeric, processive, and cap-interacting Poly(A)-specific 3' exonuclease. *J Biol Chem* 275, 24222-24230.

Matranga C, Tomari Y, Shin C, Bartel DP and Zamore PD (2005) Passenger-strand cleavage facilitates assembly of siRNA into Ago2-containing RNAi enzyme complexes. *Cell* 123, 607-620.

Mccall MN, Kim MS, Adil M, Patil AH, Lu Y, Mitchell CJ et al. (2017) Toward the human cellular microRNAome. *Genome Res* 27, 1769-1781.

Meister G, Landthaler M, Patkaniowska A, Dorsett Y, Teng G and Tuschl T (2004) Human Argonaute2 mediates RNA cleavage targeted by miRNAs and siRNAs. *Mol Cell* 15, 185-197.

Meister G, Landthaler M, Peters L, Chen PY, Urlaub H, Luhrmann R et al. (2005) Identification of novel argonaute-associated proteins. *Curr Biol* 15, 2149-2155.

Miller TE and Gomez-Cambronero J (2017) A feedback mechanism between PLD and deadenylase PARN for the shortening of eukaryotic poly(A) mRNA tails that is deregulated in cancer cells. *Biol Open* 6, 176-186.

Milligan JF, Groebe DR, Witherell GW and Uhlenbeck OC (1987) Oligoribonucleotide synthesis using T7 RNA polymerase and synthetic DNA templates. *Nucleic Acids Res* 15, 8783-8798.

Miska EA, Alvarez-Saavedra E, Abbott AL, Lau NC, Hellman AB, Mcgonagle SM et al. (2007) Most Caenorhabditis elegans microRNAs are individually not essential for development or viability. *PLoS Genet* 3, e215.

Moffat J, Grueneberg DA, Yang X, Kim SY, Kloepfer AM, Hinkle G et al. (2006) A lentiviral RNAi library for human and mouse genes applied to an arrayed viral high-content screen. *Cell* 124, 1283-1298.

Monecke T, Schell S, Dickmanns A and Ficner R (2008) Crystal structure of the RRM domain of poly(A)-specific ribonuclease reveals a novel m(7)G-cap-binding mode. *J Mol Biol* 382, 827-834.

Montellese C, Montel-Lehry N, Henras AK, Kutay U, Gleizes PE and O'donohue MF (2017) Poly(A)-specific ribonuclease is a nuclear ribosome biogenesis factor involved in human 18S rRNA maturation. *Nucleic Acids Res* 45, 6822-6836.

Moon DH, Segal M, Boyraz B, Guinan E, Hofmann I, Cahan P et al. (2015) Poly(A)-specific ribonuclease (PARN) mediates 3'-end maturation of the telomerase RNA component. *Nat Genet* 47, 1482-1488.

Moraes KC, Wilusz CJ and Wilusz J (2006) CUG-BP binds to RNA substrates and recruits PARN deadenylase. *RNA* 12, 1084-1091.

Mori M, Triboulet R, Mohseni M, Schlegelmilch K, Shrestha K, Camargo FD et al. (2014) Hippo signaling regulates microprocessor and links cell-density-dependent miRNA biogenesis to cancer. *Cell* 156, 893-906.

Morin RD, O'connor MD, Griffith M, Kuchenbauer F, Delaney A, Prabhu AL et al. (2008) Application of massively parallel sequencing to microRNA profiling and discovery in human embryonic stem cells. *Genome Res* 18, 610-621.

Mourelatos Z, Dostie J, Paushkin S, Sharma A, Charroux B, Abel L et al. (2002) miRNPs: a novel class of ribonucleoproteins containing numerous microRNAs. *Genes Dev* 16, 720-728.

Murchison EP, Partridge JF, Tam OH, Cheloufi S and Hannon GJ (2005) Characterization of Dicer-deficient murine embryonic stem cells. *Proc Natl Acad Sci U S A* 102, 12135-

12140.
Nagata T, Suzuki S, Endo R, Shirouzu M, Terada T, Inoue M et al. (2008) The RRM domain of poly(A)-specific ribonuclease has a noncanonical binding site for mRNA cap analog recognition. *Nucleic Acids Res* 36, 4754-4767.
Naruse K, Matsuura-Suzuki E, Watanabe M, Iwasaki S and Tomari Y (2018) In vitro reconstitution of chaperone-mediated human RISC assembly. *RNA* 24, 6-11.
Nguyen D, Grenier St-Sauveur V, Bergeron D, Dupuis-Sandoval F, Scott MS and Bachand F (2015a) A polyadenylation-dependent 3' end maturation pathway is required for the synthesis of the human telomerase RNA. *Cell Rep* 13, 2244-2257.
Nguyen TA, Jo MH, Choi YG, Park J, Kwon SC, Hohng S et al. (2015b) Functional anatomy of the human Microprocessor. *Cell* 161, 1374-1387.
Nicholson AW (2014) Ribonuclease III mechanisms of double-stranded RNA cleavage. *Wiley Interdiscip Rev RNA* 5, 31-48.
Nilsson P, Henriksson N, Niedzwiecka A, Balatsos NA, Kokkoris K, Eriksson J et al. (2007) A multifunctional RNA recognition motif in poly(A)-specific ribonuclease with cap and poly(A) binding properties. *J Biol Chem* 282, 32902-32911.
Okamura K, Hagen JW, Duan H, Tyler DM and Lai EC (2007) The mirtron pathway generates microRNA-class regulatory RNAs in Drosophila. *Cell* 130, 89-100.
Opyrchal M, Anderson JR, Sokoloski KJ, Wilusz CJ and Wilusz J (2005) A cell-free mRNA stability assay reveals conservation of the enzymes and mechanisms of mRNA decay between mosquito and mammalian cell lines. *Insect Biochem Mol Biol* 35, 1321-1334.
Paddison PJ, Caudy AA, Bernstein E, Hannon GJ and Conklin DS (2002) Short hairpin RNAs (shRNAs) induce sequence-specific silencing in mammalian cells. *Genes Dev* 16, 948-958.
Park CY, Jeker LT, Carver-Moore K, Oh A, Liu HJ, Cameron R et al. (2012) A resource for the conditional ablation of microRNAs in the mouse. *Cell Rep* 1, 385-391.
Park JE, Heo I, Tian Y, Simanshu DK, Chang H, Jee D et al. (2011) Dicer recognizes the 5' end of RNA for efficient and accurate processing. *Nature* 475, 201-205.
Park JH and Shin C (2015) Slicer-independent mechanism drives small-RNA strand separation during human RISC assembly. *Nucleic Acids Res* 43, 9418-9433.
Park JH, Shin SY and Shin C (2017) Non-canonical targets destabilize microRNAs in human Argonautes. *Nucleic Acids Res* 45, 1569-1583.
Parker R and Song HW (2004) The enzymes and control of eukaryotic mRNA turnover. *Nat Struct Mol Biol* 11, 121-127.
Pasquinelli AE, Reinhart BJ, Slack F, Martindale MQ, Kuroda MI, Maller B et al. (2000) Conservation of the sequence and temporal expression of let-7 heterochronic regulatory RNA. *Nature* 408, 86-89.
Petrovski S, Todd JL, Durheim MT, Wang Q, Chien JW, Kelly FL et al. (2017) An exome sequencing study to assess the role of rare genetic variation in pulmonary fibrosis. *Am J Respir Crit Care Med* 196, 82-93.
Provost P, Dishart D, Doucet J, Frendewey D, Samuelsson B and Radmark O (2002) Ribonuclease activity and RNA binding of recombinant human Dicer. *EMBO J* 21, 5864-5874.
Ran FA, Hsu PD, Wright J, Agarwala V, Scott DA and Zhang F (2013) Genome engineering using the CRISPR-Cas9 system. *Nat Protoc* 8, 2281-2308.
Rand TA, Petersen S, Du F and Wang X (2005) Argonaute2 cleaves the anti-guide strand of

siRNA during RISC activation. *Cell* 123, 621-629.
Rehwinkel J, Behm-Ansmant I, Gatfield D and Izaurralde E (2005) A crucial role for GW182 and the DCP1:DCP2 decapping complex in miRNA-mediated gene silencing. *RNA* 11, 1640-1647.
Reimao-Pinto MM, Ignatova V, Burkard TR, Hung JH, Manzenreither RA, Sowemimo I et al. (2015) Uridylation of RNA hairpins by Tailor confines the emergence of microRNAs in Drosophila. *Mol Cell* 59, 203-216.
Reinhardt HC, Hasskamp P, Schmedding I, Morandell S, Van Vugt MA, Wang X et al. (2010) DNA damage activates a spatially distinct late cytoplasmic cell-cycle checkpoint network controlled by MK2-mediated RNA stabilization. *Mol Cell* 40, 34-49.
Reinhart BJ, Slack FJ, Basson M, Pasquinelli AE, Bettinger JC, Rougvie AE et al. (2000) The 21-nucleotide let-7 RNA regulates developmental timing in Caenorhabditis elegans. *Nature* 403, 901-906.
Ren YG, Kirsebom LA and Virtanen A (2004) Coordination of divalent metal ions in the active site of poly(A)-specific ribonuclease. *J Biol Chem* 279, 48702-48706.
Ren YG, Martinez J and Virtanen A (2002) Identification of the active site of poly(A)-specific ribonuclease by site-directed mutagenesis and Fe(2+)-mediated cleavage. *J Biol Chem* 277, 5982-5987.
Roden C, Gaillard J, Kanoria S, Rennie W, Barish S, Cheng J et al. (2017) Novel determinants of mammalian primary microRNA processing revealed by systematic evaluation of hairpin-containing transcripts and human genetic variation. *Genome Res* 27, 374-384.
Ruby JG, Jan C, Player C, Axtell MJ, Lee W, Nusbaum C et al. (2006) Large-scale sequencing reveals 21U-RNAs and additional microRNAs and endogenous siRNAs in C. elegans. *Cell* 127, 1193-1207.
Ruby JG, Jan CH and Bartel DP (2007a) Intronic microRNA precursors that bypass Drosha processing. *Nature* 448, 83-86.
Ruby JG, Stark A, Johnston WK, Kellis M, Bartel DP and Lai EC (2007b) Evolution, biogenesis, expression, and target predictions of a substantially expanded set of Drosophila microRNAs. *Genome Res* 17, 1850-1864.
Ruvkun G, Wightman B and Ha I (2004) The 20 years it took to recognize the importance of tiny RNAs. *Cell* S116, S93-96.
Saito K, Ishizuka A, Siomi H and Siomi MC (2005) Processing of pre-microRNAs by the Dicer-1-Loquacious complex in Drosophila cells. *PLoS Biol* 3, e235.
Salomon WE, Jolly SM, Moore MJ, Zamore PD and Serebrov V (2015) Single-molecule imaging reveals that Argonaute reshapes the binding properties of its nucleic acid guides. *Cell* 162, 84-95.
Schirle NT and Macrae IJ (2012) The crystal structure of human Argonaute2. *Science* 336, 1037-1040.
Schirle NT, Sheu-Gruttadauria J and Macrae IJ (2014) Structural basis for microRNA targeting. *Science* 346, 608-613.
Schmittgen TD and Livak KJ (2008) Analyzing real-time PCR data by the comparative C(T) method. *Nat Protoc* 3, 1101-1108.
Schurer H, Lang K, Schuster J and Morl M (2002) A universal method to produce in vitro transcripts with homogeneous 3' ends. *Nucleic Acids Res* 30, e56.
Schwarz DS, Hutvagner G, Du T, Xu Z, Aronin N and Zamore PD (2003) Asymmetry in the assembly of the RNAi enzyme complex. *Cell* 115, 199-208.

Selbach M, Schwanhausser B, Thierfelder N, Fang Z, Khanin R and Rajewsky N (2008) Widespread changes in protein synthesis induced by microRNAs. *Nature* 455, 58-63.

Seong Y, Lim DH, Kim A, Seo JH, Lee YS, Song H et al. (2014) Global identification of target recognition and cleavage by the Microprocessor in human ES cells. *Nucleic Acids Res* 42, 12806-12821.

Shin C, Nam JW, Farh KK, Chiang HR, Shkumatava A and Bartel DP (2010) Expanding the microRNA targeting code: functional sites with centered pairing. *Mol Cell* 38, 789-802.

Shukla S and Parker R (2017) PARN modulates Y RNA stability and its 3'-end formation. *Mol Cell Biol* 37.

Shukla S, Schmidt JC, Goldfarb KC, Cech TR and Parker R (2016) Inhibition of telomerase RNA decay rescues telomerase deficiency caused by dyskerin or PARN defects. *Nat Struct Mol Biol* 23, 286-292.

Slack FJ, Basson M, Liu Z, Ambros V, Horvitz HR and Ruvkun G (2000) The lin-41 RBCC gene acts in the C. elegans heterochronic pathway between the let-7 regulatory RNA and the LIN-29 transcription factor. *Mol Cell* 5, 659-669.

Son A, Park JE and Kim VN (2018) PARN and TOE1 constitute a 3' end maturation module for nuclear non-coding RNAs. *Cell Rep* 23, 888-898.

Song Y, Liu KJ and Wang TH (2015) Efficient synthesis of stably adenylated DNA and RNA adapters for microRNA capture using T4 RNA ligase 1. *Sci Rep* 5, 15620.

Starega-Roslan J, Krol J, Koscianska E, Kozlowski P, Szlachcic WJ, Sobczak K et al. (2011) Structural basis of microRNA length variety. *Nucleic Acids Res* 39, 257-268.

Stuart BD, Choi J, Zaidi S, Xing C, Holohan B, Chen R et al. (2015) Exome sequencing links mutations in PARN and RTEL1 with familial pulmonary fibrosis and telomere shortening. *Nat Genet* 47, 512-517.

Subtelny AO, Eichhorn SW, Chen GR, Sive H and Bartel DP (2014) Poly(A)-tail profiling reveals an embryonic switch in translational control. *Nature* 508, 66-71.

Suzuki HI, Katsura A, Yasuda T, Ueno T, Mano H, Sugimoto K et al. (2015) Small-RNA asymmetry is directly driven by mammalian Argonautes. *Nat Struct Mol Biol* 22, 512-521.

Telonis AG, Magee R, Loher P, Chervoneva I, Londin E and Rigoutsos I (2017) Knowledge about the presence or absence of miRNA isoforms (isomiRs) can successfully discriminate amongst 32 TCGA cancer types. *Nucleic Acids Res* 45, 2973-2985.

Thomas MF, L'etoile ND and Ansel KM (2014) Eri1: a conserved enzyme at the crossroads of multiple RNA-processing pathways. *Trends Genet* 30, 298-307.

Thornton JE, Du P, Jing L, Sjekloca L, Lin S, Grossi E et al. (2014) Selective microRNA uridylation by Zcchc6 (TUT7) and Zcchc11 (TUT4). *Nucleic Acids Res* 42, 11777-11791.

Tian Y, Simanshu DK, Ma JB, Park JE, Heo I, Kim VN et al. (2014) A phosphate-binding pocket within the platform-PAZ-connector helix cassette of human Dicer. *Mol Cell* 53, 606-616.

Tseng CK, Wang HF, Burns AM, Schroeder MR, Gaspari M and Baumann P (2015) Human telomerase RNA processing and quality control. *Cell Rep* 13, 2232-2243.

Tsutsumi A, Kawamata T, Izumi N, Seitz H and Tomari Y (2011) Recognition of the pre-miRNA structure by Drosophila Dicer-1. *Nat Struct Mol Biol* 18, 1153-1158.

Tummala H, Walne A, Collopy L, Cardoso S, De La Fuente J, Lawson S et al. (2015) Poly(A)-

specific ribonuclease deficiency impacts telomere biology and causes dyskeratosis congenita. *J Clin Invest* 125, 2151-2160.
Tycowski KT, Shu MD and Steitz JA (1993) A small nucleolar RNA is processed from an intron of the human gene encoding ribosomal protein S3. *Genes Dev* 7, 1176-1190.
Udagawa T, Swanger SA, Takeuchi K, Kim JH, Nalavadi V, Shin J et al. (2012) Bidirectional control of mRNA translation and synaptic plasticity by the cytoplasmic polyadenylation complex. *Mol Cell* 47, 253-266.
Uhlen M, Oksvold P, Fagerberg L, Lundberg E, Jonasson K, Forsberg M et al. (2010) Towards a knowledge-based Human Protein Atlas. *Nat Biotechnol* 28, 1248-1250.
Valdar WS (2002) Scoring residue conservation. *Proteins* 48, 227-241.
Vanacova S and Stefl R (2007) The exosome and RNA quality control in the nucleus. *EMBO Rep* 8, 651-657.
Vasquez-Rifo A, Jannot G, Armisen J, Labouesse M, Bukhari SI, Rondeau EL et al. (2012) Developmental characterization of the microRNA-specific C. elegans Argonautes alg-1 and alg-2. *PLoS One* 7, e33750.
Vella MC, Choi EY, Lin SY, Reinert K and Slack FJ (2004) The C. elegans microRNA let-7 binds to imperfect let-7 complementary sites from the lin-41 3'UTR. *Genes Dev* 18, 132-137.
Vermeulen A, Behlen L, Reynolds A, Wolfson A, Marshall WS, Karpilow J et al. (2005) The contributions of dsRNA structure to Dicer specificity and efficiency. *RNA* 11, 674-682.
Virtanen A, Henriksson N, Nilsson P and Nissbeck M (2013) Poly(A)-specific ribonuclease (PARN): an allosterically regulated, processive and mRNA cap-interacting deadenylase. *Crit Rev Biochem Mol Biol* 48, 192-209.
Walker SC, Avis JM and Conn GL (2003) General plasmids for producing RNA in vitro transcripts with homogeneous ends. *Nucleic Acids Res* 31, e82.
Wang HW, Noland C, Siridechadilok B, Taylor DW, Ma E, Felderer K et al. (2009) Structural insights into RNA processing by the human RISC-loading complex. *Nat Struct Mol Biol* 16, 1148-1153.
Wang Y, Medvid R, Melton C, Jaenisch R and Blelloch R (2007) DGCR8 is essential for microRNA biogenesis and silencing of embryonic stem cell self-renewal. *Nat Genet* 39, 380-385.
Wee LM, Flores-Jasso CF, Salomon WE and Zamore PD (2012) Argonaute divides its RNA guide into domains with distinct functions and RNA-binding properties. *Cell* 151, 1055-1067.
Wienholds E, Koudijs MJ, Van Eeden FJ, Cuppen E and Plasterk RH (2003) The microRNA-producing enzyme Dicer1 is essential for zebrafish development. *Nat Genet* 35, 217-218.
Wightman B, Ha I and Ruvkun G (1993) Posttranscriptional regulation of the heterochronic gene lin-14 by lin-4 mediates temporal pattern formation in C. elegans. *Cell* 75, 855-862.
Wilson RC, Tambe A, Kidwell MA, Noland CL, Schneider CP and Doudna JA (2015) Dicer-TRBP complex formation ensures accurate mammalian microRNA biogenesis. *Mol Cell* 57, 397-407.
Wu H, Xu H, Miraglia LJ and Crooke ST (2000) Human RNase III is a 160-kDa protein involved in preribosomal RNA processing. *J Biol Chem* 275, 36957-36965.
Wu H, Ye C, Ramirez D and Manjunath N (2009a) Alternative processing of primary

microRNA transcripts by Drosha generates 5' end variation of mature microRNA. *PLoS One* 4, e7566.

Wu M, Nilsson P, Henriksson N, Niedzwiecka A, Lim MK, Cheng Z et al. (2009b) Structural basis of m(7)GpppG binding to poly(A)-specific ribonuclease. *Structure* 17, 276-286.

Wu MS, Reuter M, Lilie H, Liu YY, Wahle E and Song HW (2005) Structural insight into poly(A) binding and catalytic mechanism of human PARN. *EMBO J* 24, 4082-4093.

Wyman SK, Knouf EC, Parkin RK, Fritz BR, Lin DW, Dennis LM et al. (2011) Post-transcriptional generation of miRNA variants by multiple nucleotidyl transferases contributes to miRNA transcriptome complexity. *Genome Res* 21, 1450-1461.

Xie M, Li M, Vilborg A, Lee N, Shu MD, Yartseva V et al. (2013) Mammalian 5'-capped microRNA precursors that generate a single microRNA. *Cell* 155, 1568-1580.

Yamane D, Selitsky SR, Shimakami T, Li Y, Zhou M, Honda M et al. (2017) Differential hepatitis C virus RNA target site selection and host factor activities of naturally occurring miR-122 3' variants. *Nucleic Acids Res* 45, 4743-4755.

Yamashita A, Chang TC, Yamashita Y, Zhu W, Zhong Z, Chen CY et al. (2005) Concerted action of poly(A) nucleases and decapping enzyme in mammalian mRNA turnover. *Nat Struct Mol Biol* 12, 1054-1063.

Yang JS, Maurin T, Robine N, Rasmussen KD, Jeffrey KL, Chandwani R et al. (2010) Conserved vertebrate mir-451 provides a platform for Dicer-independent, Ago2-mediated microRNA biogenesis. *Proc Natl Acad Sci U S A* 107, 15163-15168.

Yekta S, Shih IH and Bartel DP (2004) MicroRNA-directed cleavage of HOXB8 mRNA. *Science* 304, 594-596.

Yi H, Park J, Ha M, Lim J, Chang H and Kim VN (2018) PABP cooperates with the CCR4-NOT complex to promote mRNA deadenylation and block precocious decay. *Mol Cell* 70, 1081-1088.

Yi R, Qin Y, Macara IG and Cullen BR (2003) Exportin-5 mediates the nuclear export of pre-microRNAs and short hairpin RNAs. *Genes Dev* 17, 3011-3016.

Yoda M, Cifuentes D, Izumi N, Sakaguchi Y, Suzuki T, Giraldez AJ et al. (2013) Poly(A)-specific ribonuclease mediates 3'-end trimming of Argonaute2-cleaved precursor microRNAs. *Cell Rep* 5, 715-726.

Yoda M, Kawamata T, Paroo Z, Ye X, Iwasaki S, Liu Q et al. (2010) ATP-dependent human RISC assembly pathways. *Nat Struct Mol Biol* 17, 17-23.

Zamudio JR, Kelly TJ and Sharp PA (2014) Argonaute-bound small RNAs from promoter-proximal RNA polymerase II. *Cell* 156, 920-934.

Zeng Y, Yi R and Cullen BR (2005) Recognition and cleavage of primary microRNA precursors by the nuclear processing enzyme Drosha. *EMBO J* 24, 138-148.

Zhang A, Liu WF and Yan YB (2007) Role of the RRM domain in the activity, structure and stability of poly(A)-specific ribonuclease. *Arch Biochem Biophys* 461, 255-262.

Zhang H, Kolb FA, Jaskiewicz L, Westhof E and Filipowicz W (2004) Single processing center models for human Dicer and bacterial RNase III. *Cell* 118, 57-68.

Zhang LN and Yan YB (2015) Depletion of poly(A)-specific ribonuclease (PARN) inhibits proliferation of human gastric cancer cells by blocking cell cycle progression. *Biochim Biophys Acta* 1853, 522-534.

Zhang X, Devany E, Murphy MR, Glazman G, Persaud M and Kleiman FE (2015) PARN deadenylase is involved in miRNA-dependent degradation of TP53 mRNA in mammalian cells. *Nucleic Acids Res* 43, 10925-10938.

Zhang X and Zeng Y (2010) The terminal loop region controls microRNA processing by Drosha and Dicer. *Nucleic Acids Res* 38, 7689-7697.

Zhu Y, Chen G, Lv F, Wang X, Ji X, Xu Y et al. (2011) Zinc-finger antiviral protein inhibits HIV-1 infection by selectively targeting multiply spliced viral mRNAs for degradation. *Proc Natl Acad Sci U S A* 108, 15834-15839.

Zuker M (2003) Mfold web server for nucleic acid folding and hybridization prediction. *Nucleic Acids Res* 31, 3406-3415.

Zuo YH and Deutscher MP (2001) Exoribonuclease superfamilies: structural analysis and phylogenetic distribution. *Nucleic Acids Res* 29, 1017-1026.

ABSTRACT IN KOREAN

마이크로RNA는 약 22개의 뉴클레오타이드로 이루어진 짧은 비암호화 RNA의 일종으로, 세포 내에서 유전자 발현을 억제하는 방식으로 조절자의 기능을 수행한다. 차세대 염기서열 분석 기술의 발달에 힘입어 한 종류의 마이크로RNA가 실제 세포 내에서는 말단 부위 서열이나 내부 서열이 약간씩 다른 일련의 동형체로 존재하고 있다는 사실이 알려져 왔다. 그러한 변형 중에서 가장 빈번하게 일어나는 것은 3′ 말단 부근의 변형이다. 예를 들어 말단뉴클레오타이드전달효소라 불리는 일련의 효소들은 마이크로RNA의 3′ 말단에 몇 개의 뉴클레오타이드를 첨가하는데, 이러한 “꼬리”가 때로는 마이크로RNA의 안정성이나 기능을 조절하기도 한다. 말단뉴클레오타이드전달효소에 의한 마이크로RNA의 길이 연장은 여러 전사체 수준에서의 연구에 의해 그 효소학이 잘 정립된 편인 반면, 마이크로RNA의 길이를 줄이는 효소 활성에 대해서는 알려진 바가 많지 않다. 본 연구에서 나는 Poly(A)-specific ribonuclease (PARN) 라 불리는 RNA 말단분해효소가 인간 세포에서 마이크로RNA의 3′ 말단을 조각한다는 사실을 보고하였다. PARN이 결핍된 세포를 제작하고 그 세포의 마이크로RNA들을 차세대 염기서열 분석법을 통해 조사한 결과, 나는 PARN이 유전체에서 유래하였거나 또는 말단뉴클레오타이드전달효소에 의해 부착된 마이크로RNA의 3′ 말단 연장을 제거하고, 결과적으로 마이크로RNA의 길이를 줄인다는 사실을 발견하였다. 놀랍게도 PARN에 의한 마이크로RNA의 길이 감소는 마이크로RNA의 안정성을 크게 변화시키지 않았고, 따라서 이러한 과정은 마이크로RNA 분해 경로에서 작동한다기보다는 마이크로RNA 성숙을 완료하는 역할을 하는 것으로 생각된다. PARN에 의한 마이크로RNA의 길이 감소는 대부분의 마이크로RNA에서 폭넓게 일어나며, 척추동물 전반에서 마이크로RNA의 3′

말단 형성에 기여하는 보존된 메커니즘으로 보여진다. 결과적으로 본 연구는 마이크로 RNA 생합성 및 3′ 말단 형성에 대한 이해를 한층 확장하였으며, 최근 들어 급속도로 늘어나고 있는 PARN의 비암호화 RNA 기질 목록에 마이크로RNA를 추가하였다.

주요어: 꼬리달기, 마이크로RNA, 마이크로RNA동형체, 말단뉴클레오타이드첨가, RNA 말단분해효소, 잘라다듬기, PARN, poly(A)-specific ribonuclease

학번: 2010-23461

CURRICULUM VITAE

Name : Dooyoung Lee

Gender : Male

Date of birth : February 14, 1988

Place of birth : Seoul, Republic of Korea

Address : Department of Agricultural Biotechnology,
Seoul National University, Seoul 08826, Republic of Korea

Phone : +82-2-880-4653

Fax : +82-2-873-3112

E-mail : freeblue@snu.ac.kr

Education

2006. 3. – 2010. 2.

B. S. in Applied Life Chemistry (*summa cum laude*),
Department of Applied Biology and Chemistry,
College of Agriculture and Life Sciences,
Seoul National University, Seoul, Republic of Korea

2010. 9. – 2019. 2.

Ph. D. in Agricultural Biotechnology,
Department of Agricultural Biotechnology,
College of Agriculture and Life Sciences,
Seoul National University, Seoul, Republic of Korea
Study on the role of poly(A)-specific ribonuclease in microRNA 3′ end formation (Advisor: Chanseok Shin)

PUBLICATIONS

Lee D*, Park D*, Park JH and Shin C (2019) Poly(A)-specific ribonuclease sculpts the 3' ends of microRNAs. *RNA*, in press. (*co-first authors)

Kang I, Choi Y, Jung S, Lim JY, **Lee D**, Gupta S et al. (2018) Identification of target genes regulated by the Drosophila histone methyltransferase Eggless reveals a role of Decapentaplegic in apoptotic signaling. *Sci Rep* 8, 7123.

Kim Y, Kang YG, Choe JY, **Lee D**, Shin C, Hong SW et al. (2018) RNA interference-mediated gene silencing by branched tripodal RNAs does not require Dicer processing. *Nucleic Acid Ther* 28, 44-49.

Lee D and Shin C (2018) Emerging roles of DROSHA beyond primary microRNA processing. *RNA Biol* 15, 186-193.

Lee D, Nam JW and Shin C (2017) DROSHA targets its own transcript to modulate alternative splicing. *RNA* 23, 1035-1047.

Lee TY, Chang CI, **Lee D**, Hong SW, Shin C, Li CJ et al. (2013) RNA interference-mediated simultaneous silencing of four genes using cross-shaped RNA. *Mol Cells* 35, 320-326.

Lee D and Shin C (2012) MicroRNA-target interactions: new insights from genome-wide approaches. *Ann N Y Acad Sci* 1271, 118-128.